Neutrino Masses, Mixing, and Oscillations

note finali coverpage

(Article begins on next page)

19 April 2024

14. Neutrino Masses, Mixing, and Oscillations

Updated November 2017 by K. Nakamura (Kavli IPMU (WPI), U. Tokyo, KEK), and S.T. Petcov (SISSA/INFN Trieste, Kavli IPMU (WPI), U. Tokyo, Bulgarian Academy of Sciences).

June 5, 2018   19:50

The experiments with solar, atmospheric, reactor and accelerator neutrinos have provided compelling evidences for oscillations of neutrinos caused by nonzero neutrino masses and neutrino mixing. The data imply the existence of 3-neutrino mixing in vacuum. We review the theory of neutrino oscillations, the phenomenology of neutrino mixing, the problem of the nature - Dirac or Majorana, of massive neutrinos, the issue of CP violation in the lepton sector, and the current data on the neutrino masses and mixing parameters. The open questions and the main goals of future research in the field of neutrino mixing and oscillations are outlined.

14.1. Introduction: Massive neutrinos and neutrino mixing

It is a well-established experimental fact that the neutrinos and antineutrinos which take part in the standard charged current (CC) and neutral current (NC) weak interaction are of three varieties (types) or flavours: electron, ν_e and $\bar{\nu}_e$, muon, ν_μ and $\bar{\nu}_\mu$, and tauon, ν_τ and $\bar{\nu}_\tau$. The notion of neutrino type or flavour is dynamical: ν_e is the neutrino which is produced with e^+, or produces an e^-, in CC weak interaction processes; ν_μ is the neutrino which is produced with μ^+, or produces μ^-, *etc.* The flavour of a given neutrino is Lorentz invariant. Among the three different flavour neutrinos and antineutrinos, no two are identical. Correspondingly, the states which describe different flavour neutrinos must be orthogonal (within the precision of the current data): $\langle \nu_{l'}|\nu_l \rangle = \delta_{l'l}$, $\langle \bar{\nu}_{l'}|\bar{\nu}_l \rangle = \delta_{l'l}$, $\langle \bar{\nu}_{l'}|\nu_l \rangle = 0$.

It is also well-known from the existing data (all neutrino experiments were done so far with relativistic neutrinos or antineutrinos), that the flavour neutrinos ν_l (antineutrinos $\bar{\nu}_l$), are always produced in weak interaction processes in a state that is predominantly left-handed (LH) (right-handed (RH)). To account for this fact, ν_l and $\bar{\nu}_l$ are described in the Standard Model (SM) by a chiral LH flavour neutrino field $\nu_{lL}(x)$, $l = e, \mu, \tau$. For massless ν_l, the state of ν_l ($\bar{\nu}_l$) which the field $\nu_{lL}(x)$ annihilates (creates) is with helicity (-1/2) (helicity +1/2). If ν_l has a non-zero mass $m(\nu_l)$, the state of ν_l ($\bar{\nu}_l$) is a linear superposition of the helicity (-1/2) and (+1/2) states, but the helicity +1/2 state (helicity (-1/2) state) enters into the superposition with a coefficient $\propto m(\nu_l)/E$, E being the neutrino energy, and thus is strongly suppressed. Together with the LH charged lepton field $l_L(x)$, $\nu_{lL}(x)$ forms an $SU(2)_L$ doublet. In the absence of neutrino mixing and zero neutrino masses, $\nu_{lL}(x)$ and $l_L(x)$ can be assigned one unit of the additive lepton charge L_l and the three charges L_l, $l = e, \mu, \tau$, are conserved by the weak interaction.

At present there is no compelling evidence for the existence of states of relativistic neutrinos (antineutrinos), which are predominantly right-handed, ν_R (left-handed, $\bar{\nu}_L$). If RH neutrinos and LH antineutrinos exist, their interaction with matter should be much weaker than the weak interaction of the flavour LH neutrinos ν_l and RH antineutrinos $\bar{\nu}_l$, *i.e.*, ν_R ($\bar{\nu}_L$) should be "sterile" or "inert" neutrinos (antineutrinos) [1]. In the formalism of the Standard Model, the sterile ν_R and $\bar{\nu}_L$ can be described by $SU(2)_L$ singlet RH neutrino fields $\nu_R(x)$. In this case, ν_R and $\bar{\nu}_L$ will have no gauge interactions, *i.e.*, will not couple to the weak $W^\pm$ and Z^0 bosons. If present in an extension of the Standard Model, the RH neutrinos can play a crucial role i) in the generation of neutrino masses and mixing, ii) in understanding the remarkable disparity between the

magnitudes of neutrino masses and the masses of the charged leptons and quarks, and iii) in the generation of the observed matter-antimatter asymmetry of the Universe (via the leptogenesis mechanism [2]) . In this scenario which is based on the see-saw theory [3], there is a link between the generation of neutrino masses and the generation of the baryon asymmetry of the Universe. The simplest hypothesis (based on symmetry considerations) is that to each LH flavour neutrino field $\nu_{lL}(x)$ there corresponds a RH neutrino field $\nu_{lR}(x)$, $l = e, \mu, \tau$, although schemes with less (more) than three RH neutrinos are also being considered.

There have been remarkable discoveries in the field of neutrino physics in the last 20 years. The experiments with solar, atmospheric, reactor and accelerator neutrinos have provided compelling evidences for the existence of neutrino oscillations [4,5], transitions in flight between the different flavour neutrinos ν_e, ν_μ, ν_τ (antineutrinos $\bar{\nu}_e$, $\bar{\nu}_\mu$, $\bar{\nu}_\tau$), caused by nonzero neutrino masses and neutrino mixing. The existence of flavour neutrino oscillations implies that if a neutrino of a given flavour, say ν_μ, with energy E is produced in some weak interaction process, at a sufficiently large distance L from the ν_μ source the probability to find a neutrino of a different flavour, say ν_τ, $P(\nu_\mu \rightarrow \nu_\tau; E, L)$, is different from zero. $P(\nu_\mu \rightarrow \nu_\tau; E, L)$ is called the $\nu_\mu \rightarrow \nu_\tau$ oscillation or transition probability. If $P(\nu_\mu \rightarrow \nu_\tau; E, L) \neq 0$, the probability that ν_μ will not change into a neutrino of a different flavour, i.e., the "ν_μ survival probability" $P(\nu_\mu \rightarrow \nu_\mu; E, L)$, will be smaller than one. If only muon neutrinos ν_μ are detected in a given experiment and they take part in oscillations, one would observe a "disappearance" of muon neutrinos on the way from the ν_μ source to the detector. Disappearance of the solar ν_e, reactor $\bar{\nu}_e$ and of atmospheric ν_μ and $\bar{\nu}_\mu$ due to the oscillations have been observed respectively, in the solar neutrino [6–14], KamLAND [15,16] and Super-Kamiokande [17,18] experiments. Strong evidences for ν_μ disappearance due to oscillations were obtained also in the long-baseline accelerator neutrino experiments K2K [19]. Subsequently, the MINOS [20,21] and T2K [22,23] long baseline experiments reported compelling evidence for ν_μ disappearance due to oscillations, while evidences for ν_τ appearance due to $\nu_\mu \rightarrow \nu_\tau$ oscillations were published by the Super-Kamiokande [24] and OPERA [25] collaborations. As a consequence of the results of the experiments quoted above the existence of oscillations or transitions of the solar ν_e, atmospheric ν_μ and $\bar{\nu}_\mu$, accelerator ν_μ (at $L \sim 250$ km, $L \sim 295$ km and $L \sim 730$ km) and reactor $\bar{\nu}_e$ (at $L \sim 180$ km), driven by nonzero neutrino masses and neutrino mixing, was firmly established. There are strong indications that the solar ν_e transitions are affected by the solar matter [26,27].

The experimental discovery of oscillations of atmospheric muon neutrinos and antineutrinos and of the flavor conversion of solar (electron) neutrinos led to the 2015 Nobel Prize for Physics awarded to Takaaki Kajita [28](from the SuperKamiokande Collaboration) and Arthur McDonald [29](from the SNO Collaboration).

Further important developments took place in the period starting from June 2011. First, the T2K Collaboration reported [30] indications for $\nu_\mu \rightarrow \nu_e$ oscillations, i.e., of "appearance" of ν_e in a beam of ν_μ, which had a statistical significance of 2.5σ. The MINOS [31] Collaboration also obtained data consistent with $\nu_\mu \rightarrow \nu_e$ oscillations. Subsequently, the Double Chooz Collaboration reported [32] indications for disappearance of reactor $\bar{\nu}_e$ at $L \sim 1.1$ km. Strong evidences for reactor $\bar{\nu}_e$ disappearance at $L \sim 1.65$

km and $L \sim 1.38$ km and (with statistical significance of 5.2σ and 4.9σ) were obtained respectively in the Daya Bay [33] and RENO [34] experiments. Further evidences for reactor $\bar{\nu}_e$ disappearance (at 2.9σ) and for $\nu_\mu \rightarrow \nu_e$ oscillations (at 3.1σ) were reported by the Double Chooz [35] and T2K [36] experiments, while the Daya Bay and RENO Collaborations presented updated, more precise results on reactor $\bar{\nu}_e$ disappearance [37,38,39]. More recently the NOνA experiment reported results on $\nu_\mu \rightarrow \nu_e$ oscillations [40,42], while T2K presented data on $\bar{\nu}_\mu \rightarrow \bar{\nu}_e$ oscillation [43](for the latest results of the Daya Bay [44], RENO [45], Double Chooz [46], MINOS [47], T2K [48] and NOνA experiments, see Section 14.12).

Oscillations of neutrinos are a consequence of the presence of flavour neutrino mixing, or lepton mixing, in vacuum. In the formalism of local quantum field theory, used to construct the Standard Model, this means that the LH flavour neutrino fields $\nu_{l\mathrm{L}}(x)$, which enter into the expression for the lepton current in the CC weak interaction Lagrangian, are linear combinations of the fields of three (or more) neutrinos ν_j, having masses $m_j \neq 0$:

$$\nu_{l\mathrm{L}}(x) = \sum_j U_{lj} \, \nu_{j\mathrm{L}}(x), \quad l = e, \mu, \tau, \tag{14.1}$$

where $\nu_{j\mathrm{L}}(x)$ is the LH component of the field of ν_j possessing a mass m_j and U is a unitary matrix - the neutrino mixing matrix [1,4,5]. The matrix U is often called the Pontecorvo-Maki-Nakagawa-Sakata (PMNS) or Maki-Nakagawa-Sakata (MNS) mixing matrix. Obviously, Eq. (14.1) implies that the individual lepton charges L_l, $l = e, \mu, \tau$, are not conserved.

All compelling neutrino oscillation data can be described assuming 3-flavour neutrino mixing in vacuum. The data on the invisible decay width of the Z-boson is compatible with only 3 light flavour neutrinos coupled to Z [49]. The number of massive neutrinos ν_j, n, can, in general, be bigger than 3, $n > 3$, if, for instance, there exist sterile neutrinos and they mix with the flavour neutrinos. It is firmly established on the basis of the current data that at least 3 of the neutrinos ν_j, say ν_1, ν_2, ν_3, must be light, $m_{1,2,3} \lesssim 1$ eV (Section 14.12), and must have different masses, $m_1 \neq m_2 \neq m_3$. At present there are several experimental hints for existence of one or two light sterile neutrinos at the eV scale, which mix with the flavour neutrinos, implying the presence in the neutrino mixing of additional one or two neutrinos, ν_4 or $\nu_{4,5}$, with masses m_4 $(m_{4,5}) \sim 1$ eV. These hints will be briefly discussed in Section 14.14 of the present review.

Being electrically neutral, the neutrinos with definite mass ν_j can be Dirac fermions or Majorana particles [50,51]. The first possibility is realized when there exists a lepton charge carried by the neutrinos ν_j, which is conserved by the particle interactions. This could be, *e.g.*, the total lepton charge $L = L_e + L_\mu + L_\tau$: $L(\nu_j) = 1$, $j = 1, 2, 3$. In this case the neutrino ν_j has a distinctive antiparticle $\bar{\nu}_j$: $\bar{\nu}_j$ differs from ν_j by the value of the lepton charge L it carries, $L(\bar{\nu}_j) = -1$. The massive neutrinos ν_j can be Majorana particles if no lepton charge is conserved (see, *e.g.*, Refs. [52,53]) . A massive Majorana particle χ_j is identical with its antiparticle $\bar{\chi}_j$: $\chi_j \equiv \bar{\chi}_j$. On the basis of the existing neutrino data it is impossible to determine whether the massive neutrinos are Dirac or Majorana fermions.

In the case of n neutrino flavours and n massive neutrinos, the $n \times n$ unitary neutrino mixing matrix U can be parametrized by $n(n-1)/2$ Euler angles and $n(n+1)/2$ phases. If the massive neutrinos ν_j are Dirac particles, only $(n-1)(n-2)/2$ phases are physical and can be responsible for CP violation in the lepton sector. In this respect the neutrino (lepton) mixing with Dirac massive neutrinos is similar to the quark mixing.

For $n = 3$ there is just one CP violating phase in U, which is usually called "the Dirac CP violating phase." CP invariance holds if (in a certain standard convention) U is real, $U^* = U$.

If, however, the massive neutrinos are Majorana fermions, $\nu_j \equiv \chi_j$, the neutrino mixing matrix U contains $n(n-1)/2$ CP violation phases [54,55], *i.e.*, by $(n-1)$ phases more than in the Dirac neutrino case: in contrast to Dirac fields, the massive Majorana neutrino fields cannot "absorb" phases. In this case U can be cast in the form [54]

$$U = V\,P \tag{14.2}$$

where the matrix V contains the $(n-1)(n-2)/2$ Dirac CP violation phases, while P is a diagonal matrix with the additional $(n-1)$ Majorana CP violation phases $\alpha_{21}, \alpha_{31},...,\alpha_{n1}$,

$$P = diag\left(1, e^{i\frac{\alpha_{21}}{2}}, e^{i\frac{\alpha_{31}}{2}}, ..., e^{i\frac{\alpha_{n1}}{2}}\right). \tag{14.3}$$

The Majorana phases will conserve CP if [56] $\alpha_{j1} = \pi q_j$, $q_j = 0, 1, 2$, $j = 2, 3, ..., n$. In this case $\exp[i(\alpha_{j1} - \alpha_{k1})] = \pm 1$ has a simple physical interpretation: this is the relative CP-parity of Majorana neutrinos χ_j and χ_k. The condition of CP invariance of the leptonic CC weak interaction in the case of mixing and massive Majorana neutrinos reads [52]:

$$U_{lj}^* = U_{lj}\,\rho_j, \quad \rho_j = \frac{1}{i}\eta_{CP}(\chi_j) = \pm 1, \tag{14.4}$$

where $\eta_{CP}(\chi_j) = i\rho_j = \pm i$ is the CP parity of the Majorana neutrino χ_j [56]. Thus, if CP invariance holds, all elements of any given column of U are either real or purely imaginary.

In the case of $n = 3$ there are altogether 3 CP violation phases - one Dirac and two Majorana. Even in the mixing involving only 2 massive Majorana neutrinos there is one physical CP violation Majorana phase. In contrast, the CC weak interaction is automatically CP-invariant in the case of mixing of two massive Dirac neutrinos or of two quarks.

14.2.   The three neutrino mixing

All existing compelling data on neutrino oscillations can be described assuming 3-flavour neutrino mixing in vacuum. This is the minimal neutrino mixing scheme which can account for the currently available data on the oscillations of the solar (ν_e), atmospheric (ν_μ and $\bar{\nu}_\mu$), reactor ($\bar{\nu}_e$) and accelerator (ν_μ and $\bar{\nu}_\mu$) neutrinos. The (left-handed) fields of the flavour neutrinos ν_e, ν_μ and ν_τ in the expression for the weak charged lepton current in the CC weak interaction Lagrangian, are linear combinations of the LH components of the fields of three massive neutrinos ν_j:

$$\mathcal{L}_{\mathrm{CC}} = -\frac{g}{\sqrt{2}} \sum_{l=e,\mu,\tau} \overline{l_L}(x)\, \gamma_\alpha\, \nu_{lL}(x)\, W^{\alpha\dagger}(x) + h.c.\,,$$

$$\nu_{l\mathrm{L}}(x) = \sum_{j=1}^{3} U_{lj}\, \nu_{j\mathrm{L}}(x), \tag{14.5}$$

where U is the 3×3 unitary neutrino mixing matrix [4,5].   As we have discussed in the preceding Section, the mixing matrix U can be parameterized by 3 angles, and, depending on whether the massive neutrinos ν_j are Dirac or Majorana particles, by 1 or 3 CP violation phases [54,55]:

$$U = \begin{bmatrix} c_{12}c_{13} & s_{12}c_{13} & s_{13}e^{-i\delta} \\ -s_{12}c_{23} - c_{12}s_{23}s_{13}e^{i\delta} & c_{12}c_{23} - s_{12}s_{23}s_{13}e^{i\delta} & s_{23}c_{13} \\ s_{12}s_{23} - c_{12}c_{23}s_{13}e^{i\delta} & -c_{12}s_{23} - s_{12}c_{23}s_{13}e^{i\delta} & c_{23}c_{13} \end{bmatrix}$$

$$\times \operatorname{diag}(1,\ e^{i\frac{\alpha_{21}}{2}},\ e^{i\frac{\alpha_{31}}{2}})\ . \tag{14.6}$$

where $c_{ij} = \cos\theta_{ij}$, $s_{ij} = \sin\theta_{ij}$, the angles $\theta_{ij} = [0, \pi/2)$, $\delta = [0, 2\pi]$ is the Dirac CP violation phase and α_{21}, α_{31} are two Majorana CP violation (CPV) phases. Thus, in the case of massive Dirac neutrinos, the neutrino mixing matrix U is similar, in what concerns the number of mixing angles and CPV phases, to the CKM quark mixing matrix. The presence of two additional physical CPV phases in U if ν_j are Majorana particles is a consequence of the special properties of the latter (see, *e.g.*, Refs. [52,54]) .

As we see, the fundamental parameters characterizing the 3-neutrino mixing are: i) the 3 angles θ_{12}, θ_{23}, θ_{13}, ii) depending on the nature of massive neutrinos ν_j - 1 Dirac (δ), or 1 Dirac + 2 Majorana ($\delta, \alpha_{21}, \alpha_{31}$), CPV phases, and iii) the 3 neutrino masses, m_1, m_2, m_3. Thus, depending on whether the massive neutrinos are Dirac or Majorana particles, this makes 7 or 9 additional parameters in the minimally extended Standard Model of particle interactions with massive neutrinos.

The angles θ_{12}, θ_{23} and θ_{13} can be defined via the elements of the neutrino mixing matrix:

$$c_{12}^2 \equiv \cos^2\theta_{12} = \frac{|U_{e1}|^2}{1 - |U_{e3}|^2}\,, \quad s_{12}^2 \equiv \sin^2\theta_{12} = \frac{|U_{e2}|^2}{1 - |U_{e3}|^2}\,, \tag{14.7}$$

$$s_{13}^2 \equiv \sin^2\theta_{13} = |U_{e3}|^2,\ \ s_{23}^2 \equiv \sin^2\theta_{23} = \frac{|U_{\mu3}|^2}{1 - |U_{e3}|^2}\,,$$

$$c_{23}^2 \equiv \cos^2\theta_{23} = \frac{|U_{\tau3}|^2}{1 - |U_{e3}|^2}\,. \tag{14.8}$$

The neutrino oscillation probabilities depend (Section 14.7), in general, on the neutrino energy, E, the source-detector distance L, on the elements of U and, for relativistic neutrinos used in all neutrino experiments performed so far, on $\Delta m_{ij}^2 \equiv (m_i^2 - m_j^2)$, $i \neq j$. In the case of 3-neutrino mixing there are only two independent neutrino mass squared differences, say $\Delta m_{21}^2 \neq 0$ and $\Delta m_{31}^2 \neq 0$. The numbering of massive neutrinos ν_j is arbitrary. It proves convenient from the point of view of relating the mixing angles θ_{12}, θ_{23} and θ_{13} to observables, to identify $|\Delta m_{21}^2|$ with the smaller of the two neutrino mass squared differences, which, as it follows from the data, is responsible for the solar ν_e and, the observed by KamLAND, reactor $\bar{\nu}_e$ oscillations. We will number (just for convenience) the massive neutrinos in such a way that $m_1 < m_2$, so that $\Delta m_{21}^2 > 0$. With these choices made, there are two possibilities: either $m_1 < m_2 < m_3$, or $m_3 < m_1 < m_2$. Then the larger neutrino mass square difference $|\Delta m_{31}^2|$ or $|\Delta m_{32}^2|$, can be associated with the experimentally observed oscillations of the atmospheric and accelerator ν_μ and $\bar{\nu}_\mu$, as well as of the reactor $\bar{\nu}_e$ at $L \sim 1$ km. The effects of Δm_{31}^2 or Δm_{32}^2 in the oscillations of solar ν_e, and of Δm_{21}^2 in the oscillations of atmospheric and accelerator ν_μ and $\bar{\nu}_\mu$ or of the reactor $\bar{\nu}_e$ at $L \sim 1$ km, are relatively small and subdominant as a consequence of the facts that i) L, E and L/E in the experiments with solar ν_e and with atmospheric and accelerator ν_μ and $\bar{\nu}_\mu$, or with reactor $\bar{\nu}_e$ and baseline $L \sim 1$ km, are very different, ii) the conditions of production and propagation (on the way to the detector) of the solar ν_e and of the atmospheric or accelerator ν_μ and $\bar{\nu}_\mu$ and of the reactor $\bar{\nu}_e$, are very different, and iii) Δm_{21}^2 and $|\Delta m_{31}^2|$ ($|\Delta m_{32}^2|$) in the case of $m_1 < m_2 < m_3$ ($m_3 < m_1 < m_2$), as it follows from the data, differ by approximately a factor of 30, $\Delta m_{21}^2 \ll |\Delta m_{31(32)}^2|$, $\Delta m_{21}^2/|\Delta m_{31(32)}^2| \cong 0.03$. This implies that in both cases of $m_1 < m_2 < m_3$ and $m_3 < m_1 < m_2$ we have $\Delta m_{32}^2 \cong \Delta m_{31}^2$ with $|\Delta m_{31}^2 - \Delta m_{32}^2| = \Delta m_{21}^2 \ll |\Delta m_{31,32}^2|$. Obviously, in the case of $m_1 < m_2 < m_3$ ($m_3 < m_1 < m_2$) we have $\Delta m_{31(32)}^2 > 0$ ($\Delta m_{31(32)}^2 < 0$).

It followed from the results of the Chooz experiment [57] with reactor $\bar{\nu}_e$ and from the more recent data of the Daya Bay, RENO, Double Chooz and T2K experiments (which will be discussed in Section14.12), that, in the convention we use, in which $0 < \Delta m_{21}^2 < |\Delta m_{31(32)}^2|$, the element $|U_{e3}|=\sin\theta_{13}$ of the neutrino mixing matrix U is relatively small. This makes it possible to identify the angles θ_{12} and θ_{23} as the neutrino mixing angles associated with the solar ν_e and the dominant atmospheric ν_μ (and $\bar{\nu}_\mu$) oscillations, respectively. The angles θ_{12} and θ_{23} are sometimes called "solar" and "atmospheric" neutrino mixing angles, and are sometimes denoted as $\theta_{12} = \theta_\odot$ and $\theta_{23} = \theta_A$ (or θ_{atm}), while Δm_{21}^2 and Δm_{31}^2 are often referred to as the "solar" and "atmospheric" neutrino mass squared differences and are often denoted as $\Delta m_{21}^2 \equiv \Delta m_\odot^2$, $\Delta m_{31}^2 \equiv \Delta m_A^2$ (or Δm_{atm}^2).

The solar neutrino data tell us that $\Delta m_{21}^2 \cos 2\theta_{12} > 0$. In the convention employed by us we have $\Delta m_{21}^2 > 0$. Correspondingly, in this convention one must have $\cos 2\theta_{12} > 0$.

The enormous amount of neutrino oscillation data accumulated over many years of research allow us to determine the parameters which are responsible for the solar ν_e oscillations (flavour conversion), Δm_{21}^2 and $\sin^2\theta_{12}$, for the dominant oscillations of the

atmospheric ν_μ and $\bar{\nu}_\mu$, $|\Delta m^2_{31}|$ ($|\Delta m^2_{32}|$) and $\sin^2 \theta_{23}$, and the angle θ_{13} responsible for the $\nu_\mu \rightarrow \nu_e$ and $\bar{\nu}_\mu \rightarrow \bar{\nu}_e$ ($\nu_\mu \rightarrow \nu_e$) oscillations observed in the T2K (NOνA) experiment as well as for the reactor $\bar{\nu}_e$ oscillations observed in the Daya Bay, RENO and Double Chooz experiments. In the two most recent global analyses of the neutrino oscillation data [58,59] the indicated 3-neutrino oscillation parameters Δm^2_{21}, θ_{12}, $|\Delta m^2_{31}|$ ($|\Delta m^2_{32}|$), θ_{23} and θ_{13} have been determined with an impressively high precision. The new data included in these analyses were, in particular, the latest T2K $\bar{\nu}_\mu \rightarrow \bar{\nu}_e$ oscillation data [43] and the latest NOνA data on ν_μ disappearance [60] and $\nu_\mu \rightarrow \nu_e$ oscillations [42], reported first at the XXVII International Conference on Neutrino Physics and Astrophysics, held in London at the beginning of July 2016, and published at the beginning of 2017. The authors of the two independent analyses [58,59] report practically the same (within 1σ) results on Δm^2_{21}, $\sin^2 \theta_{12}$, $|\Delta m^2_{31}|$, $\sin^2 \theta_{13}$, $\sin^2 \theta_{23}$ and δ. We present in Table 14.1 the best fit values and the 99.73% confidence level (CL) allowed ranges of the neutrino oscillation parameters, as well as the 95% CL allowed range of the CP violation phases δ, found in Ref. 58.

In both analyses [58,59] the authors find, in particular, that $\sin^2 \theta_{23} = 0.5$ lies outside the 2σ range allowed by the current data. This results is mainly driven by the NOνA data [60] on $\sin^2 \theta_{23}$. Both groups also find that the best fit value of the Dirac CPV phases δ is close to $3\pi/2$: in [58], for example, the values found are $\delta = 1.38\pi$ (1.31π) for $\Delta m^2_{31(32)} > 0$ ($\Delta m^2_{31(32)} < 0$). The absolute χ^2 minimum takes place for $\Delta m^2_{31(32)} > 0$, the local minimum in the case of $\Delta m^2_{31(32)} < 0$ being approximately by 0.7σ higher. According to Ref. 58, the CP conserving values $\delta = 0$ or 2π are disfavored at 2.4σ (3.2σ) for $\Delta m^2_{31(32)} > 0$ ($\Delta m^2_{31(32)} < 0$); the CP conserving value $\delta = \pi$ in the case of $\Delta m^2_{31(32)} > 0$ ($\Delta m^2_{31(32)} < 0$) is statistically approximately 2.0σ (2.5σ) away from the best fit value $\delta \cong 1.38\pi$ (1.31π). In what concerns the CP violating value $\delta = \pi/2$, it is strongly disfavored at 3.4σ (3.9σ) for $\Delta m^2_{31(32)} > 0$ ($\Delta m^2_{31(32)} < 0$). The quoted confidence levels for $\delta = 0, \pi$ and $\pi/2$ are all with respect to the absolute χ^2 minimum. At 3σ, δ/π is found to lie in the case of $\Delta m^2_{31(32)} > 0$ ($\Delta m^2_{31(32)} < 0$) in the following intervals [58]: $(0.00 - 0.17(0.16)) \oplus (0.76(0.69) - 2.00))$. Similar results are obtained in [59].

It follows from the results given in Table 14.1 that the value of θ_{23} can deviate by about ± 0.1 from $\pi/4$, $\pi/4$ belonging to the 3σ allowed region, $\theta_{12} \cong \pi/5.4$ and that $\theta_{13} \cong \pi/20$. Correspondingly, the pattern of neutrino mixing is drastically different from the pattern of quark mixing.

Note also that Δm^2_{21}, $\sin^2 \theta_{12}$, $|\Delta m^2_{31(32)}|$, $\sin^2 \theta_{23}$ and $\sin^2 \theta_{13}$ are determined from the data with a 1σ uncertainty (= $1/6$ of the 3σ range) of approximately 2.3%, 5.8%, 1.6%, 9.6% and 4.0%, respectively.

Further, the existing SK atmospheric neutrino, K2K, MINOS, T2K and NOνA data do not allow to determine the sign of $\Delta m^2_{31(32)}$. Maximal solar neutrino mixing, *i.e.*, $\theta_{12} = \pi/4$, is ruled out at more than 6σ by the data. Correspondingly, one has $\cos 2\theta_{12} \geq 0.29$ (at 99.73% CL).

Apart from the hint that the Dirac phase $\delta \cong 3\pi/2$, no other experimental information

Table 14.1: The best-fit values and 3σ allowed ranges of the 3-neutrino oscillation parameters, derived from a global fit of the current neutrino oscillation data (from [58]) . For the Dirac phase δ we give the best fit value and the 2σ allowed range. The values (values in brackets) correspond to $m_1 < m_2 < m_3$ ($m_3 < m_1 < m_2$). The definition of Δm^2, which is determined in the global analysis in [58] is: $\Delta m^2 = m_3^2 - (m_2^2 + m_1^2)/2$. Thus, $\Delta m^2 = \Delta m_{31}^2 - \Delta m_{21}^2/2 > 0$, if $m_1 < m_2 < m_3$, and $\Delta m^2 = \Delta m_{32}^2 + \Delta m_{21}^2/2 < 0$ for $m_3 < m_1 < m_2$. We give the values of $\Delta m_{31}^2 > 0$ for $m_1 < m_2 < m_3$, and of Δm_{23}^2 for $m_3 < m_1 < m_2$, obtained from those for Δm^2 quoted in [58].

Parameter	best-fit	3σ
Δm_{21}^2 [10^{-5} eV ^{2}]	7.37	$6.93 - 7.96$
$\Delta m_{31(23)}^2$ [10^{-3} eV ^{2}]	2.56 (2.54)	$2.45 - 2.69$ $(2.42 - 2.66)$
$\sin^2 \theta_{12}$	0.297	$0.250 - 0.354$
$\sin^2 \theta_{23}, \Delta m_{31(32)}^2 > 0$	0.425	$0.381 - 0.615$
$\sin^2 \theta_{23}, \Delta m_{32(31)}^2 < 0$	0.589	$0.384 - 0.636$
$\sin^2 \theta_{13}, \Delta m_{31(32)}^2 > 0$	0.0215	$0.0190 - 0.0240$
$\sin^2 \theta_{13}, \Delta m_{32(31)}^2 < 0$	0.0216	$0.0190 - 0.0242$
δ/π	1.38 (1.31)	2σ: (1.0 - 1.9)
		$(2\sigma$: (0.92-1.88))

on the Dirac and Majorana CPV phases in the neutrino mixing matrix is available at present. Thus, the status of CP symmetry in the lepton sector is essentially unknown. With $\theta_{13} \cong 0.15 \neq 0$, the Dirac phase δ can generate CP violating effects in neutrino oscillations [54,61,62], *i.e.*, a difference between the probabilities of the $\nu_l \to \nu_{l'}$ and $\bar{\nu}_l \to \bar{\nu}_{l'}$ oscillations, $l \neq l' = e, \mu, \tau$. The magnitude of CP violation in $\nu_l \to \nu_{l'}$ and $\bar{\nu}_l \to \bar{\nu}_{l'}$ oscillations, $l \neq l' = e, \mu, \tau$, is determined by [63] the rephasing invariant J_{CP}, associated with the Dirac CPV phase in U:

$$J_{\mathrm{CP}} = \mathrm{Im}\left(U_{\mu 3}\, U_{e3}^*\, U_{e2}\, U_{\mu 2}^* \right) . \tag{14.9}$$

It is analogous to the rephasing invariant associated with the Dirac CPV phase in the CKM quark mixing matrix [64]. In the "standard" parametrization of the neutrino mixing matrix (Eq. (14.6)), J_{CP} has the form:

$$J_{CP} \equiv \mathrm{Im}\left(U_{\mu 3}\, U_{e3}^*\, U_{e2}\, U_{\mu 2}^* \right) = \frac{1}{8}\, \cos\theta_{13} \sin 2\theta_{12} \sin 2\theta_{23} \sin 2\theta_{13} \sin\delta . \tag{14.10}$$

Thus, given the fact that $\sin 2\theta_{12}$, $\sin 2\theta_{23}$ and $\sin 2\theta_{13}$ have been determined experimentally with a relatively good precision, the size of CP violation effects in

neutrino oscillations depends essentially only on the magnitude of the currently not well determined value of the Dirac phase δ. The current data implies $0.026(0.027)|\sin\delta| \lesssim |J_{CP}| \lesssim 0.035|\sin\delta|$, where we have used the 3σ ranges of $\sin^2\theta_{12}$, $\sin^2\theta_{23}$ and $\sin^2\theta_{13}$ given in Table 14.1. For the current best fit values of $\sin^2\theta_{12}$, $\sin^2\theta_{23}$, $\sin^2\theta_{13}$ and δ we find in the case of $\Delta m^2_{31(2)} > 0$ ($\Delta m^2_{31(2)} < 0$): $J_{CP} \cong 0.032\sin\delta \cong -0.030$ ($J_{CP} \cong 0.032\sin\delta \cong -0.027$). Thus, if the indication that δ has a value close to $3\pi/2$ is confirmed by future more precise data, i) the $J_{CP}-$ factor in the lepton sector would be approximately by 3 orders of magnitude larger in absolute value than corresponding $J_{CP}-$ factor in the quark sector, and ii) the CP violation effects in neutrino oscillations would be relatively large.

If the neutrinos with definite masses ν_i, $i = 1, 2, 3$, are Majorana particles, the 3-neutrino mixing matrix contains two additional Majorana CPV phases [54]. However, the flavour neutrino oscillation probabilities $P(\nu_l \to \nu_{l'})$ and $P(\bar{\nu}_l \to \bar{\nu}_{l'})$, $l, l' = e, \mu, \tau$, do not depend on the Majorana phases [54,65]. The Majorana phases can play important role, e.g., in $|\Delta L| = 2$ processes like neutrinoless double beta $((\beta\beta)_{0\nu}-)$ decay $(A, Z) \to (A, Z + 2) + e^- + e^-$, L being the total lepton charge, in which the Majorana nature of massive neutrinos ν_i manifests itself (see, e.g., Refs. [52,66]) . Our interest in the CPV phases present in the neutrino mixing matrix is stimulated also by the intriguing possibility that the Dirac phase and/or the Majorana phases in U_{PMNS} can provide the CP violation necessary for the generation of the observed baryon asymmetry of the Universe [67,68].

As we have indicated, the existing data do not allow one to determine the sign of $\Delta m^2_{31(32)}$. In the case of 3-neutrino mixing, the two possible signs of $\Delta m^2_{31(32)}$ correspond to two types of neutrino mass spectrum. In the widely used conventions of numbering the neutrinos with definite mass in the two cases employed by us, the two spectra read:

  – *i) spectrum with normal ordering (NO)*:

$$m_1 < m_2 < m_3, \quad \Delta m^2_{31} = \Delta m^2_{\mathrm{A}} > 0,$$

$$\Delta m^2_{21} \equiv \Delta m^2_{\odot} > 0, \;\; m_{2(3)} = (m_1^2 + \Delta m^2_{21(31)})^{\frac{1}{2}}. \tag{14.11}$$

  – *ii) spectrum with inverted ordering (IO)*:

$$m_3 < m_1 < m_2, \quad \Delta m^2_{32} = \Delta m^2_{\mathrm{A}} < 0, \quad \Delta m^2_{21} \equiv \Delta m^2_{\odot} > 0,$$

$$m_2 = (m_3^2 + \Delta m^2_{23})^{\frac{1}{2}}, \quad m_1 = (m_3^2 + \Delta m^2_{23} - \Delta m^2_{21})^{\frac{1}{2}}. \tag{14.12}$$

Depending on the values of the lightest neutrino mass [69], $\min(m_j)$, the neutrino mass spectrum can be:

  – *Normal Hierarchical (NH)*:

$$m_1 \ll m_2 < m_3, \;\; m_2 \cong (\Delta m^2_{21})^{\frac{1}{2}} \cong 0.0086 \text{ eV},$$

$$m_3 \cong |\Delta m^2_{31}|^{\frac{1}{2}} \cong 0.0506 \text{ eV}; \text{ or} \tag{14.13}$$

– *Inverted Hierarchical (IH)*:

$$m_3 \ll m_1 < m_2, \ \ m_1 \cong (|\Delta m_{32}^2| - \Delta m_{21}^2)^{\frac{1}{2}} \cong 0.0497 \ \text{eV},$$
$$m_2 \cong |\Delta m_{32}^2|^{\frac{1}{2}} \cong 0.0504 \ \text{eV}; \ \ \text{or} \tag{14.14}$$

– *Quasi-Degenerate (QD)*:

$$m_1 \cong m_2 \cong m_3 \cong m_0, \ \ m_j^2 \gg |\Delta m_{31(32)}^2|, \ \ m_0 \gtrsim 0.10 \ \text{eV}. \tag{14.15}$$

Sometimes the determination of the neutrino mass spectrum is referred to in the literature on the subject as determination of "neutrino mass hierarchy". However, as we have seen, the neutrino mass spectrum might not be hierarchical. Therefore, determination of "neutrino mass ordering" is a more precise expression and we are going to use this expression in the present review article.

Eq. (14.11) and Eq. (14.12) suggest that, for consistency, the data on the larger neutrino mass squared difference, obtained in 3-neutrino oscillation analyses, should be presented i) either on the value of Δm_{32}^2 in the case of NO spectrum and on Δm_{31}^2 for IO spectrum, or ii) on the value of Δm_{31}^2 for the NO spectrum and on Δm_{32}^2 for IO spectrum. It would be preferable that all experimental groups which provide data on the larger neutrino mass squared difference, choose one of the indicated two possibilities to present their data - this will make straightforward the comparison of the results obtained in different experiments.

All types of neutrino mass spectrum, discussed above, are compatible with the existing constraints on the absolute scale of neutrino masses m_j. Information about the latter can be obtained, *e.g.*, by measuring the spectrum of electrons near the end point in ^{3}H β-decay experiments [70–74] and from cosmological and astrophysical data. The most stringent upper bounds on the $\bar{\nu}_e$ mass were obtained in the Troitzk [74,71] experiment:

$$m_{\bar{\nu}_e} < 2.05 \ \text{eV} \quad \text{at} \ 95\% \ \text{CL}. \tag{14.16}$$

Similar result was obtained in the Mainz experiment [72]: $m_{\bar{\nu}_e} < 2.3$ eV at 95% CL. We have $m_{\bar{\nu}_e} \cong m_{1,2,3}$ in the case of QD spectrum. The upcoming KATRIN experiment [73] is planned to reach sensitivity of $m_{\bar{\nu}_e} \sim 0.20$ eV, *i.e.*, it will probe the region of the QD spectrum.

The Cosmic Microwave Background (CMB) data of the WMAP and PLANCK experiments, combined with supernovae and other cosmological and astrophysical data can be used to obtain an upper limit on the sum of neutrinos masses (see review on "Neutrinos in Cosmology", Section 25 [75], and, *e.g.*, Ref. 76). Depending on the model complexity and the input data used one typically obtains [76]: $\sum_j m_j \lesssim (0.3 - 1.3)$ eV, 95% CL.

In March of 2013 the Planck Collaboration published their first constraints on $\sum_j m_j$ [77]. These constraints were updated in 2016 in [78]. Assuming the existence of three light massive neutrinos and the validity of the Λ CDM (Cold Dark Matter) model, and

using their data on the CMB temperature power spectrum anisotropies, polarization, on gravitational lensing effects, the low l CMB polarization spectrum data (the "low P" data), etc. the Planck Collaboration reported the updated upper limit on the sum of the neutrino masses [78], which, depending on the data-set used, varies in the interval: $\sum_j m_j < (0.340 - 0.715)$ eV, 95% CL. Adding data on the Baryon Acoustic Oscillations (BAO) lowers the limit to [78]:

$$\sum_j m_j < 0.170 \ eV, \quad 95\% \ CL.$$

The quoted cosmological bound on the sum of neutrino masses might not be valid if, e.g., the neutrino masses are generated dynamically at certain relatively late epoch in the evolution of the Universe (see, e.g., Ref. [79]) .

It follows from these data that neutrino masses are much smaller than the masses of charged leptons and quarks. If we take as an indicative upper limit $m_j \lesssim 0.5$ eV, we have $m_j/m_{l,q} \lesssim 10^{-6}$, $l = e, \mu, \tau$, $q = d, s, b, u, c, t$. It is natural to suppose that the remarkable smallness of neutrino masses is related to the existence of a new fundamental mass scale in particle physics, and thus to new physics beyond that predicted by the Standard Model.

14.3. Future progress

After the spectacular experimental progress made in the studies of neutrino oscillations, further understanding of the pattern of neutrino masses and neutrino mixing, of their origins and of the status of CP symmetry in the lepton sector requires an extensive and challenging program of research. The main goals of such a research program include:

- Determining the nature - Dirac or Majorana, of massive neutrinos ν_j. This is of fundamental importance for making progress in our understanding of the origin of neutrino masses and mixing and of the symmetries governing the lepton sector of particle interactions.
- Determination of the sign of Δm_{31}^2 (or Δm_{32}^2), *i.e.*, the "neutrino mass ordering", or of the type of spectrum neutrino masses obey.
- Determining, or obtaining significant constraints on, the absolute scale of neutrino masses. This, in particular, would help obtain information about the detailed structure (hierarchical, quasidegenerate, etc.) of the neutrino mass spectrum.
- Determining the status of CP symmetry in the lepton sector.
- High precision measurement of θ_{13}, Δm_{21}^2, θ_{12}, $|\Delta m_{31}^2|$ and θ_{23}.
- Understanding at a fundamental level the mechanism giving rise to neutrino masses and mixing and to L_l-non-conservation. This includes understanding the origin of the patterns of ν-mixing and ν-masses suggested by the data. Are the observed patterns of ν-mixing and of $\Delta m_{21,31}^2$ related to the existence of a new fundamental symmetry of particle interactions? Is there any relation between quark mixing and neutrino mixing? What is the physical origin of CP violation phases in the neutrino

mixing matrix U? Is there any relation (correlation) between the (values of) CP violation phases and mixing angles in U? Progress in the theory of neutrino mixing might also lead to a better understanding of the mechanism of generation of baryon asymmetry of the Universe.

The high precision measurement of the value of $\sin^2 2\theta_{13}$ from the Daya Bay experiment and the subsequent results on θ_{13} obtained by the RENO, Double Chooz and T2K collaborations (see Section 1.11), have far reaching implications. The measured relatively large value of θ_{13} opened up the possibilities, in particular,

i) for searching for CP violation effects in neutrino oscillation experiments with high intensity accelerator neutrino beams, like T2K, NOνA, etc. (the sensitivities of T2K and NOνA on CP violation in neutrino oscillations are discussed in, *e.g.*, Refs. [80,81]) ; ii) for determining the sign of Δm^2_{32}, and thus the type of neutrino mass spectrum ("neutrino mass ordering") in the long baseline neutrino oscillation experiments at accelerators (NOνA, etc.), in the experiments studying the oscillations of atmospheric neutrinos (PINGU [82], ORCA [83,84], Hyper-Kamiokande [200], INO [85]) , as well as in experiments with reactor antineutrinos [86–91](for reviews see, *e.g.*, Ref. 92).

There are also long term plans extending beyond 2025 for searches for CP violation and neutrino mass spectrum (ordering) determination in long baseline neutrino oscillation experiments with accelerator neutrino beams (see, *e.g.*, Refs. [93,94]) . The successful realization of this research program would be a formidable task and would require many years of extraordinary experimental efforts aided by intensive theoretical investigations and remarkable investments.

Before reviewing in detail i) the different neutrino sources and the specific characteristics of the corresponding neutrino fluxes, which have been and are being used in neutrino oscillation experiments (Section 14.6), ii) the theory and phenomenology of neutrino oscillations (Sections 14.7 and 14.8), and iii) the compelling experimental evidences of neutrino oscillations and, more generally, the results obtained in the neutrino oscillation experiments (Sections 14.9 – 14.14), we would like to discuss briefly the problem of determination of the nature - Dirac or Majorana - of massive neutrinos as well as the (type I) seesaw mechanism of neutrino mass generation.

14.4. The nature of massive neutrinos

The experiments studying flavour neutrino oscillations cannot provide information on the nature - Dirac or Majorana, of massive neutrinos [54,65]. Establishing whether the neutrinos with definite mass ν_j are Dirac fermions possessing distinct antiparticles, or Majorana fermions, *i.e.*, spin 1/2 particles that are identical with their antiparticles, is of fundamental importance for understanding the origin of ν-masses and mixing and the underlying symmetries of particle interactions (see, *e.g.*, Ref. 95). The neutrinos with definite mass ν_j will be Dirac fermions if the particle interactions conserve some additive lepton number, *e.g.*, the total lepton charge $L = L_e + L_\mu + L_\tau$. If no lepton charge is conserved, ν_j will be Majorana fermions (see, *e.g.*, Refs. [52,53]) . The massive

neutrinos are predicted to be of Majorana nature by the see-saw mechanism of neutrino mass generation [3]. The observed patterns of neutrino mixing and of neutrino mass squared differences can be related to Majorana massive neutrinos and the existence of an approximate flavour symmetry in the lepton sector (see, *e.g.*, Ref. 96). Determining the nature of massive neutrinos ν_j is one of the fundamental and most challenging problems in the future studies of neutrino mixing.
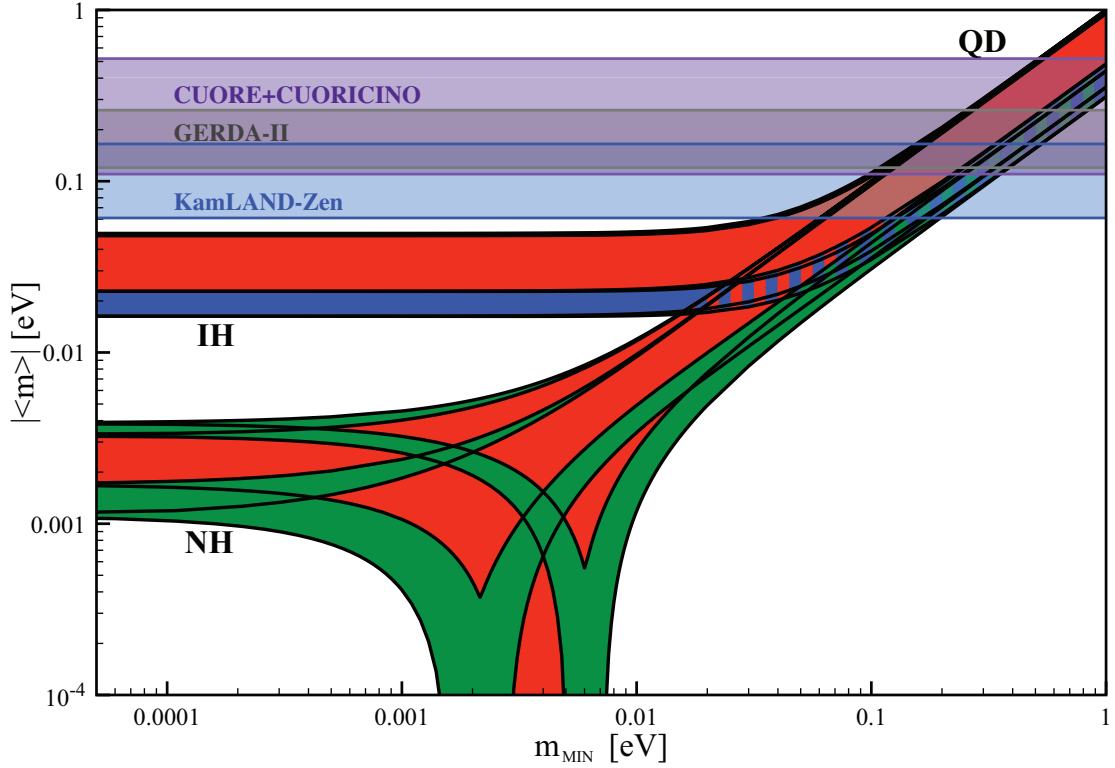

Figure 14.1:   The effective Majorana mass $|<m>|$ (including a 2σ uncertainty), as a function of $\min(m_j)$. The figure is obtained using the best fit values and the 1σ ranges of allowed values of Δm^2_{21}, $\sin^2\theta_{12}$, $\sin^2\theta_{13}$ and $|\Delta m^2_{31(32)}|$ from Ref. 58 (see Table 14.1), propagated to $|<m>|$ and then taking a 2σ uncertainty. The phases α_{21} and $(\alpha_{31} - 2\delta)$ are varied in the interval $[0,2\pi]$. The predictions for the NH, IH and QD spectra as well as the GERDA-II, KamLAND-Zen and the combined CUORE+CUORICINO limits, Eq. (14.20) and Eq. (14.21), are indicated. The black lines determine the ranges of values of $|<m>|$ for the different pairs of CP conserving values of α_{21} and $(\alpha_{31} - 2\delta)$: $(0, 0)$, $(0, \pi)$, $(\pi, 0)$ and (π, π). The red regions correspond to at least one of the phases α_{21} and $(\alpha_{31} - 2\delta)$ having a CP violating value, while the blue and green areas correspond to α_{21} and $(\alpha_{31} - 2\delta)$ possessing CP conserving values. (Update by S. Pascoli of a figure from Ref. 112.)

The Majorana nature of massive neutrinos ν_j manifests itself in the existence of processes in which the total lepton charge L changes by two units: $K^+ \rightarrow \pi^- + \mu^+ + \mu^+$, $\mu^- + (A, Z) \rightarrow \mu^+ + (A, Z - 2)$, *etc.* Extensive studies have shown that the only

feasible experiments having the potential of establishing that the massive neutrinos are Majorana particles are at present the experiments searching for $(\beta\beta)_{0\nu}$-decay: $(A, Z) \rightarrow (A, Z + 2) + e^- + e^-$ (see, *e.g.*, [97–99]) . The observation of $(\beta\beta)_{0\nu}$-decay and the measurement of the corresponding half-life with sufficient accuracy, would not only be a proof that the total lepton charge is not conserved, but might also provide unique information on the i) type of neutrino mass spectrum [102], ii) Majorana phases in U [66,103] and iii) the absolute scale of neutrino masses (for details see [98–104] and references quoted therein).

Under the assumptions of 3-ν mixing, of massive neutrinos ν_j being Majorana particles, and of $(\beta\beta)_{0\nu}$-decay generated only by the (V-A) charged current weak interaction via the exchange of the three Majorana neutrinos ν_j having masses $m_j \lesssim$ few MeV, the $(\beta\beta)_{0\nu}$-decay amplitude has the form (see, *e.g.*, Refs. [52,99]) : $A(\beta\beta)_{0\nu} \cong G_F^2 <m> M(A, Z)$, where G_F is the Fermi coupling constant, $M(A, Z)$ is the corresponding nuclear matrix element (NME) which does not depend on the neutrino mixing parameters, and

$$|<m>| = \left| m_1 U_{e1}^2 + m_2 U_{e2}^2 + m_3 U_{e3}^2 \right|$$
$$= \left| \left(m_1 c_{12}^2 + m_2 s_{12}^2 e^{i\alpha_{21}} \right) c_{13}^2 + m_3 s_{13}^2 e^{i(\alpha_{31} - 2\delta)} \right|, \qquad (14.17)$$

is the effective Majorana mass in $(\beta\beta)_{0\nu}$-decay. In the case of CP-invariance one has [56], $\eta_{21} \equiv e^{i\alpha_{21}} = \pm 1$, $\eta_{31} \equiv e^{i\alpha_{31}} = \pm 1$, $e^{-i2\delta} = 1$. The three neutrino masses $m_{1,2,3}$ can be expressed in terms of the two measured Δm_{jk}^2 and, *e.g.*, $\min(m_j)$. Thus, given the neutrino oscillation parameters Δm_{21}^2, $\sin^2\theta_{12}$, Δm_{31}^2 and $\sin^2\theta_{13}$, $|<m>|$ is a function of the lightest neutrino mass $\min(m_j)$, the type of neutrino mass spectrum, the Majorana phase α_{21}, and – in the standard parametrisation of the neutrino mixing matrix U – of the Majorana-Dirac phase difference $(\alpha_{31} - 2\delta)$. In the case of NH, IH and QD spectrum we have (see, *e.g.*, Ref. 66 and Ref. 104):

$$|<m>| \cong \left| \sqrt{\Delta m_{21}^2} s_{12}^2 c_{13}^2 + \sqrt{\Delta m_{31}^2} s_{13}^2 e^{i(\alpha_{31} - \alpha_{21} - 2\delta)} \right|, \quad \text{NH}, \qquad (14.18)$$

$$|<m>| \cong \tilde{m} \left(1 - \sin^2 2\theta_{12} \sin^2 \frac{\alpha_{21}}{2} \right)^{\frac{1}{2}}, \quad \text{IH (IO) and QD}, \qquad (14.19)$$

where $\tilde{m} \equiv \sqrt{\Delta m_{23}^2}$ $(\tilde{m} \equiv \sqrt{\Delta m_{23}^2 + m_3^2})$ and $\tilde{m} \equiv m_0$ for IH (IO) and QD spectrum, respectively. In Eq. (14.19) we have exploited the fact that $\sin^2\theta_{13} \ll \cos 2\theta_{12}$. The CP conserving values of the Majorana phase α_{21} and the Majorana-Dirac phase difference $(\alpha_{31} - \alpha_{21} - 2\delta)$ determine the intervals of possible values of $|<m>|$, corresponding to the different types of neutrino mass spectrum. Using the 3σ ranges of the allowed values of the neutrino oscillation parameters from Table 14.1 one finds that: i) 0.78×10^{-3} eV $\lesssim |<m>| \lesssim 4.32 \times 10^{-3}$ eV in the case of NH spectrum; ii) $\sqrt{\Delta m_{23}^2} \cos 2\theta_{12} \, c_{13}^2 \lesssim |<m>| \lesssim \sqrt{\Delta m_{23}^2} \, c_{13}^2$, or 1.4×10^{-2} eV $\lesssim |<m>| \lesssim 5.1 \times 10^{-2}$ eV in the case of IH spectrum; iii) $m_0 \cos 2\theta_{12} \lesssim |<m>| \lesssim m_0$, or 2.9×10^{-2} eV $\lesssim |<m>| \lesssim m_0$

eV, $m_0 \gtrsim 0.10$ eV, in the case of QD spectrum. The difference in the ranges of $|\!<\!m\!>\!|$ in the cases of NH, IH and QD spectrum opens up the possibility to get information about the type of neutrino mass spectrum from a measurement of $|\!<\!m\!>\!|$ [102]. The predicted $(\beta\beta)_{0\nu}$-decay effective Majorana mass $|\!<\!m\!>\!|$ as a function of the lightest neutrino mass $\min(m_j)$ is shown in Fig. 14.1.

The experimental searches for $(\beta\beta)_{0\nu}$-decay have a long history (see, *e.g.*, [105]) . The current best limits on $|\!<\!m\!>\!|$ have been obtained by the KamLAND-Zen [106] and GERDA phase II [107] experiments searching for $(\beta\beta)_{0\nu}$-decay of ^{136}Xe and ^{76}Ge, respectively:

$$|\!<\!m\!>\!| < (0.061 - 0.165)eV \,, \quad ^{136}\text{Xe} \quad \text{and} \quad |\!<\!m\!>\!| < (0.12 - 0.26)eV \,, \quad ^{76}\text{Ge}. \quad (14.20)$$

both at 90% CL. The intervals reflect the estimated uncertainties in the relevant NMEs used to extract the limits on $|\!<\!m\!>\!|$ from the experimentally obtained lower bounds on the ^{136}Xe and ^{76}Ge $(\beta\beta)_{0\nu}$-decay half-lives, $T_{1/2}^{0\nu}(^{136}\text{Xe}) > 1.07 \times 10^{26}$yr (90% CL) [106], $T_{1/2}^{0\nu}(^{76}\text{Ge}) > 8.0 \times 10^{25}$yr (90% CL) [107]. (For a review of the limits on $|\!<\!m\!>\!|$ obtained in other $(\beta\beta)_{0\nu}$-decay experiments and a detailed discussion of the NME calculations for $(\beta\beta)_{0\nu}$-decay and their uncertainties see, *e.g.*, Ref. 99.) In October 2017 the first results of the CUORE experiment searching for $(\beta\beta)_{0\nu}$-decay of ^{130}Te were published [108]. In this experiment the following lower limit of the half-live of ^{130}Te was obtained: $T_{1/2}^{0\nu}(^{130}\text{Te}) > 1.3 \times 10^{25}$yr (90% CL). Combining this limit with the limits on $T_{1/2}^{0\nu}(^{130}\text{Te})$ obtained earlier in the Cuoricino [109] and CUORE-0 [110] experiments leads to [108] $T_{1/2}^{0\nu}(^{130}\text{Te}) > 1.5 \times 10^{25}$yr (90% CL). Taking into account the estimated uncertainties in the relevant NMEs of the process, the following upper limit on $|\!<\!m\!>\!|$ was reported in [108]:

$$|\!<\!m\!>\!| < (0.11 - 0.52)eV \,, \quad ^{130}\text{Te}. \quad (14.21)$$

The "conservative" upper limit $|\!<\!m\!>\!|_{exp}^{max} = 0.165$ eV, which is in the range of the QD spectrum, implies, as it is not difficult to show, the following upper limit on the absolute Majorana neutrino mass scale: $m_0 \cong m_{1,2,3} \lesssim |\!<\!m\!>\!|_{exp}^{max} / \cos 2\theta_{12} \lesssim 0.57$ eV.

A large number of experiments of a new generation aims at a sensitivity to $|\!<\!m\!>\!| \sim (0.01 - 0.05)$ eV, which will allow to probe the whole range of the predictions for $|\!<\!m\!>\!|$ in the case of IO neutrino mass spectrum [102] (see, *e.g.*, Refs. [98,99,100] for reviews of the currently running and future planned $(\beta\beta)_{0\nu}$-decay experiments and their prospective sensitivities).

Obtaining quantitative information on the neutrino mixing parameters from a measurement of $(\beta\beta)_{0\nu}$-decay half-life would be impossible without sufficiently precise knowledge of the corresponding NME of the process. At present the variation of the values of the different $(\beta\beta)_{0\nu}$-decay NMEs calculated using the various currently employed methods is typically by factors $\sim (2 - 3)$ (for a discussion of the current status of the calculations of the NMEs for the $(\beta\beta)_{0\nu}$-decay see [99]) . Additional source of uncertainty is the effective value of the axial-vector coupling constant g_A in $(\beta\beta)_{0\nu}$-decay. This constant is renormalized by nuclear medium effects, which tend to quench, i.e., reduce,

the vacuum value of g_A. The problem of the g_A quenching arose in connection with the efforts to describe theoretically the experimental data on the two-neutrino double beta decay [101]. The physical origin of the quenching is not fully understood, and the magnitude of the quenching of g_A in $(\beta\beta)_{0\nu}$-decay is subject to debates (for further details see, e.g., [99]) . The importance of the effective value of g_A in $(\beta\beta)_{0\nu}$-decay stems from the fact that, to a good approximation, the $(\beta\beta)_{0\nu}$-decay rate is proportional to the fourth power of the effective g_A.

The observation of $(\beta\beta)_{0\nu}$-decay of one nucleus is likely to lead to the searches and observation of the decay of other nuclei. The data on the $(\beta\beta)_{0\nu}$-decay of several nuclei might help to reduce the uncertainties in the calculations of the $(\beta\beta)_{0\nu}$-decay NMEs (see, *e.g.*, [111]) .

If the future $(\beta\beta)_{0\nu}$-decay experiments show that $|<m>| < 0.01$ eV, both the IH and the QD spectrum will be ruled out for massive Majorana neutrinos. If in addition it is established in neutrino oscillation experiments that $\Delta m^2_{31(32)} < 0$ (IO spectrum), one would be led to conclude that either the massive neutrinos ν_j are Dirac fermions, or that ν_j are Majorana particles but there are additional contributions to the $(\beta\beta)_{0\nu}$-decay amplitude which interfere destructively with that due to the exchange of ν_j. If, however, $\Delta m^2_{31(32)}$ is determined to be positive, the upper limit $|<m>| < 0.01$ eV would be perfectly compatible with massive Majorana neutrinos possessing NH mass spectrum, or NO spectrum with partial hierarchy, and the quest for $|<m>|$ would still be open (see, *e.g.*, Ref. 112).

The $(\beta\beta)_{0\nu}$-decay can be generated, in principle, by a $\Delta L = 2$ mechanism other than the light Majorana neutrino exchange considered here, or by a combination of mechanisms one of which is the light Majorana neutrino exchange (for a discussion of different mechanisms which can trigger $(\beta\beta)_{0\nu}$-decay, see, *e.g.*, Refs. [113,114] and the articles quoted therein). Actually, the predictions for $|<m>|$ in the cases of the NH, IH and QD neutrino mass spectra can be drastically modified by the existence of lepton charge non-conserving ($|\Delta L| = 2$) new physics beyond that predicted by the SM: eV or GeV to TeV scale sterile neutrinos, etc. (see, *e.g.*, Refs. [115,116]) . There is a potential synergy between the searches for $(\beta\beta)_{0\nu}$-decay and the searches for neutrino-related $|\Delta L| = 2$ beyond the SM physics at LHC: $(\beta\beta)_{0\nu}$-decay experiments with a sensitivity to half-lives of $T^{0\nu}_{1/2} = 10^{25}$ yr probe approximately values of $|<m>| \sim 0.1$ eV and "new physics" at the scale $\Lambda_{LNV} \sim 1$ TeV (see, *e.g.*, Ref. [116] and references quoted therein).

If the $(\beta\beta)_{0\nu}$-decay will be observed, it will be of fundamental importance to determine which mechanism (or mechanisms) is (are) inducing the decay. The discussion of the problem of determining the mechanisms which possibly are operative in $(\beta\beta)_{0\nu}$-decay, including the case when more than one mechanism is involved, is out of the scope of the present article. This problem has been investigated in detail in, *e.g.*, Refs. [114,117] and we refer the reader to these articles and the articles quoted therein.

14.5. The see-saw mechanism and the baryon asymmetry of the Universe

A natural explanation of the smallness of neutrino masses is provided by the (type I) see-saw mechanism of neutrino mass generation [3]. An integral part of this rather simple mechanism [118] are the RH neutrinos ν_{lR} (RH neutrino fields $\nu_{lR}(x)$). The latter are assumed to possess a Majorana mass term as well as Yukawa type coupling $\mathcal{L}_Y(x)$ with the Standard Model lepton and Higgs doublets, $\psi_{lL}(x)$ and $\Phi(x)$, respectively, $(\psi_{lL}(x))^T = (\nu_{lL}^T(x) \quad l_L^T(x))$, $l = e, \mu, \tau$, $(\Phi(x))^T = (\Phi^{(0)}(x) \quad \Phi^{(-)}(x))$. In the basis in which the Majorana mass matrix of RH neutrinos is diagonal, we have:

$$\mathcal{L}_{Y,M}(x) = \left(\lambda_{il} \, \overline{N_{iR}}(x) \, \Phi^\dagger(x) \, \psi_{lL}(x) + \text{h.c.} \right) - \frac{1}{2} \, M_i \, \overline{N_i}(x) \, N_i(x) \,, \qquad (14.22)$$

where λ_{il} is the matrix of neutrino Yukawa couplings and N_i ($N_i(x)$) is the heavy Majorana neutrino (field) possessing a mass $M_i > 0$. When the electroweak symmetry is broken spontaneously, the neutrino Yukawa coupling generates a Dirac mass term: $m_{il}^D \, \overline{N_{iR}}(x) \, \nu_{lL}(x) + \text{h.c.}$, with $m^D = v\lambda$, $v = 174$ GeV being the Higgs doublet v.e.v. In the case when the elements of m^D are much smaller than M_k, $|m_{il}^D| \ll M_k$, $i, k = 1, 2, 3$, $l = e, \mu, \tau$, the interplay between the Dirac mass term and the mass term of the heavy (RH) Majorana neutrinos N_i generates an effective Majorana mass (term) for the LH flavour neutrinos [3]:

$$m_{l'l}^{LL} \cong -(m^D)_{l'j}^T M_j^{-1} m_{jl}^D = -v^2 (\lambda)_{l'j}^T M_j^{-1} \lambda_{jl} \,. \qquad (14.23)$$

In grand unified theories, m^D is typically of the order of the charged fermion masses. In $SO(10)$ theories, for instance, m^D is related to the up-quark mass matrix. Taking indicatively $m^{LL} \sim 0.1$ eV, $m^D \sim 100$ GeV, one finds $M \sim 10^{14}$ GeV, which is close to the scale of unification of the electroweak and strong interactions, $M_{GUT} \cong 2 \times 10^{16}$ GeV. In GUT theories with RH neutrinos one finds that indeed the heavy Majorana neutrinos N_j naturally obtain masses which are by few to several orders of magnitude smaller than M_{GUT}. Thus, the enormous disparity between the neutrino and charged fermion masses is explained in this approach by the huge difference between effectively the electroweak symmetry breaking scale and M_{GUT}.

An additional attractive feature of the see-saw scenario is that the generation and smallness of neutrino masses is related via the leptogenesis mechanism [2] to the generation of the baryon asymmetry of the Universe. The Yukawa coupling in Eq. (14.22), in general, is not CP conserving. Due to this CP-nonconserving coupling the heavy Majorana neutrinos undergo, *e.g.*, the decays $N_j \to l^+ + \Phi^{(-)}$, $N_j \to l^- + \Phi^{(+)}$, which have different rates: $\Gamma(N_j \to l^+ + \Phi^{(-)}) \neq \Gamma(N_j \to l^- + \Phi^{(+)})$. When these decays occur in the Early Universe at temperatures somewhat below the mass of, say, N_1, so that the latter are out of equilibrium with the rest of the particles present at that epoch, CP violating asymmetries in the individual lepton charges L_l, and in the total lepton charge L, of the Universe are generated. These lepton asymmetries are converted into a baryon

asymmetry by $(B - L)$ conserving, but $(B + L)$ violating, sphaleron processes, which exist in the Standard Model and are effective at temperatures $T \sim (100 - 10^{12})$ GeV. If the heavy neutrinos N_j have hierarchical spectrum, $M_1 \ll M_2 \ll M_3$, the observed baryon asymmetry can be reproduced provided the mass of the lightest one satisfies $M_1 \gtrsim 10^9$ GeV [119]. Thus, in this scenario, the neutrino masses and mixing and the baryon asymmetry have the same origin - the neutrino Yukawa couplings and the existence of (at least two) heavy Majorana neutrinos. Moreover, quantitative studies [67,68], based on advances in leptogenesis theory [120], have shown that the CP violation necessary in leptogenesis for the generation of the observed baryon asymmetry of the Universe, can be provided exclusively by the Dirac and/or Majorana phases in the neutrino mixing matrix U. This implies, in particular, that if the CP symmetry is established not to hold in the lepton sector due to U, at least some fraction (if not all) of the observed baryon asymmetry might be due to the Dirac and/or Majorana CP violation present in the neutrino mixing. More specifically, the necessary condition that the requisite CP violation for a successful leptogenesis with heirarchical in mass heavy Majorana neutrinos is due *entirely* to the Dirac CPV phase in U reads [68]: $|\sin\theta_{13}\sin\delta| \gtrsim 0.09$. This condition is comfortably compatible with the measured value of $\sin\theta_{13} \cong 0.15$ and the hint that $\delta \cong 3\pi/2$, found in the global analyses of the neutrino oscillation data. The scenario, in which the requisite CP violation in leptogenesis is provided exclusively by the Dirac and/or Majorana CPV phases of the neutrino mixing matrix, considered in [67,68] on purely phenomenological grounds, was shown recently to be realised in theories of lepton flavour based on non-Abelian discrete symmetries (see, *e.g.*, Ref. [121]) .

14.6. Neutrino sources

In the experimental part of this review (Sections 14.9 - 14.14), we mainly discuss neutrino oscillation experiments using neutrinos or antineutrinos produced by the Sun, cosmic-ray interactions in the air, proton accelerators, and nuclear reactors. We call neutrinos from these sources as solar neutrinos, atmospheric neutrinos, accelerator neutrinos, and reactor (anti)neutrinos. Neutrinos (and/or antineutrinos) from each of these sources have very different properties, *e.g.*, energy spectra, flavour components, and directional distributions, at production. In the literature, neutrino flavour conversion of neutrinos from gravitationally collapsed supernova explosions (supernova neutrinos) is also discussed, but this topic is out of the scope of the present review.

Solar neutrinos and atmospheric neutrinos are naturally produced neutrinos; their fluxes as well as the distance between the (point or distributed) neutrino source and the detector cannot be controlled artificially. While the atmospheric neutrino flux involves ν_μ, $\bar{\nu}_\mu$, ν_e, and $\bar{\nu}_e$ components at production, solar neutrinos are produced as pure electron neutrinos due to thermo-nuclear fusion reactions of four protons, producing a helium nucleus. For atmospheric neutrinos with energy $\gtrsim 1$ GeV, which undergo charged-current interactions in the detector, directional correlation of the charged lepton with the parent neutrino gives the way to know, within the resolution, the distance traveled by the neutrino between the production and detection.

Accelerator neutrinos and reactor (anti)neutrinos are man-made neutrinos. In principle, it is possible to choose the distance between the neutrino source and the

detector arbitrarily. Accelerator neutrinos used for neutrino oscillation experiments so far have been produced by the decay of secondary mesons (pions and kaons) produced by the collision of a primary proton beam with a nuclear target. A dominant component of the accelerator neutrino flux is ν_μ or $\bar{\nu}_\mu$, depending on the secondary meson's sign selection, but a wrong-sign muon neutrino component as well as ν_e and $\bar{\nu}_e$ components are also present. The fluxes of accelerator neutrinos depend on a number of factors, *e.g.*, energy and intensity of the primary proton beam, material and geometry of the target, selection of the momentum and charge of the secondary mesons that are focused, and production angle of the secondary mesons with respect to the primary beam. In other words, it is possible to control the peak energy, energy spread, and dominant neutrino flavour, of the neutrino beam.

From the nuclear reactor, almost pure electron antineutrinos are produced by β-decays of fission products of the nuclear fuel. However, experimental groups cannot control the normalization and spectrum of the $\bar{\nu}_e$ flux from commercial nuclear reactors. They are dependent on the initial fuel composition and history of the nuclear fuel burnup. These data are provided by the power plant companies.

For neutrino oscillation experiments, knowledge of the flux of each neutrino and antineutrino flavour at production is needed for planning and designing the experiment, analyzing the data, and estimating systematic errors. Basically, for all neutrino sources, flux models are constructed and validation is made by comparing various experimentally observed quantities with the model predictions. Many of the modern accelerator long baseline and reactor neutrino oscillation experiments employ a two- or multi-detector configuration. In the accelerator long baseline experiment, a "near" detector measures non-oscillated neutrino flux. In the two- or multi-baseline reactor experiments, even a near detector measures the neutrino flux with oscillations developed to some extent. However, comparing the quantities measured with different baselines, it is possible to validate the reactor flux model and measure the oscillation parameters at the same time, or to make an analysis with minimal dependence on flux models.

14.6.1. *Standard solar model predictions of the solar neutrino fluxes* :

The Sun is an intense, well-defined neutrino source. It provides an important opportunities to investigate neutrino oscillations including matter effects, because of the wide range of matter density and the great distance from the Sun to the Earth. The solar neutrinos are produced by some of the fusion reactions in the pp chain and CNO cycle, shown in Table 14.2. In addition, electron capture on ^{13}N, ^{15}O, and ^{17}F produces line spectra of neutrinos called ecCNO neutrinos [122,123].   The combined effect of these reactions is written as

$$4p \rightarrow {}^4\mathrm{He} + 2e^+ + 2\nu_e. \tag{14.24}$$

Positrons annihilate with electrons. Therefore, when considering the solar thermal energy generation, a relevant expression is

$$4p + 2e^- \rightarrow {}^4\mathrm{He} + 2\nu_e + 26.73~\mathrm{MeV} - E_\nu~, \tag{14.25}$$

where E_ν represents the energy taken away by neutrinos, the average value being $\langle E_\nu \rangle \sim 0.6$ MeV.

Table 14.2: Neutrino-producing reactions in the Sun (first column) and their abbreviations (second column). The neutrino fluxes predicted by the B16-GS98 standard solar model [130] are listed in the third column.

Reaction	Abbr.	Flux (cm^{-2} s^{-1})
$pp \to d\,e^+\,\nu$	pp	$5.98(1 \pm 0.006) \times 10^{10}$
$pe^-p \to d\,\nu$	pep	$1.44(1 \pm 0.01) \times 10^8$
$^3\mathrm{He}\,p \to {}^4\mathrm{He}\,e^+\nu$	hep	$7.98(1 \pm 0.30) \times 10^3$
$^7\mathrm{Be}\,e^- \to {}^7\mathrm{Li}\,\nu + (\gamma)$	$^7\mathrm{Be}$	$4.93(1 \pm 0.06) \times 10^9$
$^8\mathrm{B} \to {}^8\mathrm{Be}^*\,e^+\nu$	$^8\mathrm{B}$	$5.46(1 \pm 0.12) \times 10^6$
$^{13}\mathrm{N} \to {}^{13}\mathrm{C}\,e^+\nu$	$^{13}\mathrm{N}$	$2.78(1 \pm 0.15) \times 10^8$
$^{15}\mathrm{O} \to {}^{15}\mathrm{N}\,e^+\nu$	$^{15}\mathrm{O}$	$2.05(1 \pm 0.17) \times 10^8$
$^{17}\mathrm{F} \to {}^{17}\mathrm{O}\,e^+\nu$	$^{17}\mathrm{F}$	$5.29(1 \pm 0.20) \times 10^6$
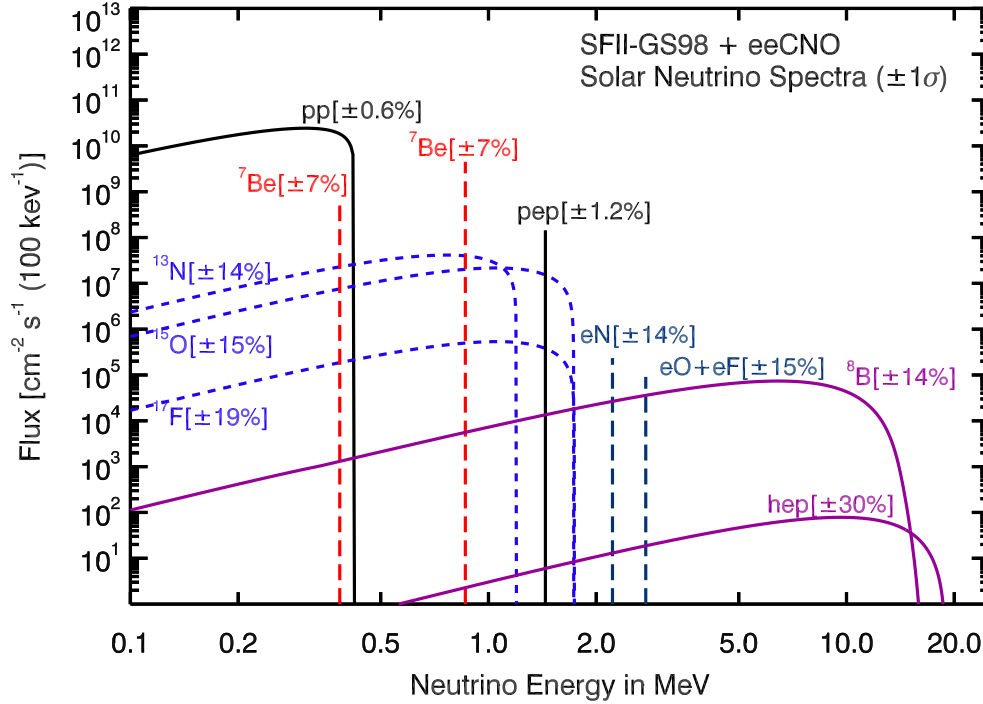
Figure 14.2: The solar neutrino spectrum predicted by the SFII-GS98 standard solar model [129].   In addition to the standard fluxes, the line spectra of the ecCNO neutrinos [123] are added. The neutrino fluxes are given in units of cm^{-2}s^{-1}MeV^{-1} for continuous spectra and cm^{-2}s^{-1} for line spectra. The numbers associated with the neutrino sources show theoretical errors of the fluxes. This figure is taken from Ref. 134.

The fluxes of the solar neutrinos are predicted by the calculations based on the Standard Solar Model (SSM), which describes the internal solar structure and follows its evolution from zero age to the present. A variety of input information is needed for the evolutionary calculations in the SSM, including the luminosity, age, radius, and mass of the Sun, its surface abundances of elements, radiative opacities, and nuclear reaction rates relevant to the pp chain and CNO cycle. Bahcall and his collaborators defined the SSM as the solar model which is constructed with the best available physics and input data [124,125,126]. Therefore, SSM calculations have been rather frequently updated in response to the changes or improvements of relevant physics and input data: there have been efforts over several decades to improve the SSM [124–130]. Observation of solar neutrinos directly addresses the theory of stellar structure and evolution, which is the basis of the SSM. There was a large discrepancy between the "observed" and predicted ^{8}B solar neutrino fluxes before the discovery of neutrino oscillations. Later, the SSM calculations of the ^{8}B solar neutrino flux turned out to be basically correct. This is one of the major successes of the SSM.

In 2011, Serenelli, Haxton, and Peña-Garay published a new SSM calculations [129] by adopting the newly analyzed solar fusion cross sections recommended in the Solar Fusion II paper by Adelberger *et al.* [131]. Hence, their SSM is referred to as the SFII SSM by Vinyoles *et al.*, who published the latest SSM calculations (referred to as the Barcelona 2016 or B16 SSM by the authors) [130]. The B16 SSM shares with the SFII SSM much of the physics but some important nuclear fusion rates are updated and the treatment of opacity uncertainties improved. Both the SFII and B16 SSM calculations used two sets of solar abundances, GS98 [132] and AGSS09met [133]. GS98 abundances are characterized by high metal-to-hydrogen ratio $Z/X = 0.0229$ (all elements more massive than Helium are called metals and their total abundance by mass is denote by Z, while the hydrogen abundance by mass is denoted by X) and AGSS09met abundances are characterized by low Z/X (=0.0178). High-Z SSMs are referred to as SFII-GS98 and B16-GS98. These high-Z models show generally better agreement with solar data than the low-Z models with AGSS09met abundances. With regard to the solar neutrino fluxes, however, predictions of the high-Z and low-Z models are almost comparable.

The prediction of the B16-GS98 SSM [130] for the fluxes from neutrino-producing reactions is given in Table 14.2. Fig. 14.2 shows the solar-neutrino spectra calculated with the SFII-GS98 model [129], together with the line spectra of the ecCNO neutrinos [123].

14.6.2. *Atmospheric neutrino fluxes* :

Atmospheric neutrinos are produced by the decays of π and K mesons produced in the nuclear interactions of the primary component of cosmic rays in the atmosphere ((A) in Table 14.3). The primary cosmic ray components above 2 GeV/nucleon are protons ($\sim 95\%$), helium nuclei ($\sim 4.5\%$), and heavier nuclei. For neutrino producing hadronic interactions at high energies, a nucleus can be simply regarded as a sum of individual nucleons. Pions are dominantly produced in these interactions, and they predominantly decay according to (B1) in Table 14.3, followed by muon decay (E) in Table 14.3. The interactions in massive underground detectors of atmospheric neutrinos provide a means of studying neutrino oscillations because of the large range of distances traveled by

these neutrinos ($\sim$10 to 1.27×10^4 km) to reach a detector on Earth and relatively well-understood atmospheric neutrino fluxes.

Table 14.3: Reactions and decays relevant to atmospheric neutrino and accelerator neutrino production. The first column shows the index of the reaction or decay, and the second column shows the reaction or decay channel. The third column shows the branching ratio [135]. (For K_L decay, the sum of the branching ratios to charge conjugate modes is shown).

	Reaction/Decay	Branching ratio (%)
(A)	$p\,(n) + A \rightarrow \pi^{\pm}X,\ K^{\pm}X,\ K_L X$	
(B1)	$\pi^{\pm} \rightarrow \mu^{\pm} + \nu_\mu\,(\bar{\nu}_\mu)$	99.9877
(B2)	$\rightarrow e^{\pm} + \nu_e\,(\bar{\nu}_e)$	0.0123
(C1)	$K^{\pm} \rightarrow \mu^{\pm} + \nu_\mu\,(\bar{\nu}_\mu)$	63.56
(C2)	$\rightarrow \pi^0 + \mu^{\pm} + \nu_\mu\,(\bar{\nu}_\mu)$	3.352
(C3)	$\rightarrow \pi^0 + e^{\pm} + \nu_e\,(\bar{\nu}_e)$	5.07
(D1)	$K_L \rightarrow \pi^{\pm} + \mu^{\mp} + \bar{\nu}_\mu\,(\nu_\mu)$	27.04
(D2)	$\rightarrow \pi^{\pm} + e^{\mp} + \bar{\nu}_e\,(\nu_e)$	40.55
(E)	$\mu^{\pm} \rightarrow e^{\pm} + \bar{\nu}_\mu(\nu_\mu) + \nu_e\,(\bar{\nu}_e)$	100

Calculation of the atmospheric neutrino fluxes requires knowledge of the primary cosmic-ray fluxes and composition, and the hadronic interactions. Atmospheric neutrinos with energy of $\sim$a few GeV are mostly produced by primary cosmic rays with energy of $\sim$100 GeV. For primary cosmic-rays in this energy range, a flux modulation due to the solar activity and the effects of Earth's geomagnetic fields should be taken into account. In particular, the atmospheric neutrino fluxes in the low-energy region depend on the location on the Earth. Detailed calculations of the atmospheric neutrino fluxes are performed by Honda et al. [136,137], Barr et al. [138], and Battistoni et al. [139], with a typical uncertainty of $10 \sim 20\%$.

From the dominant production mechanism of the atmospheric neutrinos, we can readily understand some relations that exist between the atmospheric ν_μ, $\bar{\nu}_\mu$, ν_e, and $\bar{\nu}_e$ fluxes without detailed calculations. For the ratio of the fluxes of $(\nu_\mu + \bar{\nu}_\mu)$ and $(\nu_e + \bar{\nu}_e)$ at low energies ($\lesssim 1$ GeV), where almost all produced muons decay before reaching the ground, we have approximately $(\nu_\mu + \bar{\nu}_\mu)/(\nu_e + \bar{\nu}_e) \approx 2$. As the neutrino energy increases, this ratio increases because an increasing fraction of muons do not decay before reaching the ground (the Earth surface) and being absorbed. We also have $\nu_\mu/\bar{\nu}_\mu \approx 1$ at low energies. However, as the $\nu_e/\bar{\nu}_e$ ratio reflects the parent π^+/π^- ratio (see (B1) and (B2) in Table 14.3), it is expected to be slightly greater than 1 because the dominance of protons in the primary component of the cosmic rays means a π^+ excess in the secondary
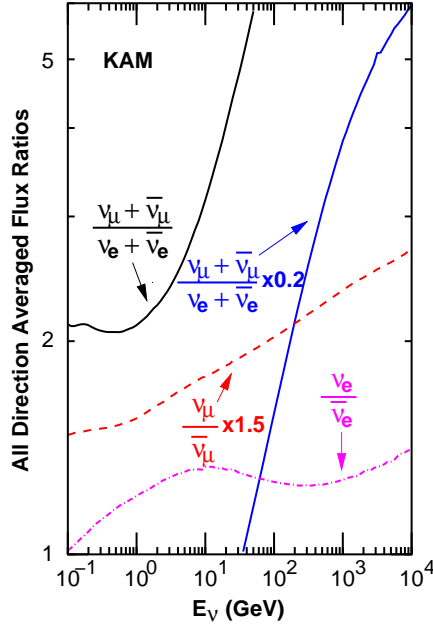
Figure 14.3: Neutrino flavour ratios calculated with the all-direction and one-year averaged atmospheric neutrino fluxes at Kamioka. This figure is provided by M. Honda, and is a part of Fig. 5 in Ref. [137], where similar plots at the INO site, the South Pole, and the Pyhäsalmi mine are also shown.

component. Fig. 14.3 shows these ratios at the Super-Kamiokande site, averaged over all directions and over a year, as a function of neutrino energy.

Another important feature of the atmospheric neutrino fluxes is that the zenith angle distribution for each neutrino type is up-down symmetric above ~ 1 GeV, if there are no neutrino oscillations. As the neutrino energy becomes lower than ~ 1 GeV, however, zenith angle distributions start to show deviations from up-down symmetric shapes due to the geomagnetic effects on primary cosmic rays.

14.6.3. *Accelerator neutrino beams* :

Conventional method to produce neutrino beams at a high-energy proton accelerator facility is to guide an intense proton beam onto a nuclear target of $1 \sim 2$ interaction lengths. For a comprehensive description of the accelerator neutrino beams, see Ref. 140. From the pA collisions, mesons are produced and their decays then produce neutrinos (see Table 14.3). In the high-energy collisions, pions are dominantly produced, with kaons produced at an order of 10% of the pion production rate. Therefore, the dominant component of the accelerator neutrinos is the muon neutrino or muon antineutrino. Mesons decay in the free space called a decay pipe or decay tunnel. This free space is evacuated or filled with helium gas. The decay tunnel is followed by a muon absorber (Earth ground or concrete), which can be several hundred meters long.

To increase the neutrino flux, it is necessary to focus the secondary pions. Modern neutrino oscillation experiments at high-energy accelerators exploit two or three magnetic horns as an approximately point-to-parallel focusing system for this purpose. A magnetic

horn is a high-current pulse magnet with toroidal magnetic fields. Therefore, the use of horns also means sign selection of the secondary hadrons that are focused, which in turn means muon neutrino sign selection. Even so, a fraction of wrong sign muon neutrinos contaminate the beam. Also, there is a small ν_e and $\bar{\nu}_e$ contamination from kaon, pion, and muon decay ((C3), (B2), and (E) in Table 14.3). Precise knowledge of ν_e and $\bar{\nu}_e$ components in the neutrino flux is important for the $\nu_\mu \rightarrow \nu_e$ ($\bar{\nu}_\mu \rightarrow \bar{\nu}_e$) appearance measurement.

With a given neutrino beam line configuration, the expected neutrino fluxes are calculated by using a simulation program tuned to that configuration. Re-interactions of the primary protons in the target and interactions of the secondary particles in the target and in the material outside the target have to be taken into account. An important input is hadron production cross sections from pA collisions for relevant target materials over wide energy and angular regions. For this purpose, some dedicated experiments such as SPY [141], HARP [142], MIPP [143], and NA61/SHINE [144] have been conducted. The data are fit to specific hadron production models to determine the model parameters.

The predicted neutrino fluxes have to be validated in some way. Modern long baseline neutrino oscillation experiments often have a two-detector configuration, with a near detector to measure an unoscillated neutrino flux immediately after the production. In the single detector experiment, the muon-neutrino flux model is calibrated by using a muon monitor which is located behind the beam dump. Since low-energy muons are absorbed in the beam dump, it is not possible to calibrate the low-energy part of the neutrino spectrum. Even in the two-detector experiments, it should be noted that the near detector does not see the same neutrino flux as the far detector sees, because the neutrino source looks like a line source for the near detector, while it looks as a point source for the far detector.

The energy E_ν of the neutrino emitted at an angle θ with respect to the parent pion direction is given by

$$E_\nu = \frac{m_\pi^2 - m_\mu^2}{2(E_\pi - p_\pi \cos\theta)}, \tag{14.26}$$

where E_π and p_π are the energy and momentum of the parent pion, m_π is the charged pion mass, m_μ is the muon mass. Suppose an ideal case that the pions are completely focused in parallel. Then, for $\theta = 0$, it can be seen from the above equation that E_ν is proportional to E_π for $E_\pi \gg m_\pi$. As the secondary pions have a wide energy spectrum, a 0 degree neutrino beam also has a wide spectrum and is called a "wide-band beam".

For a given angle θ, differentiating the above expression with respect to E_π, it can be shown that E_ν takes a maximum value $E_\nu^{\mathrm{max}} = (m_\pi^2 - m_\mu^2)/(2E_\pi^\circ \sin^2\theta)$ at $E_\pi^\circ = m_\pi/\sin\theta$. Numerical calculations show that a wide range of E_π, in particular that of $E_\pi \geq E_\pi^\circ$, contributes to a narrow range of $E_\nu \leq E_\nu^{\mathrm{max}}$ [145]. It is expected, therefore, that a narrow neutrino spectrum peaked at around E_ν^{max} can be obtained by the off-axis beam. Fig. 14.4 shows an example of the simulated muon neutrino fluxes at $\theta = 0$ degree and $2.0°$ and $2.5°$ off-axis configurations corresponding to the T2K experiment [146]. As expected, an off-axis beam has a narrower spectrum than the 0 degree wide-band beam. Therefore, an off-axis beam is called a "narrow-band beam". This idea of an off-axis

beam was proposed for BNL E889 experiment [145]. It has been employed for the T2K experiment for the first time. Currently, it is also used in the NOνA experiment [147]. For the off-axis beam, obviously the effect of a line neutrino source, namely the difference between the neutrino fluxes measured at the near and far detectors, is enhanced, and it has to be properly taken into account.
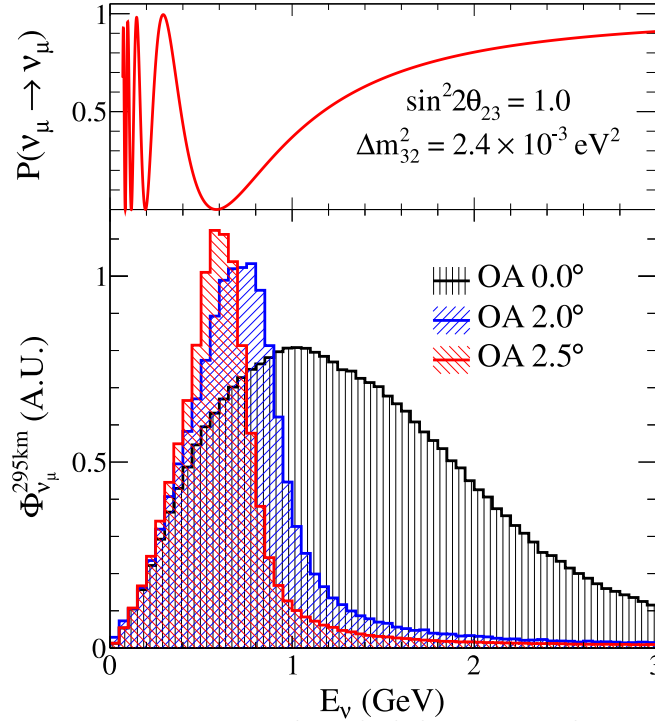

Figure 14.4: Muon neutrino survival probability at 295 km and neutrino fluxes for different off-axis angles. This figure is taken from Ref. 146.

14.6.4. *Reactor neutrino fluxes* :

In nuclear reactors, power is generated mainly by nuclear fission of four heavy isotopes, ^{235}U, ^{238}U, ^{239}Pu, and ^{241}Pu. These isotopes account for more than 99% of fissions in the reactor core. β-decays of fission products produce almost pure $\bar{\nu}_e$ flux. The rate of ν_e production is less than 10^{-5} of the rate of $\bar{\nu}_e$ production [148]. As the daughter isotopes of each fission undergo 6 β-decays on average, 6 electron antineutrinos are emitted per fission. The thermal power outputs of nuclear power reactors are usually quoted in thermal GW, $GW_{\rm th}$. The effective energy released per fission is $\sim$ 200 MeV [150]. Therefore, with 1 $GW_{\rm th}$ output, $\sim 2 \times 10^{20}$ electron antineutrinos are produced per second and emitted isotropically. Typical power plant light-water reactors have thermal power outputs of order 3 $GW_{\rm th}$. The total $\bar{\nu}_e$ flux $S(E_\nu)$ emitted from a reactor is given as a sum of contributions from the four fissioning isotopes, $S(E_\nu) = \sum_j f_j S_j(E_\nu)$, where f_j is the fission rate and $S_j(E_\nu)$ is the $\bar{\nu}_e$ flux per fission (in units of $\bar{\nu}_e/(cm^2\ fission)$) of each contributing isotope, $j = 235, 238, 239, 241$. The fission rates, and therefore $S(E_\nu)$, are dependent on the thermal power output $W_{\rm th}$ from the reactor as a function of time.

Using W_{th} and the total fission rate $F = \sum_j f_j$, $S(E_\nu)$ is rewritten as [149]

$$S(E_\nu) = \frac{W_{\text{th}}}{\sum_j (f_j/F)E_j} \sum_j (f_j/F)S_j(E_\nu), \tag{14.27}$$

where E_j is the average energy released per fission by each isotope [150]. The thermal power output and fission fractions f_j/F are provided by the power plant companies.
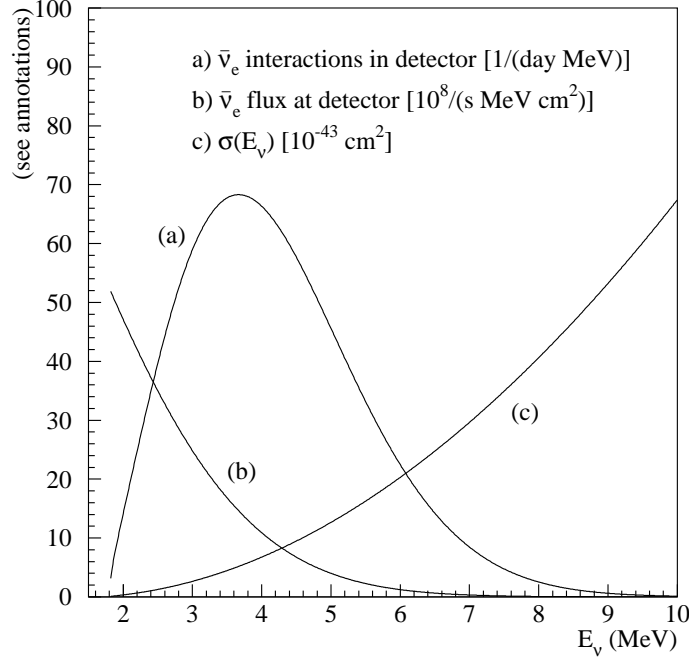

Figure 14.5: Assuming a 12-ton fiducial mass detector located 0.8 km from 12-GW$_{\text{th}}$ power reactor, $\bar{\nu}_e$ interaction spectrum in the detector (curve (a)) and reactor $\bar{\nu}_e$ flux at the detector (curve (b)) are shown as a function of energy. Inverse β-decay cross section (curve (c)) is also shown. This figure is from Ref. 162.

Electron antineutrinos from reactors are detected via the inverse β-decay (IBD) $\bar{\nu}_e + p \rightarrow e^+ + n$. This reaction has a threshold of 1.8 MeV, so that the $\bar{\nu}_e$ flux above this threshold is detected. The event rate as a function of $\bar{\nu}_e$ energy E_ν is proportional to $\sigma(E_\nu)S(E_\nu)$, where $\sigma(E_\nu)$ is the IBD cross section. Fig. 14.5 shows $\sigma(E_\nu)$. This figure also shows the flux and event rate for a particular detector configuration (see caption to this figure) in a reactor neutrino oscillation experiment.

To estimate the flux per fission $S_j(E_\nu)$ for each fuel isotope j, two methods have been employed [151,152]. One is an *ab initio* type approach called the "summation" method. It makes use of available nuclear data information of all fission fragments and their β-decays. Then, the $\bar{\nu}_e$ spectrum of each β-decay branch is summed up with its cumulative yield in fission as a weight to give $S_j(E_\nu)$. While the conversion of the

electron spectrum in β-decay to the $\bar{\nu}_e$ spectrum is trivial for a single β-decay branch, fission of the four main fuel isotopes involve > 1000 daughter isotopes and > 6000 individual β-decay branches. Incomplete knowledge of the nuclear data would cause rather large uncertainties in both the normalization and shape of the reactor $\bar{\nu}_e$ flux. The other method is an empirical approach called the "conversion" method. It relies on the measured cumulative electron spectrum associated with the β-decays of all fission fragments of the fuel isotope j. This spectrum is fitted by the superposition of a set of virtual allowed branches with different end points. $S_j(E_\nu)$ is then given as the sum of the $\bar{\nu}_e$ spectrum converted from each virtual β-branch.

The cumulative electron spectra were measured at the Institut Laue-Langevin (ILL) reactor in Grenoble, France in the 1980s for ^{235}U, ^{239}Pu, and ^{241}Pu, irradiated with thermal neutrons, and converted to the $\bar{\nu}_e$ spectra [153]. However, as ^{238}U undergoes fission with fast neutrons, its cumulative electron spectrum could not be measured at the ILL reactor. It was later measured at the scientific neutron source FRM II in Garching, Germany in 2014 [154].

Until 2011, a conventionally employed reactor $\bar{\nu}_e$ flux model was the predictions from the ILL conversion for ^{235}U, ^{239}Pu, and ^{241}Pu spectra [153]. For the ^{238}U $\bar{\nu}_e$ spectrum, the prediction from Vogel *et al.*'s summation [152] calculation was often used. (We refer to this reactor $\bar{\nu}_e$ flux model as the "ILL-Vogel" flux model or the "old" flux model.)

In 2011 the reactor $\bar{\nu}_e$ flux predictions were reevaluated with improved theoretical treatments [155]. The authors of [155] calculated the ^{238}U $\bar{\nu}_e$ spectrum with an improved *ab initio* approach and obtained predictions for ^{235}U, ^{239}Pu, and ^{241}Pu $\bar{\nu}_e$ spectra with a strategy to use the nuclear database information as much as possible. Their predictions for the ^{235}U, ^{239}Pu, and ^{241}Pu $\bar{\nu}_e$ spectra were found about 3% higher in normalization compared to the ILL predictions [153]. It was further pointed out in [156] that the mean ratio of the IBD event rate observed in previous short baseline reactor neutrino oscillation experiments to the rate predicted in [155] is 0.943 ± 0.023. The authors of [156] called this discrepancy (more than 2σ effect) the "reactor antineutrino anomaly."

Subsequently, the accuracy of theoretical electron spectrum in β-decay was further improved in [157]. The author of [157] took the strategy of minimizing the use of nuclear databases as much as possible, in contrast to that employed in [155], to predict the ^{235}U, ^{239}Pu, and ^{241}Pu $\bar{\nu}_e$ spectra by the conversion method. He also found that his predictions for the ^{235}U, ^{239}Pu, and ^{241}Pu $\bar{\nu}_e$ spectra were about 3% higher in normalization than the ILL predictions [153].

In view of the improved predictions of the reactor antineutrino spectra after 2011, the reactor $\bar{\nu}_e$ flux model often quoted in the literature is based on the prediction from the Huber conversion [157] for ^{235}U, ^{239}Pu, and ^{241}Pu and the prediction from Mueller *et al.*'s *ab initio* calculation for ^{238}U [155]. (We refer to this reactor $\bar{\nu}_e$ flux model as the "Saclay-Huber" flux model or the "new" flux model.) For the ^{238}U $\bar{\nu}_e$ flux, the prediction based on the measured electron spectrum [154] is also used.

If true, the results obtained with the "new" $\bar{\nu}_e$ flux model hint at possible oscillations involving sterile neutrinos (see Section 14.14). However, the reactor antineutrino flux measurement at Daya Bay [158] is consistent with the flux measurement results in the

previous short-baseline reactor neutrino oscillation experiments, and shows a 7.8% lower observed IBD yield from fission of ^{235}U with respect to the prediction of the "new" flux model [159]. This result suggests that the primary source of the reactor antineutrino anomaly may be an incorrect prediction of the ^{235}U $\bar{\nu}_e$ flux by the "new" flux model. A combined analysis of the Daya Bay measurement and other reactor measurements of the $\bar{\nu}_e$ fluxes was performed also in [160], where statistically stronger results confirming the Daya Bay's observation were obtained. These results have an impact on the sterile neutrino search in reactor neutrino oscillation experiments.

In what concerns the shape of the reactor $\bar{\nu}_e$ flux, all the current reactor neutrino oscillation experiments, Daya Bay [158], RENO [45], and Double Chooz [46], observe an excess of $\bar{\nu}_e$ flux in the energy region from 4 to 6 MeV, relative to current predictions. The excess rate is found to be time independent and correlated with the reactor power. Because of this, an unknown background is unlikely for its explanation. There are certain suggestions on the possible nuclear physics origins of this excess, but this problem is not completely solved yet [161].

14.7. Neutrino oscillations in vacuum

Neutrino oscillations are a quantum mechanical consequence of the existence of nonzero neutrino masses and neutrino (lepton) mixing, Eq. (14.1), and of the relatively small splitting between the neutrino masses. The neutrino mixing and oscillation phenomena are analogous to the $K^0 - \bar{K}^0$ and $B^0 - \bar{B}^0$ mixing and oscillations.

In what follows we will present a simplified version of the derivation of the expressions for the neutrino and antineutrino oscillation probabilities. The complete derivation would require the use of the wave packet formalism for the evolution of the massive neutrino states, or, alternatively, of the field-theoretical approach, in which one takes into account the processes of production, propagation and detection of neutrinos [163].

Suppose the flavour neutrino ν_l is produced in a CC weak interaction process and after a time T it is observed by a neutrino detector, located at a distance L from the neutrino source and capable of detecting also neutrinos $\nu_{l'}$, $l' \neq l$. We will consider the evolution of the neutrino state $|\nu_l\rangle$ in the frame in which the detector is at rest (laboratory frame). The oscillation probability, as we will see, is a Lorentz invariant quantity. If lepton mixing, Eq. (14.1), takes place and the masses m_j of all neutrinos ν_j are sufficiently small, the state of the neutrino ν_l, $|\nu_l\rangle$, will be a coherent superposition of the states $|\nu_j\rangle$ of neutrinos ν_j:

$$|\nu_l\rangle = \sum_j U^*_{lj} |\nu_j; \tilde{p}_j\rangle, \quad l = e, \mu, \tau\,, \tag{14.28}$$

where U is the neutrino mixing matrix and $\tilde{p}_j$ is the 4-momentum of ν_j [164].

We will consider the case of relativistic neutrinos ν_j, which corresponds to the conditions in both past and currently planned future neutrino oscillation experiments [166]. In this case the state $|\nu_j; \tilde{p}_j\rangle$ practically coincides with the helicity (-1) state $|\nu_j, L; \tilde{p}_j\rangle$ of the neutrino ν_j, the admixture of the helicity (+1) state $|\nu_j, R; \tilde{p}_j\rangle$ in $|\nu_j; \tilde{p}_j\rangle$ being suppressed due to the factor $\sim m_j/E_j$, where E_j is the energy of ν_j. If ν_j are Majorana particles,

$\nu_j \equiv \chi_j$, due to the presence of the helicity $(+1)$ state $|\chi_j, R; \tilde{p}_j\rangle$ in $|\chi_j; \tilde{p}_j\rangle$, the neutrino ν_l can produce an l^+ (instead of l^-) when it interacts, *e.g.*, with nucleons. The cross section of such a $|\Delta L_l| = 2$ process is suppressed by the factor $(m_j/E_j)^2$, which renders the process unobservable at present.

If the number n of massive neutrinos ν_j is bigger than 3 due to a mixing between the active flavour and sterile neutrinos, one will have additional relations similar to that in Eq. (14.28) for the state vectors of the (predominantly LH) sterile antineutrinos. In the case of just one RH sterile neutrino field $\nu_{sR}(x)$, for instance, we will have in addition to Eq. (14.28):

$$|\bar{\nu}_{sL}\rangle = \sum_{j=1}^{4} U_{sj}^* |\nu_j; \tilde{p}_j\rangle \cong \sum_{j=1}^{4} U_{sj}^* |\nu_j, L; \tilde{p}_j\rangle, \tag{14.29}$$

where the neutrino mixing matrix U is now a 4×4 unitary matrix.

For the state vector of RH flavour antineutrino $\bar{\nu}_l$, produced in a CC weak interaction process we similarly get:

$$|\bar{\nu}_l\rangle = \sum_j U_{lj} |\bar{\nu}_j; \tilde{p}_j\rangle \cong \sum_{j=1} U_{lj} |\bar{\nu}_j, R; \tilde{p}_j\rangle, \quad l = e, \mu, \tau, \tag{14.30}$$

where $|\bar{\nu}_j, R; \tilde{p}_j\rangle$ is the helicity $(+1)$ state of the antineutrino $\bar{\nu}_j$ if ν_j are Dirac fermions, or the helicity $(+1)$ state of the neutrino $\nu_j \equiv \bar{\nu}_j \equiv \chi_j$ if the massive neutrinos are Majorana particles. Thus, in the latter case we have in Eq. (14.30): $|\bar{\nu}_j; \tilde{p}_j\rangle \cong |\nu_j, R; \tilde{p}_j\rangle \equiv |\chi_j, R; \tilde{p}_j\rangle$. The presence of the matrix U in Eq. (14.30) (and not of U^*) follows directly from Eq. (14.1).

We will assume in what follows that the spectrum of masses of neutrinos is not degenerate: $m_j \neq m_k$, $j \neq k$. Then the states $|\nu_j; \tilde{p}_j\rangle$ in the linear superposition in the r.h.s. of Eq. (14.28) will have, in general, different energies and different momenta, independently of whether they are produced in a decay or interaction process: $\tilde{p}_j \neq \tilde{p}_k$, or $E_j \neq E_k$, $\mathbf{p}_j \neq \mathbf{p}_k$, $j \neq k$, where $E_j = \sqrt{p_j^2 + m_j^2}$, $p_j \equiv |\mathbf{p}_j|$. The deviations of E_j and p_j from the values for a massless neutrino E and $p = E$ are proportional to m_j^2/E_0, E_0 being a characteristic energy of the process, and are extremely small. In the case of $\pi^+ \to \mu^+ + \nu_\mu$ decay at rest, for instance, we have: $E_j = E + m_j^2/(2m_\pi)$, $p_j = E - \xi m_j^2/(2E)$, where $E = (m_\pi/2)(1 - m_\mu^2/m_\pi^2) \cong 30$ MeV, $\xi = (1 + m_\mu^2/m_\pi^2)/2 \cong 0.8$, and m_μ and m_π are the μ^+ and π^+ masses. Taking $m_j = 1$ eV we find: $E_j \cong E(1 + 1.2 \times 10^{-16})$ and $p_j \cong E(1 - 4.4 \times 10^{-16})$.

Given the uncorrelated uncertainties δE and δp in the knowledge of the neutrino energy E and momentum p, the quantum mechanical condition that neutrinos with definite mass ν_1, ν_2, ..., whose states are part of the linear superposition of states corresponding, for example, to $|\nu_l\rangle$ in Eq. (14.28), are emitted coherently when $|\nu_l\rangle$ is produced in some weak interaction process, has the form [167]:

$$\delta m^2 = \sqrt{(2E\delta E)^2 + (2p\delta p)^2} > \max(|m_i^2 - m_j^2|), \quad i, j = 1, 2, ..., n, \tag{14.31}$$

where δm^2 is the uncertainty in the square of the neutrino mass due to the uncertainties in the energy and momentum of the neutrino. Equation Eq. (14.31) follows from the well known relativistic relation $E^2 = p^2 + m^2$. In the context under discussion, δE and δp should be understood as the intrinsic quantum mechanical uncertainties in the neutrino energy and momentum for the given neutrino production and detection processes, *i.e.*, δE and δp are the minimal uncertainties with which E and p can be determined in the considered production and detection processes. Then δm^2 is the quantum mechanical uncertainty of the inferred squared neutrino mass.

Suppose that the neutrinos are observed via a CC weak interaction process and that in the detector's rest frame they are detected after time T after emission, after traveling a distance L. Then the amplitude of the probability that neutrino $\nu_{l'}$ will be observed if neutrino ν_l was produced by the neutrino source can be written as [163,165,168]:

$$A(\nu_l \to \nu_{l'}) = \sum_j U_{l'j} \, D_j \, U_{jl}^\dagger \,, \qquad l, l' = e, \mu, \tau \,, \tag{14.32}$$

where $D_j = D_j(p_j; L, T)$ describes the propagation of ν_j between the source and the detector, $U_{jl}^\dagger$ and $U_{l'j}$ are the amplitudes to find

ν_j in the initial and in the final flavour neutrino state, respectively. It follows from relativistic Quantum Mechanics considerations that [163,165]

$$D_j \equiv D_j(\tilde{p}_j; L, T) = e^{-i\tilde{p}_j \, (x_f - x_0)} = e^{-i(E_j T - p_j L)} \,, \qquad p_j \equiv |\mathbf{p}_j| \,, \tag{14.33}$$

where [169] x_0 and x_f are the space-time coordinates of the points of neutrino production and detection, $T = (t_f - t_0)$ and $L = \mathbf{k}(\mathbf{x}_f - \mathbf{x}_0)$, $\mathbf{k}$ being the unit vector in the direction of neutrino momentum, $\mathbf{p}_j = \mathbf{k} p_j$. What is relevant for the calculation of the probability $P(\nu_l \to \nu_{l'}) = |A(\nu_l \to \nu_{l'})|^2$ is the interference factor $D_j D_k^*$ which depends on the phase

$$\delta\varphi_{jk} = (E_j - E_k)T - (p_j - p_k)L = (E_j - E_k)\left[T - \frac{E_j + E_k}{p_j + p_k} L\right]$$

$$+ \frac{m_j^2 - m_k^2}{p_j + p_k} L \,. \tag{14.34}$$

Some authors [170] have suggested that the distance traveled by the neutrinos L and the time interval T are related by $T = (E_j + E_k) L/(p_j + p_k) = L/\bar{v}$, $\bar{v} = (E_j/(E_j + E_k))v_j + (E_k/(E_j + E_k))v_k$ being the "average" velocity of ν_j and ν_k, where $v_{j,k} = p_{j,k}/E_{j,k}$. In this case the first term in the r.h.s. of Eq. (14.34) vanishes. The indicated relation has not emerged so far from any dynamical wave packet calculations. We arrive at the same conclusion concerning the term under discussion in Eq. (14.34) if one assumes [171] that $E_j = E_k = E_0$. Finally, it was proposed in Ref. 168 and Ref. 177 that the states of ν_j and $\bar{\nu}_j$ in Eq. (14.28) and Eq. (14.30) have the same 3-momentum, $p_j = p_k = p$. Under this condition the first term in the r.h.s. of Eq. (14.34) is negligible, being suppressed by the additional factor $(m_j^2 + m_k^2)/p^2$ since for relativistic

neutrinos $L = T$ up to terms $\sim m_{j,k}^2/p^2$. We arrive at the same conclusion if $E_j \neq E_k$, $p_j \neq p_k$, $j \neq k$, and we take into account that neutrinos are relativistic and therefore, up to corrections $\sim m_{j,k}^2/E_{j,k}^2$, we have $L \cong T$ (see, *e.g.*, C. Giunti quoted in Ref. 163).

Although the cases considered above are physically quite different, they lead to the same result for the phase difference $\delta\varphi_{jk}$. Thus, we have:

$$\delta\varphi_{jk} \cong \frac{m_j^2 - m_k^2}{2p} L = 2\pi \frac{L}{L_{jk}^v} \operatorname{sgn}(m_j^2 - m_k^2), \tag{14.35}$$

where $p = (p_j + p_k)/2$ and

$$L_{jk}^v = 4\pi \frac{p}{|\Delta m_{jk}^2|} \cong 2.48 \ \mathrm{m} \ \frac{p[MeV]}{|\Delta m_{jk}^2|[eV^2]} \tag{14.36}$$

is the neutrino oscillation length associated with Δm_{jk}^2. We can safely neglect the dependence of p_j and p_k on the masses m_j and m_k and consider p to be the zero neutrino mass momentum, $p = E$. The phase difference $\delta\varphi_{jk}$, Eq. (14.35), is Lorentz-invariant.

Eq. (14.33) corresponds to a plane-wave description of the propagation of neutrinos ν_j. It accounts only for the movement of the center of the wave packet describing ν_j. In the wave packet treatment of the problem, the interference between the states of ν_j and ν_k is subject to a number of conditions [163], the localization condition and the condition of overlapping of the wave packets of ν_j and ν_k at the detection point being the most important. For relativistic neutrinos, the localisation condition in space, for instance, reads: $\sigma_{xP}, \sigma_{xD} < L_{jk}^v/(2\pi)$, $\sigma_{xP(D)}$ being the spatial width of the production (detection) wave packet. Thus, the interference will not be suppressed if the spatial width of the neutrino wave packets determined by the neutrino production and detection processes is smaller than the corresponding oscillation length in vacuum. In order for the interference to be nonzero, the wave packets describing ν_j and ν_k should also overlap in the point of neutrino detection. This requires that the spatial separation between the two wave packets at the point of neutrinos detection, caused by the two wave packets having different group velocities $v_j \neq v_k$, satisfies $|(v_j - v_k)T| \ll \max(\sigma_{xP}, \sigma_{xD})$. If the interval of time T is not measured, T in the preceding condition must be replaced by the distance L between the neutrino source and the detector (for further discussion see, *e.g.*, Refs. [163,165,168]) .

For the $\nu_l \to \nu_{l'}$ and $\bar{\nu}_l \to \bar{\nu}_{l'}$ oscillation probabilities we get from Eq. (14.32), Eq. (14.33), and Eq. (14.35):

$$P(\nu_l \to \nu_{l'}) = \sum_j |U_{l'j}|^2 |U_{lj}|^2 + 2\sum_{j>k} |U_{l'j} U_{lj}^* U_{lk} U_{l'k}^*|$$
$$\cos(\frac{\Delta m_{jk}^2}{2p} L - \phi_{l'l;jk}), \tag{14.37}$$

$$P(\bar{\nu}_l \to \bar{\nu}_{l'}) = \sum_j |U_{l'j}|^2 |U_{lj}|^2 + 2 \sum_{j>k} |U_{l'j} U_{lj}^* U_{lk} U_{l'k}^*|$$

$$\cos(\frac{\Delta m_{jk}^2}{2p} L + \phi_{l'l;jk}), \tag{14.38}$$

where $l, l' = e, \mu, \tau$ and $\phi_{l'l;jk} = \arg\left(U_{l'j} U_{lj}^* U_{lk} U_{l'k}^*\right)$. It follows from Eq. (14.32) - Eq. (14.34) that in order for neutrino oscillations to occur, at least two neutrinos ν_j should not be degenerate in mass and lepton mixing should take place, $U \neq \mathbf{1}$. The neutrino oscillations effects can be large if we have

$$\frac{|\Delta m_{jk}^2|}{2p} L = 2\pi \frac{L}{L_{jk}^v} \gtrsim 1, \quad j \neq k. \tag{14.39}$$

at least for one Δm_{jk}^2. This condition has a simple physical interpretation: the neutrino oscillation length L_{jk}^v should be of the order of, or smaller, than source-detector distance L, otherwise the oscillations will not have time to develop before neutrinos reach the detector.

We see from Eq. (14.37) and Eq. (14.38) that $P(\nu_l \to \nu_{l'}) = P(\bar{\nu}_{l'} \to \bar{\nu}_l)$, $l, l' = e, \mu, \tau$. This is a consequence of CPT invariance. The conditions of CP and T invariance read [54,61,62]: $P(\nu_l \to \nu_{l'}) = P(\bar{\nu}_l \to \bar{\nu}_{l'})$, $l, l' = e, \mu, \tau$ (CP), $P(\nu_l \to \nu_{l'}) = P(\nu_{l'} \to \nu_l)$, $P(\bar{\nu}_l \to \bar{\nu}_{l'}) = P(\bar{\nu}_{l'} \to \bar{\nu}_l)$, $l, l' = e, \mu, \tau$ (T). In the case of CPT invariance, which we will assume to hold throughout this article, we get for the survival probabilities: $P(\nu_l \to \nu_l) = P(\bar{\nu}_l \to \bar{\nu}_l)$, $l = e, \mu, \tau$. Thus, the study of the "disappearance" of ν_l and $\bar{\nu}_l$, caused by oscillations in vacuum, cannot be used to test whether CP invariance holds in the lepton sector. It follows from Eq. (14.37) and Eq. (14.38) that we can have CP violation effects in neutrino oscillations only if $\phi_{l'l;jk} \neq \pi q$, $q = 0, 1, 2$, *i.e.*, if $U_{l'j} U_{lj}^* U_{lk} U_{l'k}^*$, and therefore U itself, is not real. As a measure of CP and T violation in neutrino oscillations we can consider the asymmetries:

$$A_{\rm CP}^{(l'l)} \equiv P(\nu_l \to \nu_{l'}) - P(\bar{\nu}_l \to \bar{\nu}_{l'}), \quad A_{\rm T}^{(l'l)} \equiv P(\nu_l \to \nu_{l'}) - P(\nu_{l'} \to \nu_l). \tag{14.40}$$

CPT invariance implies: $A_{\rm CP}^{(l'l)} = -A_{\rm CP}^{(ll')}$, $A_{\rm T}^{(l'l)} = P(\bar{\nu}_{l'} \to \bar{\nu}_l) - P(\bar{\nu}_l \to \bar{\nu}_{l'}) = A_{\rm CP}^{(l'l)}$. It follows further directly from Eq. (14.37) and Eq. (14.38) that

$$A_{\rm CP}^{(l'l)} = 4 \sum_{j>k} {\rm Im}\left(U_{l'j} U_{lj}^* U_{lk} U_{l'k}^*\right) \sin\frac{\Delta m_{jk}^2}{2p} L, \quad l, l' = e, \mu, \tau. \tag{14.41}$$

Eq. (14.2) and Eq. (14.37) - Eq. (14.38) imply that $P(\nu_l \to \nu_{l'})$ and $P(\bar{\nu}_l \to \bar{\nu}_{l'})$ do not depend on the Majorana CP violation phases in the neutrino mixing matrix U [54]. Thus, the experiments investigating the $\nu_l \to \nu_{l'}$ and $\bar{\nu}_l \to \bar{\nu}_{l'}$ oscillations, $l, l' = e, \mu, \tau$, cannot provide information on the nature - Dirac or Majorana, of massive neutrinos.

The same conclusions hold also when the $\nu_l \to \nu_{l'}$ and $\bar{\nu}_l \to \bar{\nu}_{l'}$ oscillations take place in matter [65]. In the case of $\nu_l \leftrightarrow \nu_{l'}$ and $\bar{\nu}_l \leftrightarrow \bar{\nu}_{l'}$ oscillations in vacuum, only the Dirac phase(s) in U can cause CP violating effects leading to $P(\nu_l \to \nu_{l'}) \neq P(\bar{\nu}_l \to \bar{\nu}_{l'})$, $l \neq l'$.

In the case of 3-neutrino mixing all different $\text{Im}(U_{l'j} U_{lj}^* U_{lk} U_{l'k}^*) \neq 0$, $l' \neq l = e, \mu, \tau$, $j \neq k = 1, 2, 3$, coincide up to a sign as a consequence of the unitarity of U. Therefore one has [63]:

$$A_{\text{CP}}^{(\mu e)} = - A_{\text{CP}}^{(\tau e)} = A_{\text{CP}}^{(\tau \mu)} =$$

$$4 \, J_{\text{CP}} \, \left(\sin \frac{\Delta m_{32}^2}{2p} L + \sin \frac{\Delta m_{21}^2}{2p} L + \sin \frac{\Delta m_{13}^2}{2p} L \right) , \tag{14.42}$$

where

$$J_{\text{CP}} = \text{Im} \left(U_{\mu 3} \, U_{e3}^* \, U_{e2} \, U_{\mu 2}^* \right) , \tag{14.43}$$

is the "rephasing invariant" associated with the Dirac CP violation phase in U. It is analogous to the rephasing invariant associated with the Dirac CP violating phase in the CKM quark mixing matrix [64]. It is clear from Eq. (14.42) that J_{CP} controls the magnitude of CP violation effects in neutrino oscillations in the case of 3-neutrino mixing. If $\sin(\Delta m_{ij}^2/(2p)L) \cong 0$ for $(ij) = (32)$, or (21), or (13), we get $A_{\text{CP}}^{(l'l)} \cong 0$. Thus, if as a consequence of the production, propagation and/or detection of neutrinos, effectively oscillations due only to one non-zero neutrino mass squared difference take place, the CP violating effects will be strongly suppressed. In particular, we get $A_{\text{CP}}^{(l'l)} = 0$, unless all three $\Delta m_{ij}^2 \neq 0$, $(ij) = (32), (21), (13)$.

If the number of massive neutrinos n is equal to the number of neutrino flavours, $n = 3$, one has as a consequence of the unitarity of the neutrino mixing matrix: $\sum_{l'=e,\mu,\tau} P(\nu_l \to \nu_{l'}) = 1$, $l = e, \mu, \tau$, $\qquad \sum_{l=e,\mu,\tau} P(\nu_l \to \nu_{l'}) = 1$, $l' = e, \mu, \tau$. Similar "probability conservation" equations hold for $P(\bar{\nu}_l \to \bar{\nu}_{l'})$. If, however, the number of light massive neutrinos is bigger than the number of flavour neutrinos as a consequence, *e.g.*, of a flavour neutrino - sterile neutrino mixing, we would have $\sum_{l'=e,\mu,\tau} P(\nu_l \to \nu_{l'}) = 1 - P(\nu_l \to \bar{\nu}_{sL})$, $l = e, \mu, \tau$, where we have assumed the existence of just one sterile neutrino. Obviously, in this case $\sum_{l'=e,\mu,\tau} P(\nu_l \to \nu_{l'}) < 1$ if $P(\nu_l \to \bar{\nu}_{sL}) \neq 0$. The former inequality is used in the searches for oscillations between active and sterile neutrinos.

Consider next neutrino oscillations in the case of one neutrino mass squared difference "dominance": suppose that $|\Delta m_{j1}^2| \ll |\Delta m_{n1}^2|$, $j = 2, ..., (n-1)$, $|\Delta m_{n1}^2| \, L/(2p) \gtrsim 1$ and $|\Delta m_{j1}^2| \, L/(2p) \ll 1$, so that $\exp[i(\Delta m_{j1}^2 \, L/(2p))] \cong 1$, $j = 2, ..., (n-1)$. Under these conditions we obtain from Eq. (14.37) and Eq. (14.38), keeping only the oscillating terms involving Δm_{n1}^2:

$$P(\nu_{l(l')} \to \nu_{l'(l)}) \cong P(\bar{\nu}_{l(l')} \to \bar{\nu}_{l'(l)}) \cong \delta_{ll'} - 2|U_{ln}|^2 \left[\delta_{ll'} - |U_{l'n}|^2 \right]$$

$$(1 - \cos \frac{\Delta m_{n1}^2}{2p} L) . \tag{14.44}$$

It follows from the neutrino oscillation data discussed in Section 14.2 that in the case of 3-neutrino mixing, one of the two independent neutrino mass squared differences, $\Delta m_{21}^2 > 0$, is much smaller than the absolute value of the second one, $|\Delta m_{31}^2|$: $\Delta m_{21}^2 \ll |\Delta m_{31}^2|$, $\Delta m_{21}^2/|\Delta m_{31}^2| \cong 0.03$. Neglecting the effects due to Δm_{21}^2 we get from Eq. (14.44) by setting $n = 3$ and choosing, *e.g.*, i) $l = l' = e$ and ii) $l = e(\mu)$, $l' = \mu(e)$ [172]:

$$P(\nu_e \to \nu_e) = P(\bar{\nu}_e \to \bar{\nu}_e) \cong 1 - 2|U_{e3}|^2 \left(1 - |U_{e3}|^2\right)\left(1 - \cos\frac{\Delta m_{31}^2}{2p}L\right)$$

$$= 1 - \frac{1}{2}\sin^2 2\theta_{13}\left(1 - \cos\frac{\Delta m_{31}^2}{2p}L\right), \qquad (14.45)$$

$$P(\nu_{\mu(e)} \to \nu_{e(\mu)}) \cong 2\,|U_{\mu3}|^2\,|U_{e3}|^2\left(1 - \cos\frac{\Delta m_{31}^2}{2p}L\right)$$

$$= \frac{|U_{\mu3}|^2}{1 - |U_{e3}|^2}\,P^{2\nu}\left(|U_{e3}|^2, \Delta m_{31}^2\right) = \sin^2\theta_{23}P^{2\nu}\left(\sin^2\theta_{13}, \Delta m_{31}^2\right), \qquad (14.46)$$

and $P(\bar{\nu}_{\mu(e)} \to \bar{\nu}_{e(\mu)}) = P(\nu_{\mu(e)} \to \nu_{e(\mu)})$. Here $P^{2\nu}\left(|U_{e3}|^2, \Delta m_{31}^2\right) = 0.5\sin^2 2\theta_{13}(1 - \cos\frac{\Delta m_{31}^2}{2p}L)$ is the probability of the 2-neutrino transition $\nu_e \to (s_{23}\nu_\mu + c_{23}\nu_\tau)$ due to Δm_{31}^2 and a mixing with angle θ_{13}, where θ_{13} and θ_{23} are the reactor and atmospheric neutrino angles of the standard parametrization of the neutrino mixing matrix (see Eq. (14.6) and Eq. (14.8)). Eq. (14.45) describes with a relatively high precision the oscillations of reactor $\bar{\nu}_e$ on a distance $L \sim 1$ km in the case of 3-neutrino mixing. It was used in the analysis of the data of the Chooz [57], Double Chooz [32], Daya Bay [33] and RENO [34] experiments. Eq. (14.44) with $n = 3$ and $l = l' = \mu$ describes with a relatively good precision the effects of "disappearance" due to oscillations of the accelerator ν_μ, seen in the K2K [19] MINOS [20,21] and T2K [22,23] experiments. The $\nu_\mu \to \nu_\tau$ transitions due to the oscillations, which the OPERA experiment [173,174] is observing, can be described by Eq. (14.44) with $n = 3$ and $l = \mu$, $l' = \tau$. Finally, the probability Eq. (14.46) describes with a good precision the $\nu_\mu \to \nu_e$ and $\bar{\nu}_\mu \to \bar{\nu}_e$ oscillations under the conditions of the K2K experiment [175].

It follows from the expressions for the probabilities in Eq. (14.45) and Eq. (14.46), obtained in the one Δm^2 dominance approximation, that they are not sensitive to the sign of Δm_{31}^2, i.e., to the neutrino mass ordering. However, the exact 3-neutrino mixing ν_e and $\bar{\nu}_e$ survival probabilities, $P(\bar{\nu}_e \to \bar{\nu}_e) = P(\nu_e \to \nu_e)$ (we assume CPT invariance), depend on the neutrino mass ordering [86,176]. Indeed, the expression of interest can be cast in the form [86,176](see also [87,89]) :

$$P^{(X)}(\bar{\nu}_e \to \bar{\nu}_e) = P^X(\nu_e \to \nu_e) = 1 - \frac{1}{2}\sin^2 2\theta_{13}\left(1 - \cos\frac{\Delta m_{atm}^2\,L}{2\,E_\nu}\right)$$

$$- 2\cos^4\theta_{13}\,X^2\,(1 - X^2)\left(1 - \cos\frac{\Delta m_\odot^2\,L}{2\,E_\nu}\right)$$

$$+ \frac{1}{2} \sin^2 2\theta_{13} \, X^2 \left(\cos\left(\frac{\Delta m_{atm}^2 \, L}{2 \, E_\nu} - \frac{\Delta m_\odot^2 \, L}{2 \, E_\nu} \right) - \cos\frac{\Delta m_{atm}^2 \, L}{2 \, E_\nu} \right) \quad (14.47)$$

where $\Delta m_\odot^2 \equiv \Delta m_{21}^2$, $\Delta m_{atm}^2 \equiv \Delta m_{31}^2$ in the NO case, $\Delta m_{atm}^2 \equiv -\Delta m_{32}^2$ in the IO case, and we have used the fact that $\Delta m_{31}^2(NO) = -\Delta m_{32}^2(IO)$. Thus,

$$\Delta m_{atm}^2 \equiv \Delta m_{31}^2(NO) = -\Delta m_{32}^2(IO) \,. \quad (14.48)$$

The parameter X in Eq. (14.47) is given by:

$$\begin{aligned} X^2 &= \sin^2\theta_{12} \,, & \text{NO spectrum} \,, \\ X^2 &= \cos^2\theta_{12} \,, & \text{IO spectrum} \,, \end{aligned} \quad (14.49)$$

θ_{12} being the solar neutrino mixing angle of the standard parametrisation of the neutrino mixing matrix (see Eq. (14.6) and Eq. (14.7)). Thus, the probability of $\bar{\nu}_e$ and ν_e survival in the NO and IO cases, $P^{(NO)}(\bar{\nu}_e \to \bar{\nu}_e) = P^{(NO)}(\nu_e \to \nu_e)$ and $P^{(IO)}(\bar{\nu}_e \to \bar{\nu}_e) = P^{(IO)}(\nu_e \to \nu_e)$, differ by the coefficient X^2 in the last term in Eq. (14.47) - the interference term involving both $\Delta m_\odot^2$ and Δm_{atm}^2. For the current best fit value of $\sin^2\theta_{12} = 0.297$ quoted in Table 1.1 we have $\cos^2\theta_{12} \cong 0.703$, i.e., the coefficient under discussion in $P^{(IO)}(\bar{\nu}_e \to \bar{\nu}_e)$ is approximately by a factor of 2.3 larger than that in $P^{(NO)}(\bar{\nu}_e \to \bar{\nu}_e)$. It was suggested in [86] on the basis of an analysis of the distortion of $\bar{\nu}_e$ spectrum due to oscillations in the NO and IO cases that the indicated difference can be used for determination of the neutrino mass ordering in an experiment with reactor $\bar{\nu}_e$. This possibility was further studied in greater detail in [87,89] and, e.g., in [88,90]. Such an experiment is currently under preparation within the JUNO project in China [91].

In certain cases the dimensions of the neutrino source, ΔL, are not negligible in comparison with the oscillation length. Similarly, when analyzing neutrino oscillation data one has to include the energy resolution of the detector, ΔE, *etc.* in the analysis. As can be shown [52], if $2\pi\Delta L/L_{jk}^\nu \gg 1$, and/or $2\pi(L/L_{jk}^\nu)(\Delta E/E) \gg 1$, the oscillating terms in the neutrino oscillation probabilities will be strongly suppressed. In this case (as well as in the case of sufficiently large separation of the ν_j and ν_k wave packets at the detection point) the interference terms in $P(\nu_l \to \nu_{l'})$ and $P(\bar{\nu}_{l'} \to \bar{\nu}_l)$ will be negligibly small and the neutrino flavour conversion will be determined by the average probabilities:

$$\bar{P}(\nu_l \to \nu_{l'}) = \bar{P}(\bar{\nu}_l \to \bar{\nu}_{l'}) \cong \sum_j |U_{l'j}|^2 \, |U_{lj}|^2 \,. \quad (14.50)$$

Suppose next that in the case of 3-neutrino mixing, $|\Delta m_{21}^2| \, L/(2p) \sim 1$, while at the same time $|\Delta m_{31(32)}^2| \, L/(2p) \gg 1$, and the oscillations due to Δm_{31}^2 and Δm_{32}^2 are strongly suppressed (averaged out) due to integration over the region of neutrino production, the energy resolution function, *etc.* In this case we get for the ν_e and $\bar{\nu}_e$ survival probabilities:

$$\begin{aligned} P(\nu_e \to \nu_e) = P(\bar{\nu}_e \to \bar{\nu}_e) &\cong |U_{e3}|^4 + \left(1 - |U_{e3}|^2\right)^2 P^{2\nu}(\nu_e \to \nu_e) \\ &= \sin^4\theta_{13} + \cos^4\theta_{13} P^{2\nu}(\nu_e \to \nu_e) \,, \end{aligned} \quad (14.51)$$

where

$$P^{2\nu}(\nu_e \to \nu_e) = P^{2\nu}(\bar{\nu}_e \to \bar{\nu}_e) \equiv P^{2\nu}_{ee}(\theta_{12}, \Delta m^2_{21})$$

$$= 1 - \frac{1}{2}\sin^2 2\theta_{12}\left(1 - \cos\frac{\Delta m^2_{21}}{2p}L\right) = 1 - \sin^2 2\theta_{12}\sin^2\left(\frac{\Delta m^2_{21}}{4E}L\right) \quad (14.52)$$

are the ν_e and $\bar{\nu}_e$ survival probabilities in the case of 2-neutrino oscillations "driven" by the angle θ_{12} and Δm^2_{21}. Eq. (14.51) with $P^{2\nu}(\bar{\nu}_e \to \bar{\nu}_e)$ given by Eq. (14.52) describes the effects of neutrino oscillations of reactor $\bar{\nu}_e$ observed by the KamLAND experiment.

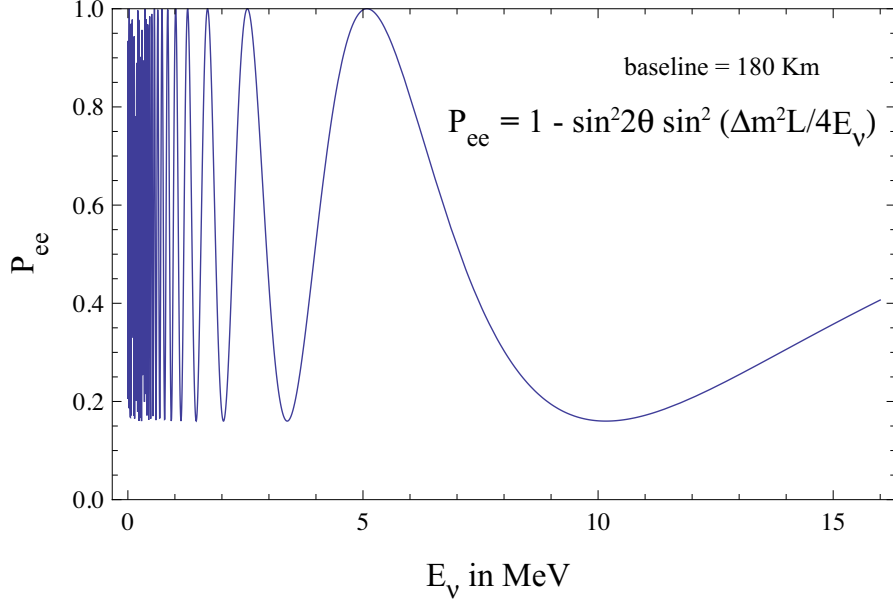**Figure 14.6:** The ν_e $(\bar{\nu}_e)$ survival probability $P(\nu_e \to \nu_e) = P(\bar{\nu}_e \to \bar{\nu}_e)$, Eq. (14.54), as a function of the neutrino energy for $L = 180$ km, $\Delta m^2 = 7.0 \times 10^{-5}$ eV^2 and $\sin^2 2\theta = 0.84$ (from Ref. 178).

The data of ν-oscillations experiments were often analyzed in the past, and in certain cases new data are still analyzed at present, assuming 2-neutrino mixing:

$$|\nu_l\rangle = |\nu_1\rangle\cos\theta + |\nu_2\rangle\sin\theta, \quad |\nu_x\rangle = -|\nu_1\rangle\sin\theta + |\nu_2\rangle\cos\theta, \quad (14.53)$$

where θ is the neutrino mixing angle in vacuum and ν_x is another flavour neutrino or sterile (anti-) neutrino, $x = l' \neq l$ or $\nu_x \equiv \bar{\nu}_{sL}$. In this case we have [177]:

$$P^{2\nu}(\nu_l \to \nu_l) = 1 - \frac{1}{2}\sin^2 2\theta\left(1 - \cos 2\pi\frac{L}{L^v}\right) = 1 - \sin^2 2\theta\left(\sin^2\frac{\Delta m^2}{4E}L\right),$$

$$P^{2\nu}(\nu_l \to \nu_x) = 1 - P^{2\nu}(\nu_l \to \nu_l), \quad (14.54)$$

where $L^v = 4\pi E/\Delta m^2$ $(p = E)$, $\Delta m^2 = m^2_2 - m^2_1 > 0$. Combining the CPT invariance constraints with the probability conservation one obtains: $P(\nu_l \to \nu_x) = P(\bar{\nu}_l \to \bar{\nu}_x) =$

$P(\nu_x \to \nu_l) = P(\bar{\nu}_x \to \bar{\nu}_l)$. These equalities and Eq. (14.54) with $l = \mu$ and $x = \tau$ were used, for instance, in the analysis of the Super-K atmospheric neutrino data [17], in which the first compelling evidence for oscillations of neutrinos was obtained. The probability $P^{2\nu}(\nu_l \to \nu_x)$, Eq. (14.54), depends on two factors: on $(1 - \cos 2\pi L/L^v)$, which exhibits oscillatory dependence on the distance L and on the neutrino energy $p = E$ (hence the name "neutrino oscillations"), and on $\sin^2 2\theta$, which determines the amplitude of the oscillations. In order to have $P^{2\nu}(\nu_l \to \nu_x) \cong 1$, two conditions have to be fulfilled: one should have $\sin^2 2\theta \cong 1$ and $L^v \lesssim 2\pi L$ with $\cos 2\pi L/L^v \cong -1$. If $L^v \gg 2\pi L$, the oscillations do not have enough time to develop on the way to the neutrino detector and $P(\nu_l \to \nu_x) \cong 0$, while $P(\nu_l \to \nu_l) \cong 1$. The preceding comments are illustrated in Fig. 14.6 showing the dependence of the probability $P^{2\nu}(\nu_e \to \nu_e) = P^{2\nu}(\bar{\nu}_e \to \bar{\nu}_e)$ on the neutrino energy.

Table 14.4: Sensitivity of different oscillation experiments.

Source	Type of ν	$\overline{E}$[MeV]	L[km]	$\min(\Delta m^2)$[eV^2]
Reactor	$\overline{\nu}_e$	~ 1	1	$\sim 10^{-3}$
Reactor	$\overline{\nu}_e$	~ 1	100	$\sim 10^{-5}$
Accelerator	$\nu_\mu, \overline{\nu}_\mu$	$\sim 10^3$	1	~ 1
Accelerator	$\nu_\mu, \overline{\nu}_\mu$	$\sim 10^3$	1000	$\sim 10^{-3}$
Atmospheric ν's	$\nu_{\mu,e}, \overline{\nu}_{\mu,e}$	$\sim 10^3$	10^4	$\sim 10^{-4}$
Sun	ν_e	~ 1	1.5×10^8	$\sim 10^{-11}$

A given experiment searching for neutrino oscillations is specified, in particular, by the average energy of the neutrinos being studied, $\bar{E}$, and by the source-detector distance L. The requirement $L^v_{jk} \lesssim 2\pi L$ determines the minimal value of a generic neutrino mass squared difference $\Delta m^2 > 0$, to which the experiment is sensitive (figure of merit of the experiment): $\min(\Delta m^2) \sim 2\bar{E}/L$. Because of the interference nature of neutrino oscillations, experiments can probe, in general, rather small values of Δm^2 (see, *e.g.*, Ref. 168). Values of $\min(\Delta m^2)$, characterizing qualitatively the sensitivity of different experiments are given in Table 14.4. They correspond to the reactor experiments Chooz, Daya Bay, RENO, Double Chooz ($L \sim 1$ km) and KamLAND ($L \sim 100$ km), to accelerator experiments - past ($L \sim 1$ km), and current (K2K, MINOS, OPERA, T2K, NOνA [147]) , $L \sim (300 \div 1000)$ km), to the Super-Kamiokande, MINOS and IceCube-DeepCore experiments studying atmospheric neutrino oscillations, and to the solar neutrino experiments.

14.8. Matter effects in neutrino oscillations

The presence of matter can change drastically the pattern of neutrino oscillations: neutrinos can interact with the particles forming the matter. Accordingly, the Hamiltonian of the neutrino system in matter H_m, differs from the Hamiltonian in vacuum H_0, $H_m = H_0 + H_{int}$, where H_{int} describes the interaction of neutrinos with the particles of matter. When, for instance, ν_e and ν_μ propagate in matter, they can scatter (due to H_{int}) on the electrons (e^-), protons (p) and neutrons (n) present in matter. The incoherent elastic and the quasi-elastic scattering, in which the states of the initial particles change in the process (destroying the coherence between the neutrino states), are not of interest - they have a negligible effect on the solar neutrino propagation in the Sun and on the solar, atmospheric and reactor neutrino propagation in the Earth [179]: even in the center of the Sun, where the matter density is relatively high (~ 150 g/cm^3), a ν_e with energy of 1 MeV has a mean free path with respect to the indicated scattering processes $\sim 10^{10}$ km. We recall that the solar radius is much smaller: $R_\odot = 6.96 \times 10^5$ km. The oscillating ν_e and ν_μ can scatter also elastically in the forward direction on the e^-, p and n, with the momenta and the spin states of the particles remaining unchanged. In such a process the coherence of the neutrino states is preserved.

The ν_e and ν_μ coherent elastic scattering on the particles of matter generates nontrivial indices of refraction of the ν_e and ν_μ in matter [26]: $\kappa(\nu_e) \neq 1$, $\kappa(\nu_\mu) \neq 1$. Most importantly, we have $\kappa(\nu_e) \neq \kappa(\nu_\mu)$. The difference $\kappa(\nu_e) - \kappa(\nu_\mu)$ is determined essentially by the difference of the real parts of the forward $\nu_e - e^-$ and $\nu_\mu - e^-$ elastic scattering amplitudes [26] Re $[F_{\nu_e - e^-}(0)]$ − Re $[F_{\nu_\mu - e^-}(0)]$: due to the flavour symmetry of the neutrino – quark (neutrino – nucleon) neutral current interaction, the forward $\nu_e - p, n$ and $\nu_\mu - p, n$ elastic scattering amplitudes are equal and therefore do not contribute to the difference of interest [180]. The imaginary parts of the forward scattering amplitudes (responsible, in particular, for decoherence effects) are proportional to the corresponding total scattering cross-sections and in the case of interest are negligible in comparison with the real parts. The real parts of the amplitudes $F_{\nu_e - e^-}(0)$ and $F_{\nu_\mu - e^-}(0)$ can be calculated in the Standard Model. To leading order in the Fermi constant G_F, only the term in $F_{\nu_e - e^-}(0)$ due to the diagram with exchange of a virtual $W^\pm$-boson contributes to $F_{\nu_e - e^-}(0) - F_{\nu_\mu - e^-}(0)$. One finds the following result for $\kappa(\nu_e) - \kappa(\nu_\mu)$ in the rest frame of the scatters [26,181,182]:

$$
\begin{aligned}
\kappa(\nu_e) - \kappa(\nu_\mu) &= \frac{2\pi}{p^2} \left(\text{Re } [F_{\nu_e - e^-}(0)] - \text{Re } [F_{\nu_\mu - e^-}(0)] \right) \\
&= -\frac{1}{p}\sqrt{2} G_F N_e \ ,
\end{aligned}
\tag{14.55}
$$

where N_e is the electron number density in matter. Given $\kappa(\nu_e) - \kappa(\nu_\mu)$, the system of evolution equations describing the $\nu_e \leftrightarrow \nu_\mu$ oscillations in matter reads [26]:

$$
i\frac{d}{dt}\begin{pmatrix} A_e(t, t_0) \\ A_\mu(t, t_0) \end{pmatrix} = \begin{pmatrix} -\epsilon(t) & \epsilon' \\ \epsilon' & \epsilon(t) \end{pmatrix} \begin{pmatrix} A_e(t, t_0) \\ A_\mu(t, t_0) \end{pmatrix}
\tag{14.56}
$$

where $A_e(t, t_0)$ $(A_\mu(t, t_0))$ is the amplitude of the probability to find ν_e (ν_μ) at time t of the evolution of the system if at time $t_0 \leq t$ the neutrino ν_e or ν_μ has been produced and

$$\epsilon(t) = \frac{1}{2} \left[\frac{\Delta m^2}{2E} \cos 2\theta - \sqrt{2} G_F N_e(t)\right], \quad \epsilon' = \frac{\Delta m^2}{4E} \sin 2\theta. \tag{14.57}$$

The term $\sqrt{2} G_F N_e(t)$ in $\epsilon(t)$ accounts for the effects of matter on neutrino oscillations. The system of evolution equations describing the oscillations of antineutrinos $\bar{\nu}_e \leftrightarrow \bar{\nu}_\mu$ in matter has exactly the same form except for the matter term in $\epsilon(t)$ which changes sign. The effect of matter in neutrino oscillations under discussion is usually called the Mikheyev, Smirnov, Wolfenstein (or MSW) effect.

Consider first the case of $\nu_e \leftrightarrow \nu_\mu$ oscillations in matter with constant density: $N_e(t) = N_e = \ const$. Due to the interaction term H_{int} in H_m, the eigenstates of the Hamiltonian of the neutrino system in vacuum, $|\nu_{1,2}\rangle$ are not eigenstates of H_m. For the eigenstates $|\nu_{1,2}^m\rangle$ of H_m, which diagonalize the evolution matrix in the r.h.s. of the system Eq. (14.56) we have:

$$|\nu_e\rangle = |\nu_1^m\rangle \cos\theta_m + |\nu_2^m\rangle \sin\theta_m\,, \quad |\nu_\mu\rangle = -|\nu_1^m\rangle \sin\theta_m + |\nu_2^m\rangle \cos\theta_m\ . \tag{14.58}$$

Here θ_m is the neutrino mixing angle in matter [26],

$$\sin 2\theta_m = \frac{\tan 2\theta}{\sqrt{(1 - \frac{N_e}{N_e^{res}})^2 + \tan^2 2\theta}}, \quad \cos 2\theta_m = \frac{1 - N_e/N_e^{res}}{\sqrt{(1 - \frac{N_e}{N_e^{res}})^2 + \tan^2 2\theta}}, \tag{14.59}$$

where the quantity

$$N_e^{res} = \frac{\Delta m^2 \cos 2\theta}{2E\sqrt{2}G_F} \cong 6.56 \times 10^6 \ \frac{\Delta m^2 [\text{eV}^2]}{E[\text{MeV}]} \cos 2\theta \ \text{cm}^{-3} \ \text{N}_A\,, \tag{14.60}$$

is called (for $\Delta m^2 \cos 2\theta > 0$) "resonance density" [27,181], N_A being Avogadro's number. The "adiabatic" states $|\nu_{1,2}^m\rangle$ have energies $E_{1,2}^m$ whose difference is given by

$$E_2^m - E_1^m = \frac{\Delta m^2}{2E} \left((1 - \frac{N_e}{N_e^{res}})^2 \cos^2 2\theta + \sin^2 2\theta\right)^{\frac{1}{2}} \equiv \frac{\Delta M^2}{2E}\,. \tag{14.61}$$

The probability of $\nu_{\mu(e)} \rightarrow \nu_{e(\mu)}$ transition in matter with $N_e = \ const.$ has the form [26,181]

$$P_m^{2\nu}(\nu_{\mu(e)} \rightarrow \nu_{e(\mu)}) = |A_{e(\mu)}(t)|^2 = \frac{1}{2} \sin^2 2\theta_m \ [1 - \cos 2\pi \frac{L}{L_m}\ ]$$
$$L_m = 2\pi/(E_2^m - E_1^m)\,, \tag{14.62}$$

where L_m is the oscillation length in matter. As Eq. (14.59) indicates, the dependence of $\sin^2 2\theta_m$ on N_e has a resonance character [27]. Indeed, if $\Delta m^2 \cos 2\theta > 0$, for any

$\sin^2 2\theta \neq 0$ there exists a value of N_e given by N_e^{res}, such that when $N_e = N_e^{res}$ we have $\sin^2 2\theta_m = 1$ independently of the value of $\sin^2 2\theta < 1$. This implies that the presence of matter can lead to a strong enhancement of the oscillation probability $P_m^{2\nu}(\nu_{\mu(e)} \to \nu_{e(\mu)})$ even when the $\nu_{\mu(e)} \to \nu_{e(\mu)}$ oscillations in vacuum are suppressed due to a small value of $\sin^2 2\theta$. For obvious reasons

$$N_e = N_e^{res} \equiv \frac{\Delta m^2 \cos 2\theta}{2E\sqrt{2}G_F} , \tag{14.63}$$

is called the "resonance condition" [27,181], while the energy at which Eq. (14.63) holds for given N_e and $\Delta m^2 \cos 2\theta$, is referred to as the "resonance energy", E^{res}. The oscillation length at resonance is given by [27] $L_m^{res} = L^v / \sin 2\theta$, while the width in N_e of the resonance at half height reads $\Delta N_e^{res} = 2N_e^{res} \tan 2\theta$. Thus, if the mixing angle in vacuum is small, the resonance is narrow, $\Delta N_e^{res} \ll N_e^{res}$, and $L_m^{res} \gg L^v$. The energy difference $E_2^m - E_1^m$ has a minimum at the resonance: $(E_2^m - E_1^m)^{res} = \min (E_2^m - E_1^m) = (\Delta m^2/(2E)) \sin 2\theta$.

It is instructive to consider two limiting cases. If $N_e \ll N_e^{res}$, we have from Eq. (14.59) and Eq. (14.61), $\theta_m \cong \theta$, $L_m \cong L^v$ and neutrinos oscillate practically as in vacuum. In the limit $N_e \gg N_e^{res}$, $N_e^{res} \tan^2 2\theta$, one finds $\theta_m \cong \pi/2$ ($\cos 2\theta_m \cong -1$) and the presence of matter suppress the $\nu_\mu \leftrightarrow \nu_e$ oscillations. In this case $|\nu_e\rangle \cong |\nu_2^m\rangle$, $|\nu_\mu\rangle = -|\nu_1^m\rangle$, *i.e.*, ν_e practically coincides with the heavier matter-eigenstate, while ν_μ coincides with the lighter one.

Since the neutral current weak interaction of neutrinos in the Standard Model is flavour symmetric, the formulae and results we have obtained are valid for the case of $\nu_e - \nu_\tau$ mixing and $\nu_e \leftrightarrow \nu_\tau$ oscillations in matter as well. The case of $\nu_\mu - \nu_\tau$ mixing, however, is different: to a relatively good precision we have [183] $\kappa(\nu_\mu) \cong \kappa(\nu_\tau)$ and the $\nu_\mu \leftrightarrow \nu_\tau$ oscillations in the matter of the Earth and the Sun proceed practically as in vacuum [184].

The analogs of Eq. (14.59) to Eq. (14.62) for oscillations of antineutrinos, $\bar\nu_\mu \leftrightarrow \bar\nu_e$, in matter can formally be obtained by replacing N_e with $(-N_e)$ in the indicated equations. It should be clear that depending on the sign of $\Delta m^2 \cos 2\theta$, the presence of matter can lead to resonance enhancement either of the $\nu_\mu \leftrightarrow \nu_e$ or of the $\bar\nu_\mu \leftrightarrow \bar\nu_e$ oscillations, but not of both types of oscillations [181]. For $\Delta m^2 \cos 2\theta < 0$, for instance, the matter can only suppress the $\nu_{\mu(e)} \to \nu_{e(\mu)}$ oscillations, while it can enhance the $\bar\nu_{\mu(e)} \to \bar\nu_{e(\mu)}$ transitions. The dependence of the effects of matter in $\nu_\mu \to \nu_e$ and $\bar\nu_\mu \to \bar\nu_e$ oscillations on $\text{sgn}(\Delta m^2 \cos 2\theta)$ is at basis of the plans to determine the sign of $\Delta m^2_{31(32)}$, and thus the type of spectrum neutrino masses obey - with normal or inverted ordering - in long baseline neutrino oscillation experiments (NOνA, DUNE,T2HKK) and in atmospheric neutrino experiments with large volume detectors (PINGU, ORCA, INO, Hyper-Kamiokande, DUNE).

The discussed disparity between the behavior of neutrinos and that of antineutrinos is a consequence of the fact that the matter in the Sun or in the Earth we are interested in is not charge-symmetric (it contains e^-, p and n, but does not contain their antiparticles) and therefore the oscillations in matter are neither CP- nor CPT-

invariant [65].   Thus, even in the case of 2-neutrino mixing and oscillations we have, *e.g.*, $P_m^{2\nu}(\nu_\mu \to \nu_e) \neq P_m^{2\nu}(\bar{\nu}_\mu \to \bar{\nu}_e)$ and $P_m^{2\nu}(\nu_e \to \nu_{\mu(\tau)}) \neq P_m^{2\nu}(\bar{\nu}_e \to \bar{\nu}_{\mu(\tau)})$.

The $\nu_\mu \leftrightarrow \nu_e$ ($\bar{\nu}_\mu \leftrightarrow \bar{\nu}_e$) and $\nu_e \leftrightarrow \nu_{\mu(\tau)}$ ($\bar{\nu}_e \leftrightarrow \bar{\nu}_{\mu(\tau)}$) oscillations in matter will be invariant with respect to the operation of time reversal if the N_e distribution along the neutrino path is symmetric with respect to this operation [63,185].   The latter condition is fulfilled (to a good approximation) for the N_e distribution along a path of a neutrino crossing the Earth [186].

14.8.1. *Effects of Earth matter on oscillations of neutrinos. Analytic expressions for oscillation probabilities* :

The formalism we have developed can be applied, *e.g.*, to the study of matter effects in the $\nu_e \leftrightarrow \nu_{\mu(\tau)}$ ($\nu_{\mu(\tau)} \leftrightarrow \nu_e$) and $\bar{\nu}_e \leftrightarrow \bar{\nu}_{\mu(\tau)}$ ($\bar{\nu}_{\mu(\tau)} \leftrightarrow \bar{\nu}_e$) oscillations of neutrinos which traverse the Earth [187].   Indeed, the Earth density distribution in the existing Earth models [186] is assumed to be spherically symmetric and there are two major density structures - the core and the mantle, and a certain number of substructures (shells or layers). The Earth radius is $R_\oplus = 6371$ km; the Earth core has a radius of $R_c = 3486$ km, so the Earth mantle depth is 2885 km. For a spherically symmetric Earth density distribution, the neutrino trajectory in the Earth is specified by the value of the nadir angle θ_n of the trajectory. For $\theta_n \leq 33.17^o$, or path lengths $L \geq 10660$ km, neutrinos cross the Earth core. The path length for neutrinos which cross only the Earth mantle is given by $L = 2R_\oplus \cos\theta_n$. If neutrinos cross the Earth core, the lengths of the paths in the mantle, $2L^{\mathrm{man}}$, and in the core, L^{core}, are determined by: $L^{\mathrm{man}} = R_\oplus \cos\theta_n - (R_c^2 - R_\oplus^2 \sin^2\theta_n)^{\frac{1}{2}}$, $L^{\mathrm{core}} = 2(R_c^2 - R_\oplus^2 \sin^2\theta_n)^{\frac{1}{2}}$. The mean electron number densities in the mantle and in the core according to the PREM model read [186]: $\bar{N}_e^{man} \cong 2.2$ cm^{-3} N$_A$, $\bar{N}_e^c \cong 5.4$ cm^{-3} N$_A$. Thus, we have $\bar{N}_e^c \cong 2.5 \; \bar{N}_e^{man}$. The change of N_e from the mantle to the core can well be approximated by a step function [186].   The electron number density N_e changes relatively little around the indicated mean values along the trajectories of neutrinos which cross a substantial part of the Earth mantle, or the mantle and the core, and the two-layer constant density approximation, $N_e^{man} = const. = \tilde{N}_e^{man}$, $N_e^c = const. = \tilde{N}_e^c$, $\tilde{N}_e^{man}$ and $\tilde{N}_e^c$ *being the mean densities along the given neutrino path in the Earth*, was shown to be sufficiently accurate in what concerns the calculation of neutrino oscillation probabilities [63,189,190] (and references quoted in [189,190]) in a large number of specific cases. This is related to the fact that the relatively small changes of density along the path of the neutrinos in the mantle (or in the core) take place over path lengths which are typically considerably smaller than the corresponding oscillation length in matter.

In the case of 3-neutrino mixing and for neutrino energies of $E \gtrsim 2$ GeV, the effects due to Δm_{21}^2 ($|\Delta m_{21}^2| \ll |\Delta m_{31(23)}^2|$, see Table 14.1) in the neutrino oscillation probabilities are sub-dominant and to leading order can be neglected: the corresponding resonance density $|N_{e21}^{res}| \lesssim 0.25 \; cm^{-3} \; N_A \ll \bar{N}_e^{man,c}$ and the Earth matter strongly suppresses the oscillations due to Δm_{21}^2. For oscillations in vacuum this approximation is valid in the case of NO (IO) neutrino mass spectrum (see Section 2) as long as the leading order contribution due to $\Delta m_{31(23)}^2$ in the relevant probabilities is bigger than approximately 10^{-3}. In this case the 3-neutrino $\nu_e \to \nu_{\mu(\tau)}$ ($\bar{\nu}_e \to \bar{\nu}_{\mu(\tau)}$) and $\nu_{\mu(\tau)} \to \nu_e$

$(\bar{\nu}_{\mu(\tau)} \to \bar{\nu}_e)$ transition probabilities for neutrinos traversing the Earth, reduce effectively to a 2-neutrino transition probability (see, *e.g.*, Refs. [190–192]) , with $\Delta m^2_{31(23)}$ and θ_{13} playing the role of the relevant 2-neutrino vacuum oscillation parameters. We note that in the approximation of negligible Δm^2_{21} we have $\Delta m^2_{31} = \Delta m^2_{32}$. Therefore in what follows in this part of the article we will use, whenever relevant, only Δm^2_{31} in the analytic expressions.

As we have discussed in Sections 14.2 and will be discussed in greater detail in Section 14.12, the value of $\sin^2 2\theta_{13}$ has been determined with a rather high precision in the Daya Bay [44] and RENO [45] experiments. The best fit values found in the two experiments read, respectively, $\sin^2 2\theta_{13} = 0.0841$ [44] and 0.086 [45]. The 3-neutrino oscillation probabilities of the atmospheric and accelerator $\nu_{e,\mu}$ having energy $E \gtrsim 2$ GeV and crossing the Earth along a trajectory characterized by a nadir angle θ_n, for instance, have the following form in the approximation of negligible Δm^2_{21}:

$$P^{3\nu}_m(\nu_e \to \nu_e) \cong 1 - P^{2\nu}_m, \tag{14.64}$$

$$P^{3\nu}_m(\nu_e \to \nu_\mu) \cong P^{3\nu}_m(\nu_\mu \to \nu_e) \cong s^2_{23} \; P^{2\nu}_m, \qquad P^{3\nu}_m(\nu_e \to \nu_\tau) \cong c^2_{23} \; P^{2\nu}_m, \tag{14.65}$$

$$P^{3\nu}_m(\nu_\mu \to \nu_\mu) \cong 1 - s^4_{23} \; P^{2\nu}_m - 2c^2_{23}s^2_{23} \; \left[1 - Re \; (e^{-i\kappa} A^{2\nu}_m(\nu' \to \nu'))\right], \tag{14.66}$$

$$P^{3\nu}_m(\nu_\mu \to \nu_\tau) = 1 - P^{3\nu}_m(\nu_\mu \to \nu_\mu) - P^{3\nu}_m(\nu_\mu \to \nu_e). \tag{14.67}$$

Here $P^{2\nu}_m \equiv P^{2\nu}_m(\Delta m^2_{31}, \theta_{13}; E, \theta_n)$ is the probability of the 2-neutrino $\nu_e \to \nu' \equiv (s_{23}\nu_\mu + c_{23}\nu_\tau)$ oscillations in the Earth, and κ and $A^{2\nu}_m(\nu' \to \nu') \equiv A^{2\nu}_m$ are known phase and 2-neutrino transition probability amplitude (see, *e.g.*, Refs. [190,191]). We note that Eq. (14.64) to Eq. (14.66) are based only on the assumptions that $|N^{res}_{e21}|$ is much smaller than the densities in the Earth mantle and core and that $|\Delta m^2_{21}| \ll |\Delta m^2_{31(23)}|$, and does not rely on the constant density approximation. Similar results are valid for the corresponding antineutrino oscillation probabilities: one has just to replace $P^{2\nu}_m$, κ and $A^{2\nu}_m$ in the expressions given above with the corresponding quantities for antineutrinos (the latter are obtained from those for neutrinos by changing the sign in front of N_e). Obviously, we have: $P(\nu_{e(\mu)} \to \nu_{\mu(e)}), P(\bar{\nu}_{e(\mu)} \to \bar{\nu}_{\mu(e)}) \leq \sin^2 \theta_{23}$, and $P(\nu_e \to \nu_\tau), P(\bar{\nu}_e \to \bar{\nu}_\tau) \leq \cos^2 \theta_{23}$. The one Δm^2 dominance approximation and correspondingly Eq. (14.64) to Eq. (14.67) were used by the Super-Kamiokande Collaboration in their 2006 neutrino oscillation analysis of the multi-GeV atmospheric neutrino data [193].

In the case of neutrinos crossing only the Earth mantle and in the constant density approximation, $P^{2\nu}_m$ is given by the r.h.s. of Eq. (14.62) with θ, Δm^2 and N_e replaced respectively by θ_{13}, Δm^2_{31} and $\bar{N}^{man}_e$ (or $\tilde{N}^{man}_e$ corresponding to the given θ_n) in the relevant expressions Eq. (14.59), Eq. (14.60) and Eq. (14.61) for $\sin 2\theta_m$, N^{res}_e and $(E^m_2 - E^m_1)$, while for κ and $A^{2\nu}_m$ we have (see, *e.g.*, Ref. 190):

$$\kappa \cong \frac{1}{2}[\frac{\Delta m^2_{31}}{2E} \; L + \sqrt{2}G_F \bar{N}^{man}_e L - \frac{\Delta M^2_{31} L}{2E}],$$

$$A^{2\nu}_m = 1 + (e^{-i\frac{\Delta M^2_{31} L}{2E}} - 1)\cos^2 \theta^m_{13} \; , \tag{14.68}$$

where ΔM_{31}^2 and θ_{13}^m can be obtained from Eq. (14.61) and Eq. (14.59) by setting $\theta = \theta_{13}$, $\Delta m^2 = \Delta m_{31}^2 > 0$, $N_e^{res} = N_{e31}^{res} = \Delta m_{31}^2 \cos 2\theta_{13}/(2E\sqrt{2}G_F)$ and $N_e = \bar{N}_e^{man}(\theta_n)$. Clearly, θ_{13}^m is the mixing angle in the mantle which coincides in vacuum with θ_{13}. In the expressions for $P_m^{2\nu} \equiv P_m^{2\nu}(\Delta m_{31}^2, \theta_{13}; E, \theta_n, \bar{N}_e^{man})$, κ and $A_m^{2\nu}$ in the case of oscillations in the mantle, $L = 2R_\oplus \cos\theta_n$ is the distance the neutrino travels in the mantle. The corresponding expressions for antineutrino oscillations, as we have noticed earlier, can be obtained from those derived above by making the change $\bar{N}_e^{man} \to -\bar{N}_e^{man}$.

The analytic results for $P_m^{2\nu}(\Delta m_{31}^2, \theta_{13}; E, \theta_n, \bar{N}_e^{man})$, κ and $A_m^{2\nu}$, described above and obtained in the constant mantle density approximation, as we have already remarked, provide a relatively precise description of the $\nu_{\mu(e)} \to \nu_{e(\mu)}$, $\nu_e \to \nu_{e(\tau)}$, etc. oscillation probabilities in the Earth mantle if for each given trajectory of the neutrinos in the mantle, specified by the nadir angle θ_n, in the calculations one uses for $\bar{N}_e^{man}$ the mean value of the electron number density along that specific trajectory: $\bar{N}_e^{man} = \tilde{N}_e^{man}(\theta_n)$, where $\tilde{N}_e^{man}(\theta_n)$ should be calculated using the density distribution given by the existing Earth models [186].

It follows from Eq. (14.64) and Eq. (14.65) that for $\Delta m_{31}^2 \cos 2\theta_{13} > 0$, the oscillation effects of interest, *e.g.*, in the $\nu_{e(\mu)} \to \nu_{\mu(e)}$ and $\nu_e \to \nu_\tau$ transitions will be maximal if $P_m^{2\nu} \cong 1$, *i.e.*, if Eq. (14.63) leading to $\sin^2 2\theta_m \cong 1$ is fulfilled, and ii) $\cos(\Delta M^2 L/(2E)) \cong -1$. Given the value of $\bar{N}_e^{man}$, the first condition determines the neutrino's energy, while the second determines the path length L, for which one can have $P_m^{2\nu} \cong 1$. For $\Delta m_{31}^2 \cong 2.5 \times 10^{-3}$ eV^2, $\sin^2 2\theta_{13} \cong 0.090$ and $\bar{N}_e^{man} \cong 2.2$ N$_A$cm^{-3}, one finds that $E_{res} \cong 7.1$ GeV and $L \cong 3522/\sin 2\theta_{13}$ km $\cong 11740$ km. Since for neutrinos crossing only the mantle $L \lesssim 10660$ km, the second condition can be satisfied only if $\sin^2 2\theta_{13} \gtrsim 0.11$, which lies outside the 3σ range of the experimentally allowed values of $\sin^2 2\theta_{13}$. We still get a significant amplification of the probability $P_m^{2\nu}$, and therefore of $P(\nu_{e(\mu)} \to \nu_{\mu(e)})$ and $P(\nu_e \to \nu_\tau)$, even when $\cos(\Delta M^2 L/(2E)) = -0.5(-0.2)$: in this case $P_m^{2\nu} \cong 0.75$ (0.60). For $\sin^2 2\theta_{13} \cong 0.090$ we have $\cos(\Delta M^2 L/(2E)) = -0.5(-0.2)$ if $L \cong 7826$ (6622) km. Thus, for $\Delta m_{31}^2 > 0$, the Earth matter effects can amplify $P_m^{2\nu}$, and therefore $P(\nu_{e(\mu)} \to \nu_{\mu(e)})$ and $P(\nu_e \to \nu_\tau)$, significantly when the neutrinos cross only the mantle, for $E \sim 7$ GeV and sufficiently large path lengths L.

If $\Delta m_{31}^2 < 0$ the same considerations apply for the corresponding antineutrino oscillation probabilities $\bar{P}_m^{2\nu} = \bar{P}_m^{2\nu}(\bar{\nu}_e \to (s_{23}\bar{\nu}_\mu + c_{23}\bar{\nu}_\tau))$ and correspondingly for $P(\bar{\nu}_{e(\mu)} \to \bar{\nu}_{\mu(e)})$ and $P(\bar{\nu}_e \to \bar{\nu}_\tau)$. For $\Delta m_{31}^2 > 0$, the $\bar{\nu}_{e(\mu)} \to \bar{\nu}_{\mu(e)}$ and $\bar{\nu}_e \to \bar{\nu}_\tau$ oscillations are suppressed by the Earth matter, while if $\Delta m_{31}^2 < 0$, the same conclusion holds for the $\nu_{e(\mu)} \to \nu_{\mu(e)}$ and $\nu_e \to \nu_\tau$, oscillations. The dependence on sgn(Δm_{31}^2) of the effects of Earth matter - enhancement or suppression - on the $\nu_{e(\mu)} \to \nu_{\mu(e)}$ and $\bar{\nu}_{e(\mu)} \to \bar{\nu}_{\mu(e)}$ oscillations taking place when the neutrinos traverse the Earth mantle, will be exploited in the current and planned long baseline and atmospheric neutrino oscillation experiments aiming, in particular, to determine the neutrino mass ordering (NOνA, PINGU, ORCA, Hyper-Kamiokande, DUNE, INO).

The discussed features of the Earth matter effects in the $\nu_{\mu(e)} \to \nu_{e(\mu)}$ and $\bar{\nu}_{\mu(e)} \to \bar{\nu}_{e(\mu)}$ oscillation probabilities for neutrinos with a path length in the Earth mantle of 7330 km and for $\Delta m_{31}^2 > 0$, $\sin^2 2\theta_{13} = 0.10$ and $\sin^2 2\theta_{23} = 1$ are illustrated in Fig. 14.7 (taken

from Ref. 194). The amplification of the $\nu_{\mu(e)} \to \nu_{e(\mu)}$ oscillation probability due to the Earth matter effect in the region of the resonance value of $E/\Delta m^2_{31}$ and the suppression of the $\bar{\nu}_{\mu(e)} \to \bar{\nu}_{e(\mu)}$ oscillation probability in the same region are clearly seen in the figure.
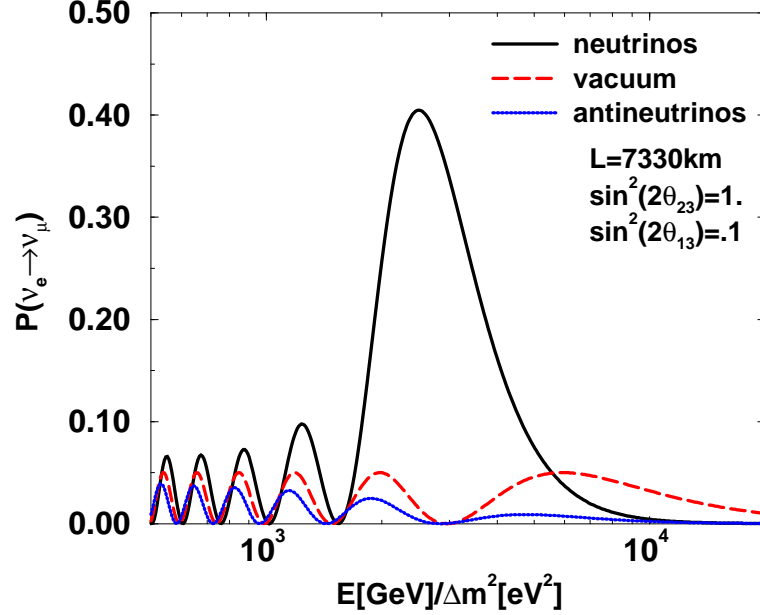

Figure 14.7: The $\nu_{e(\mu)} \to \nu_{\mu(e)}$ and $\bar{\nu}_{e(\mu)} \to \bar{\nu}_{\mu(e)}$ oscillation probabilities given in Eq. (14.65), $P(\nu_e \to \nu_\mu) = P(\nu_\mu \to \nu_e)$ (black solid line) and $P(\bar{\nu}_e \to \bar{\nu}_\mu) = P(\bar{\nu}_\mu \to \bar{\nu}_e)$ (blue solid line), as functions of $E/\Delta m^2$ for $\Delta m^2 \equiv \Delta m^2_{31} > 0$, $\sin^2 2\theta_{13} = 0.10$ and $\sin^2 2\theta_{23} = 1$. The figure is obtained for neutrinos crossing the Earth mantle along a path with length of $L = 7330$ km. The corresponding vacuum oscillation probability $P^{vac}(\nu_{e(\mu)} \to \nu_{\mu(e)}) = P^{vac}(\bar{\nu}_{e(\mu)} \to \bar{\nu}_{\mu(e)})$ is also shown (red dashed line). For $\Delta m^2 \equiv \Delta m^2_{31} < 0$, the black and blue solid lines will correspond respectively to the probabilities $P(\bar{\nu}_{e(\mu)} \to \bar{\nu}_{\mu(e)})$ and $P(\nu_{e(\mu)} \to \nu_{\mu(e)})$ (from Ref. 194).

In the case of neutrinos crossing the Earth core, new resonance-like effects become possible in the $\nu_\mu \to \nu_e$ and $\nu_e \to \nu_{\mu(\tau)}$ (or $\bar{\nu}_\mu \to \bar{\nu}_e$ and $\bar{\nu}_e \to \bar{\nu}_{\mu(\tau)}$) transitions [189–191,195–197]. For $\Delta m^2_{31} > 0$ and certain values of $\sin^2\theta_{13} \lesssim 0.05$ we can have [196] $P^{2\nu}_m(\Delta m^2_{31}, \theta_{13}) \cong 1$, and correspondingly maximal $P^{3\nu}_m(\nu_e \to \nu_\mu) = P^{3\nu}_m(\nu_\mu \to \nu_e) \cong s^2_{23}$, only due to the effect of maximal constructive interference between the amplitudes of the $\nu_e \to \nu'$ transitions in the Earth mantle and in the Earth core. The effect differs from the MSW one and the enhancement happens in the case of interest at a value of the energy between the MSW resonance energies corresponding to the density in the mantle and that of the core, or at a value of the resonance density N^{res}_e which lies between the values of N_e in the mantle and in the core [189]. In Refs. [189,190] the enhancement was called "neutrino oscillation length resonance (NOLR)", while in

Refs. [191,195] the term "parametric resonance" for the same effect was used [198]. The *mantle-core enhancement effect (or NOLR)* is caused by the existence (for a given neutrino trajectory through the Earth core) of points of resonance-like maximal neutrino conversion, $P_m^{2\nu}(\Delta m_{31}^2, \theta_{13}) = 1$, in the corresponding space of neutrino oscillation parameters [196]. For $\Delta m_{31}^2 < 0$ the mantle-core enhancement can take place for the antineutrino transitions, $\bar{\nu}_\mu \to \bar{\nu}_e$ and $\bar{\nu}_e \to \bar{\nu}_{\mu(\tau)}$. For neutrinos crossing the Earth core, analytic expressions for $P_m^{2\nu}(\Delta m_{31}^2, \theta_{13})$ and κ, $A_m^{2\nu}$ were derived in the two-layer constant density approximation for the Earth density distribution in [189] and [190], respectively.

A rather complete set of values of $\Delta m_{31}^2/E > 0$ and $\sin^2 2\theta_{13}$ for which $P_m^{2\nu}(\Delta m_{31}^2, \theta_{13}) = 1$ was found in Ref. 196. In the two-layer constant density approximation, the values of $\Delta m_{31}^2/E > 0$ and $\sin^2 2\theta_{13}$ at which $P_m^{2\nu}(\Delta m_{31}^2, \theta_{13}) = 1$ can be derived as solutions of the following system of equations [196]:

$$\tan \phi^{\mathrm{man}} = \pm \sqrt{\frac{-\cos 2\theta_{13}^{core}}{\cos(2\theta_{13}^{core} - 4\theta_{13}^{man})}} \,, \tag{14.69}$$

$$\tan \phi^{\mathrm{core}} = \pm \frac{\cos 2\theta_{13}^{man}}{\sqrt{-\cos(2\theta_{13}^{core})\cos(2\theta_{13}^{core} - 4\theta_{13}^{man})}} \,, \tag{14.70}$$

where the signs in the two equations are correlated, $2\phi^{\mathrm{man}} = (E_3^m - E_1^m)^{man} L^{man}$, $2\phi^{\mathrm{core}} = (E_3^m - E_1^m)^{core} L^{core}$, $2L^{man}$ and L^{core} are the neutrino path lengths in the Earth mantle and the core, and θ_{13}^{man} and θ_{13}^{core} are the values of the angle θ_{13} in the mantle and in the core. The expressions for $(E_3^m - E_1^m)^{man}$ $((E_3^m - E_1^m)^{core})$ and θ_{13}^{man} (θ_{13}^{core}) can be obtained respectively from Eq. (14.61) and Eq. (14.59) by setting $\theta = \theta_{13}$, $\Delta m^2 = \Delta m_{31}^2$, $N_e^{res} = N_{e31}^{res} = \Delta m_{31}^2 \cos 2\theta_{13}/(2E\sqrt{2}G_F)$ and $N_e = \tilde{N}_e^{man}(\theta_n)$ $(N_e = \tilde{N}_e^{core}(\theta_n))$.

The location of the points where $P_m^{2\nu}(\Delta m_{31}^2, \theta_{13}) = 1$ in the $\Delta m_{31}^2/E - \sin^2 2\theta_{13}$ plane determines the regions in the plane where $P_m^{2\nu}(\Delta m_{31}^2, \theta_{13})$ is large, $P_m^{2\nu}(\Delta m_{31}^2, \theta_{13}) \gtrsim 0.5$. These regions vary slowly with the nadir angle, being remarkably wide in the nadir angle and rather wide in the neutrino energy [196], so that the transitions of interest can produce noticeable effects in the measured observables. For $\sin^2 \theta_{13} \lesssim 0.05$, there are two sets of values of $(\Delta m_{31}^2/E, \sin^2 \theta_{13})$ for which $P_m^{2\nu}(\Delta m_{31}^2, \theta_{13}) = 1$, and thus two regions in $\Delta m_{31}^2/E - \sin^2 2\theta_{13}$ plane where $P_m^{2\nu}(\Delta m_{31}^2, \theta_{13}) \gtrsim 0.5$. For $\Delta m_{31}^2 = 2.5 \times 10^{-3}$ eV^2 and nadir angle, *e.g.*, $\theta_n = 0$ (Earth center crossing neutrinos), we have $P_m^{2\nu}(\Delta m_{31}^2, \theta_{13}) = 1$ at $(E, \sin^2 2\theta_{13}) = $(3.4 GeV,0.034) and (5.2 GeV,0.15). At the same time for $E = $3.4 GeV (5.2 Gev), the probability $P_m^{2\nu}(\Delta m_{31}^2, \theta_{13}) \gtrsim 0.5$ for the values of $\sin^2 2\theta_{13}$ from the interval $0.02 \lesssim \sin^2 2\theta_{13} \lesssim 0.10$ $(0.04 \lesssim \sin^2 2\theta_{13} \lesssim 0.26)$. Similar results hold for neutrinos crossing the Earth core along the trajectories with $\theta_n \neq 0$ (for further details see the last article in Ref. 196; see also the last article in Ref. 197).

The mantle-core enhancement of $P_m^{2\nu}$ (or $\bar{P}_m^{2\nu}$) is relevant, in particular, for the searches of sub-dominant $\nu_{e(\mu)} \to \nu_{\mu(e)}$ (or $\bar{\nu}_{e(\mu)} \to \bar{\nu}_{\mu(e)}$) oscillations of atmospheric neutrinos having energies $E \gtrsim 2$ GeV and crossing the Earth core on the way to the detector (see Ref. 189 to Ref. 197 and the references quoted therein).

The effects of Earth matter on the oscillations of atmospheric and accelerator neutrinos have not been observed so far. At present there are no compelling evidences for oscillations of the atmospheric ν_e and/or $\bar{\nu}_e$.

In the case of oscillations of atmospheric neutrinos in the Earth one has to take into account also the following considerations. The fluxes of atmospheric $\nu_{e,\mu}$ of energy E, which reach the detector after crossing the Earth along a given trajectory specified by the value of θ_n, $\Phi_{\nu_{e,\mu}}(E, \theta_n)$, are given by the following expressions in the case of the 3-neutrino oscillations under discussion [190,191]:

$$\Phi_{\nu_e}(E, \theta_n) \cong \Phi_{\nu_e}^0 \left(1 + [s_{23}^2 r - 1] \ P_m^{2\nu}\right), \tag{14.71}$$

$$\Phi_{\nu_\mu}(E, \theta_n) \cong \Phi_{\nu_\mu}^0 \left(1 + s_{23}^4[(s_{23}^2 \ r)^{-1} - 1]P_m^{2\nu} - 2c_{23}^2 s_{23}^2 \left[1 - Re \ (e^{-i\kappa} A_m^{2\nu}(\nu_\tau \to \nu_\tau))\right]\right), \tag{14.72}$$

where $\Phi_{\nu_{e(\mu)}}^0 = \Phi_{\nu_{e(\mu)}}^0(E, \theta_n)$ is the $\nu_{e(\mu)}$ flux in the absence of neutrino oscillations and

$$r \equiv r(E, \theta_n) \equiv \frac{\Phi_{\nu_\mu}^0(E, \theta_n)}{\Phi_{\nu_e}^0(E, \theta_n)} \quad . \tag{14.73}$$

It follows from the global analyses of the neutrino oscillation data that the neutrino mixing parameter s_{23}^2 lies (at 3σ CL) in the interval (0.38 - 0.64). For NO (IO) neutrino mass spectrum, the two groups which performed the most recent global analyses, obtained the following best values of s_{23}^2: 0.425 (0.589) [58] and 0.441 (0.587) [59]. For the predicted ratio $r(E, \theta_n)$ of the atmospheric ν_μ and ν_e fluxes for i) the Earth core crossing and ii) only mantle crossing neutrinos, having trajectories for which $0.3 \lesssim \cos\theta_n \le 1.0$, one has [199] $r(E, \theta_n) \cong (2.6 \div 4.5)$ for neutrinos giving the main contribution to the multi-GeV samples, $E \cong (2 \div 10)$ GeV. Thus, for $s_{23}^2 = 0.5$ (0.64) one finds for the multi-GeV neutrinos: $s_{23}^4[1 - (s_{23}^2 \ r(E, \theta_z))^{-1}] \cong 0.06 - 0.14$ (0.16 − 0.27) and $(s_{23}^2 \ r(E, \theta_z) - 1) \cong 0.3 - 1.3$ (0.66 − 1.9). Thus, the impact of the possible enhancement of $P_m^{2\nu} \cong 1$ would be largest for the flux of multi-GeV ν_e, $\Phi_{\nu_e}(E, \theta_n)$, traversing the Earth. As the preceding discussion suggests and detailed calculations show (see the first two articles quoted in Ref. 197), the sensitivity of the atmospheric neutrino experiments to the neutrino mass ordering depends strongly on the chosen value of $\sin^2\theta_{23}$ from its 3σ allowed range: it is maximal (minimal) for the maximal (minimal) allowed value of $\sin^2\theta_{23}$.

For water Cerenkov detectors, the charged current (CC) $\nu_l - N$ interaction cross section for multi-GeV neutrinos is approximately by a factor of 2 bigger than the $\bar{\nu}_l - N$ CC interaction cross section. Since these detectors do not distinguish between the neutrino and anti-neutrino induced CC events, determining that the neutrino mass spectrum is with inverted ordering would require roughly by a factor of 2 longer period of data acquisition than if the spectrum were with normal ordering.

The effects under discussion are larger, in general, for the multi-GeV neutrinos than for the sub-GeV neutrinos having energies $E \cong (0.1 - 1.0)$ GeV. Indeed, for the sub-GeV ν_e flux one finds in the limit of negligible θ_{13} [201]: $\Phi_{\nu_e}(E, \theta_n) \cong \Phi_{\nu_e}^0(1 + [c_{23}^2 r - 1]\bar{P}_m^{2\nu})$,

where $\bar{P}_m^{2\nu} \equiv \bar{P}_m^{2\nu}(\Delta m_{21}^2, \theta_{12}; E, \theta_n)$ is the probability of the 2-neutrino oscillations in the Earth due to Δm_{21}^2 and 2-neutrino mixing with angle θ_{12}. For the neutrinos giving contribution to the sub-GeV samples of Super-Kamiokande events one has [199] $r(E, \theta_z) \cong 2.0$. If $s_{23}^2 = 0.5$ and $r(E, \theta_z) \cong 2.0$, we get $(c_{23}^2 \ r(E, \theta_z) - 1) \cong 0$, and the possible effects of the $\nu_\mu \to \nu_e$ and $\nu_e \to \nu_{\mu(\tau)}$ transitions on the ν_e flux, and correspondingly in the sub-GeV $e-$like samples of events, would be rather strongly suppressed independently of the values of the corresponding transition probabilities.

The same conclusions are valid for the effects of oscillations on the fluxes of, and event rates due to, atmospheric antineutrinos $\bar{\nu}_e$ and $\bar{\nu}_\mu$. The formulae for anti-neutrino fluxes and oscillation probabilities are analogous to those for neutrinos (see, *e.g.*, Refs. [190,191,197,201]) .

The expression for the probability of the $\nu_\mu \to \nu_e$ oscillations taking place in the Earth mantle in the case of 3-neutrino mixing, in which both neutrino mass squared differences Δm_{21}^2 and Δm_{31}^2 contribute and the CP violation effects due to the Dirac phase in the neutrino mixing matrix are taken into account, has the following form in the constant density approximation and keeping terms up to second order in the two small parameters $|\alpha| \equiv |\Delta m_{21}^2|/|\Delta m_{31}^2| \ll 1$ and $\sin^2 \theta_{13} \ll 1$ [202]:

$$P_m^{3\nu \ man}(\nu_\mu \to \nu_e) \cong P_0 + P_{\sin \delta} + P_{\cos \delta} + P_3 \,. \tag{14.74}$$

Here

$$P_0 = \sin^2 \theta_{23} \ \frac{\sin^2 2\theta_{13}}{(A-1)^2} \ \sin^2[(A-1)\Delta]$$

$$P_3 = \alpha^2 \ \cos^2 \theta_{23} \ \frac{\sin^2 2\theta_{12}}{A^2} \ \sin^2(A\Delta) \,, \tag{14.75}$$

$$P_{\sin \delta} = -\alpha \ \frac{8 \, J_{CP}}{A(1-A)} \ (\sin \Delta) \, (\sin A\Delta) \, (\sin[(1-A)\Delta]) \,, \tag{14.76}$$

$$P_{\cos \delta} = \alpha \ \frac{8 \, J_{CP} \, \cot \delta}{A(1-A)} \ (\cos \Delta) \, (\sin A\Delta) \, (\sin[(1-A)\Delta]) \,, \tag{14.77}$$

where

$$\alpha = \frac{\Delta m_{21}^2}{\Delta m_{31}^2} \,, \quad \Delta = \frac{\Delta m_{31}^2 \, L}{4E} \,, \quad A = \sqrt{2} G_{\rm F} N_e^{man} \frac{2E}{\Delta m_{31}^2} \,, \tag{14.78}$$

$\cot \delta = J_{CP}^{-1} \mathrm{Re}(U_{\mu 3} U_{e3}^* U_{e2} U_{\mu 2}^*) \propto \cos \delta$, and we recall that $J_{CP} = \mathrm{Im}(U_{\mu 3} U_{e3}^* U_{e2} U_{\mu 2}^*)$. The analytic expression for $P_m^{3\nu \ man}(\nu_\mu \to \nu_e)$ given above is valid for [202] neutrino path lengths in the mantle ($L \leq 10660$ km) satisfying $L \lesssim 10560$ km $E[\mathrm{GeV}] \, (7.6 \times 10^{-5} \ \mathrm{eV}^2/\Delta m_{21}^2)$, and energies $E \gtrsim 0.34$ GeV$(\Delta m_{21}^2/7.6 \times 10^{-5} \ \mathrm{eV}^2) \, (1.4 \ \mathrm{cm}^{-3} N_A/N_e^{man})$. The expression for the $\bar{\nu}_\mu \to \bar{\nu}_e$ oscillation probability can be obtained formally from that for $P_m^{3\nu \ man}(\nu_\mu \to \nu_e)$ by making the changes $A \to -A$ and $J_{CP} \to -J_{CP}$, with $J_{CP} \cot \delta \equiv \mathrm{Re}(U_{\mu 3} U_{e3}^* U_{e2} U_{\mu 2}^*)$ remaining unchanged. The term $P_{\sin \delta}$ in $P_m^{3\nu \ man}(\nu_\mu \to \nu_e)$ would be equal to zero if the Dirac phase in the neutrino

mixing matrix U possesses a CP-conserving value. Even in this case, however, we have $A_{CP}^{(e\mu)\ man} \equiv (P_m^{3\nu\ man}(\nu_\mu \to \nu_e) - P_m^{3\nu\ man}(\bar{\nu}_\mu \to \bar{\nu}_e)) \neq 0$ due to the effects of the Earth matter. It will be important to experimentally disentangle the effects of the Earth matter and of J_{CP} in $A_{CP}^{(e\mu)\ man}$: this will allow to get information about the Dirac CP violation phase in U. This can be done, in principle, by studying the energy dependence of $P_m^{3\nu\ man}(\nu_\mu \to \nu_e)$ and $P_m^{3\nu\ man}(\bar{\nu}_\mu \to \bar{\nu}_e)$. Since the sign of $\Delta m_{31(32)}^2$ determines for given L whether the probability $P_m^{3\nu\ man}(\nu_\mu \to \nu_e)$ or $P_m^{3\nu\ man}(\bar{\nu}_\mu \to \bar{\nu}_e)$, as a function of energy, can be resonantly enhanced or suppressed by the matter effects, the study of the energy dependence of $P_m^{3\nu\ man}(\nu_\mu \to \nu_e)$ and/or of $P_m^{3\nu\ man}(\bar{\nu}_\mu \to \bar{\nu}_e)$ can provide also information on $\mathrm{sgn}(\Delta m_{31(32)}^2)$. In the vacuum limit of $N_e^{man} = 0$ ($A = 0$) we have $A_{CP}^{(e\mu)\ man} = A_{CP}^{(e\mu)}$ (see Eq. (14.42)) and only the term $P_{\sin\delta}$ contributes to the asymmetry $A_{CP}^{(e\mu)}$.

The preceding remarks apply also to the probabilities $P_m^{3\nu\ man}(\nu_e \to \nu_\mu)$ and $P_m^{3\nu\ man}(\bar{\nu}_e \to \bar{\nu}_\mu)$. The probability $P_m^{3\nu\ man}(\nu_e \to \nu_\mu)$, for example, can formally be obtained from the expression for the probability $P_m^{3\nu\ man}(\nu_\mu \to \nu_e)$ by changing the sign of the term $P_{\sin\delta}$.

The expression for the probability $P_m^{3\nu\ man}(\nu_\mu \to \nu_e)$ given in Eq. (14.74) and the corresponding expression for $P_m^{3\nu\ man}(\bar{\nu}_\mu \to \bar{\nu}_e)$ can be used for the interpretation of the data of the past, current, and future planned long baseline oscillation experiments MINOS/MINOS+, T2K, NOνA, DUNE [93] and T2HK [94].

14.8.2. *Oscillations (flavour conversion) of solar neutrinos* :

14.8.2.1. *Qualitative analysis:*

Consider next the oscillations of solar ν_e while they propagate from the central part of the Sun, where they are produced, to the surface of the Sun [27,188]   (see also Ref. 26 and, *e.g.*, Ref. 203) Details concerning the production, spectrum, magnitude and particularities of the solar neutrino flux were discussed in Section 14.6, while the methods of detection of solar neutrinos, description of solar neutrino experiments and of the data they provided will be discussed in the next section (see also Ref. 204). The electron number density N_e changes considerably along the neutrino path in the Sun: it decreases monotonically from the value of $\sim 100\ \mathrm{cm}^{-3}\ N_A$ in the center of the Sun to 0 at the surface of the Sun. According to the contemporary solar models (see, *e.g.*, Ref. 204) N_e decreases approximately exponentially in the radial direction towards the surface of the Sun:

$$N_e(t) = N_e(t_0) \exp\left\{-\frac{t - t_0}{r_0}\right\}\ , \qquad (14.79)$$

where $(t - t_0) \cong d$ is the distance traveled by the neutrino in the Sun, $N_e(t_0)$ is the electron number density at the point of ν_e production in the Sun, r_0 is the scale-height of the change of $N_e(t)$ and one has [204] $r_0 \sim 0.1 R_\odot$

Consider the case of 2-neutrino mixing, Eq. (14.58). Obviously, if N_e changes with t (or equivalently with the distance) along the neutrino trajectory, the matter-eigenstates,

their energies, the mixing angle and the oscillation length in matter, become, through their dependence on N_e, also functions of t: $|\nu_{1,2}^m\rangle = |\nu_{1,2}^m(t)\rangle$, $E_{1,2}^m = E_{1,2}^m(t)$, $\theta_m = \theta_m(t)$ and $L_m = L_m(t)$. It is not difficult to understand qualitatively the possible behavior of the neutrino system when solar neutrinos propagate from the center to the surface of the Sun if one realizes that one is dealing effectively with a two-level system whose Hamiltonian depends on time and admits "jumps" from one level to the other [205](see Eq. (14.56)). Consider the case of $\Delta m^2 \cos 2\theta > 0$. Let us assume first for simplicity that the electron number density at the point of a solar ν_e production in the Sun is much bigger than the resonance density, $N_e(t_0) \gg N_e^{res}$. Actually, this is one of the cases relevant to the solar neutrinos. In this case we have $\theta_m(t_0) \cong \pi/2$ and the state of the electron neutrino in the initial moment of the evolution of the system practically coincides with the heavier of the two matter-eigenstates:

$$|\nu_e\rangle \;\cong\; |\nu_2^m(t_0)\rangle\,. \tag{14.80}$$

Thus, at t_0 the neutrino system is in a state corresponding to the "level" with energy $E_2^m(t_0)$. When neutrinos propagate to the surface of the Sun they cross a layer of matter in which $N_e = N_e^{res}$: in this layer the difference between the energies of the two "levels" $(E_2^m(t) - E_1^m(t))$ has a minimal value on the neutrino trajectory (Eq. (14.61) and Eq. (14.63)). Correspondingly, the evolution of the neutrino system can proceed basically in two ways. First, the system can stay on the "level" with energy $E_2^m(t)$, *i.e.*, can continue to be in the state $|\nu_2^m(t)\rangle$ up to the final moment t_s, when the neutrino reaches the surface of the Sun. At the surface of the Sun $N_e(t_s) = 0$ and therefore $\theta_m(t_s) = \theta$, $|\nu_{1,2}^m(t_s)\rangle \equiv |\nu_{1,2}\rangle$ and $E_{1,2}^m(t_s) = E_{1,2}$. Thus, in this case the state describing the neutrino system at t_0 will evolve continuously into the state $|\nu_2\rangle$ at the surface of the Sun. Using Eq. (14.53) with $l = e$ and $x = \mu$, it is easy to obtain the probabilities to find ν_e and ν_μ at the surface of the Sun:

$$\begin{aligned} P(\nu_e \to \nu_e; t_s, t_0) &\cong |\langle \nu_e|\nu_2\rangle|^2 = \sin^2\theta \\ P(\nu_e \to \nu_\mu; t_s, t_0) &\cong |\langle \nu_\mu|\nu_2\rangle|^2 = \cos^2\theta\,. \end{aligned} \tag{14.81}$$

It is clear that under the assumption made and if $\sin^2\theta \ll 1$, practically a total $\nu_e \to \nu_\mu$ conversion is possible. This type of evolution of the neutrino system and the $\nu_e \to \nu_\mu$ transitions taking place during the evolution, are called [27] "adiabatic." They are characterized by the fact that the probability of the "jump" from the upper "level" (having energy $E_2^m(t)$) to the lower "level" (with energy $E_1^m(t)$), P', or equivalently the probability of the $\nu_2^m(t_0) \to \nu_1^m(t_s)$ transition, $P' \equiv P'(\nu_2^m(t_0) \to \nu_1^m(t_s))$, on the whole neutrino trajectory is negligible:

$$P' \equiv P'(\nu_2^m(t_0) \to \nu_1^m(t_s)) \cong 0 \;\; : \;\; \textit{adiabatic transitions}\,. \tag{14.82}$$

The second possibility is realized if in the resonance region, where the two "levels" approach each other most, the system "jumps" from the upper "level" to the lower "level" and after that continues to be in the state $|\nu_1^m(t)\rangle$ until the neutrino reaches the surface

of the Sun. Evidently, now we have $P' \equiv P'(\nu_2^m(t_0) \to \nu_1^m(t_s)) \sim 1$. In this case the neutrino system ends up in the state $|\nu_1^m(t_s)\rangle \equiv |\nu_1\rangle$ at the surface of the Sun and

$$
\begin{aligned}
P(\nu_e \to \nu_e; t_s, t_0) &\cong |\langle \nu_e | \nu_1 \rangle|^2 = \cos^2 \theta \\
P(\nu_e \to \nu_\mu; t_s, t_0) &\cong |\langle \nu_\mu | \nu_1 \rangle|^2 = \sin^2 \theta .
\end{aligned}
\tag{14.83}
$$

Obviously, if $\sin^2 \theta \ll 1$, practically no transitions of the solar ν_e into ν_μ will occur. The considered regime of evolution of the neutrino system and the corresponding $\nu_e \to \nu_\mu$ transitions are usually referred to as "extremely nonadiabatic."

Clearly, the value of the "jump" probability P' plays a crucial role in the the $\nu_e \to \nu_\mu$ transitions: it fixes the type of the transition and determines to a large extent the $\nu_e \to \nu_\mu$ transition probability [188,206,207]. We have considered above two limiting cases. Obviously, there exists a whole spectrum of possibilities since P' can have any value from 0 to $\cos^2 \theta$ [208,209]. In general, the transitions are called "nonadiabatic" if P' is non-negligible.

Numerical studies have shown [27] that solar neutrinos can undergo both adiabatic and nonadiabatic $\nu_e \to \nu_\mu$ transitions in the Sun and the matter effects can be substantial in the solar neutrino oscillations for 10^{-8} eV$^2 \lesssim \Delta m^2 \lesssim 10^{-4}$ eV^2, $10^{-4} \lesssim \sin^2 2\theta < 1.0$.

The condition of adiabaticity of the solar ν_e transitions in Sun can be written as [188,206]

$$
\gamma(t) \equiv \sqrt{2} G_F \frac{(N_e^{res})^2}{|\dot{N}_e(t)|} \tan^2 2\theta \left(1 + \tan^{-2} 2\theta_m(t) \right)^{\frac{3}{2}} \gg 1
$$
$$
\text{adiabatic transitions},
\tag{14.84}
$$

while if $\gamma(t) \lesssim 1$ the transitions are nonadiabatic (see also Ref. 209), where $\dot{N}_e(t) \equiv \frac{d}{dt} N_e(t)$. Condition in Eq. (14.84) implies that the $\nu_e \to \nu_{\mu(\tau)}$ transitions in the Sun will be adiabatic if $N_e(t)$ changes sufficiently slowly along the neutrino path. In order for the transitions to be adiabatic, condition in Eq. (14.84) has to be fulfilled at any point of the neutrino's path in the Sun.

14.8.2.2. *The solar ν_e survival probability:*

The system of evolution equations Eq. (14.56) can be solved exactly for N_e changing exponentially, Eq. (14.79), along the neutrino path in the Sun [208,210]. More specifically, the system in Eq. (14.56) is equivalent to one second order differential equation (with appropriate initial conditions). The latter can be shown [211] to coincide in form, in the case of N_e given by Eq. (14.79), with the Schroedinger equation for the radial part of the nonrelativistic wave function of the Hydrogen atom [212]. On the basis of the exact solution, which is expressed in terms of confluent hypergeometric functions, it was possible to derive a complete, simple and very accurate analytic description of the matter-enhanced transitions of solar neutrinos in the Sun for any values of Δm^2 and θ [26,208,209,213,214] (see also Refs. [27,188,207,215,216]) .

The probability that a ν_e, produced at time t_0 in the central part of the Sun, will not transform into $\nu_{\mu(\tau)}$ on its way to the surface of the Sun (reached at time t_s) is given by

$$P_\odot^{2\nu}(\nu_e \to \nu_e; t_s, t_0) = \bar{P}_\odot^{2\nu}(\nu_e \to \nu_e; t_s, t_0) + \ \ Oscillating \ \ terms. \tag{14.85}$$

Here

$$\bar{P}_\odot^{2\nu}(\nu_e \to \nu_e; t_s, t_0) \equiv \bar{P}_\odot = \frac{1}{2} + \left(\frac{1}{2} - \mathrm{P}'\right) \cos 2\theta_m(t_0) \cos 2\theta \ , \tag{14.86}$$

is the average survival probability for ν_e having energy $E \cong p$ [207], where

$$P' = \frac{\exp\left[-2\pi \mathrm{r}_0 \frac{\Delta m^2}{2E} \sin^2\theta\right] - \exp\left[-2\pi \mathrm{r}_0 \frac{\Delta m^2}{2E}\right]}{1 - \exp\left[-2\pi \mathrm{r}_0 \frac{\Delta m^2}{2E}\right]} \ , \tag{14.87}$$

is [208] the "jump" probability for exponentially varying N_e, and $\theta_m(t_0)$ is the mixing angle in matter at the point of ν_e production [215]. The expression for $\bar{P}_\odot^{2\nu}(\nu_e \to \nu_e; t_s, t_0)$ with P' given by Eq. (14.87) is valid for $\Delta m^2 > 0$, but for both signs of $\cos 2\theta \neq 0$ [208](see also Ref. [216]) ; it is valid for any given value of the distance along the neutrino trajectory and does not take into account the finite dimensions of the region of ν_e production in the Sun. This can be done by integrating over the different neutrino paths, *i.e.*, over the region of ν_e production.

The oscillating terms in the probability $P_\odot^{2\nu}(\nu_e \to \nu_e; t_s, t_0)$ [213,211] were shown [214] to be strongly suppressed for $\Delta m^2 \gtrsim 10^{-7}$ eV^2 by the various averagings one has to perform when analyzing the solar neutrino data. The current solar neutrino and KamLAND data suggest that $\Delta m^2 \cong 7.4 \times 10^{-5}$ eV^2. For $\Delta m^2 \gtrsim 10^{-7}$ eV^2, the averaging over the region of neutrino production in the Sun *etc.* renders negligible all interference terms which appear in the probability of ν_e survival due to the $\nu_e \leftrightarrow \nu_{\mu(\tau)}$ oscillations in vacuum taking place on the way of the neutrinos from the surface of the Sun to the surface of the Earth. Thus, the probability that ν_e will remain ν_e while it travels from the central part of the Sun to the surface of the Earth is effectively equal to the probability of survival of the ν_e while it propagates from the central part to the surface of the Sun and is given by the average probability $\bar{P}_\odot(\nu_e \to \nu_e; t_s, t_0)$ (determined by Eq. (14.86) and Eq. (14.87)). For this reason the solar ν_e transition into $\nu_{\mu(\tau)}$ is sometimes referred to as "solar neutrino flavour conversion".

If the solar ν_e transitions are adiabatic ($P' \cong 0$) and $\cos 2\theta_m(t_0) \cong -1$ (*i.e.*, $N_e(t_0)/|N_e^{res}| \gg 1, |\tan 2\theta|$, the ν_e are born "above" (in N_e) the resonance region), one has [27]

$$\bar{P}^{2\nu}(\nu_e \to \nu_e; t_s, t_0) \cong \frac{1}{2} - \frac{1}{2} \cos 2\theta. \tag{14.88}$$

The regime under discussion is realized for $\sin^2 2\theta \cong 0.84$ (suggested by the data, Sections 14.2 and 14.9.1), if $E/\Delta m^2$ lies approximately in the range $(2 \times 10^4 - 3 \times 10^7)$ MeV/eV^2 (see Ref. 209). This result is relevant for the interpretation of the Super-Kamiokande and SNO solar neutrino data. We see that depending on the sign

of $\cos 2\theta \neq 0$, $\bar{P}^{2\nu}(\nu_e \to \nu_e)$ is either bigger or smaller than $1/2$. It follows from the solar neutrino data that in the range of validity (in $E/\Delta m^2$) of Eq. (14.88) we have $\bar{P}^{2\nu}(\nu_e \to \nu_e) \cong 0.3$. Thus, the possibility of $\cos 2\theta \leq 0$ is ruled out by the data. Given the choice $\Delta m^2 > 0$ we made, the data imply that $\Delta m^2 \cos 2\theta > 0$.

If $E/\Delta m^2$ is sufficiently small so that $N_e(t_0)/|N_e^{res}| \ll 1$, we have $P' \cong 0$, $\theta_m(t_0) \cong \theta$ and the oscillations take place in the Sun as in vacuum [27]:

$$\bar{P}^{2\nu}(\nu_e \to \nu_e; t_s, t_0) \cong 1 - \frac{1}{2}\sin^2 2\theta\,, \tag{14.89}$$

which is the average two-neutrino vacuum oscillation probability. This expression describes with good precision the transitions of the solar pp neutrinos (Section 14.9.1). The extremely nonadiabatic ν_e transitions in the Sun, characterized by $\gamma(t) \ll 1$, are also described by the average vacuum oscillation probability (Eq. (14.89)) (for $\Delta m^2 \cos 2\theta > 0$ in this case we have (see *e.g.*, Refs. [208,209]) $\cos 2\theta_m(t_0) \cong -1$ and $P' \cong \cos^2 \theta$).

The probability of ν_e survival in the case 3-neutrino mixing takes a simple form for $|\Delta m^2_{31}| \cong 2.5 \times 10^{-3}$ eV$^2 \gg |\Delta m^2_{21}|$. Indeed, for the energies of solar neutrinos $E \lesssim 10$ MeV, N^{res} corresponding to $|\Delta m^2_{31}|$ satisfies $N^{res}_{e31} \gtrsim 10^3$ cm^{-3} N$_A$ and is by a factor of 10 bigger than N_e in the center of the Sun. As a consequence, the oscillations due to Δm^2_{31} proceed as in vacuum. The oscillation length associated with $|\Delta m^2_{31}|$ satisfies $L^v_{31} \lesssim 10$ km $\ll \Delta R$, ΔR being the dimension of the region of ν_e production in the Sun. We have for the different components of the solar ν_e flux [204] $\Delta R \cong (0.04 - 0.20)R_\odot$. Therefore the averaging over ΔR strongly suppresses the oscillations due to Δm^2_{31} and we get [192,217]:

$$P^{3\nu}_\odot \cong \sin^4 \theta_{13} + \cos^4 \theta_{13}\ P^{2\nu}_\odot(\Delta m^2_{21}, \theta_{12}; N_e \cos^2 \theta_{13})\,, \tag{14.90}$$

where $P^{2\nu}_\odot(\Delta m^2_{21}, \theta_{12}; N_e \cos^2 \theta_{13})$ is given by Eq. (14.85) to Eq. (14.87) in which $\Delta m^2 = \Delta m^2_{21}$, $\theta = \theta_{12}$ and the solar e^- number density N_e is replaced by $N_e \cos^2 \theta_{13}$. As can be shown [192,217], $P^{2\nu}_\odot(\Delta m^2_{21}, \theta_{12}; N_e \cos^2 \theta_{13})$ and $(1 - P^{2\nu}_\odot(\Delta m^2_{21}, \theta_{12}; N_e \cos^2 \theta_{13}))$ are respectively the average probabilities of solar ν_e survival and of the 2-neutrino $\nu_e \to \nu'' \equiv (c_{23}\nu_\mu - s_{23}\nu_\tau)$ transitions in the Sun. Thus, in the case of 3-neutrino mixing, the solar ν_e undergo transitions into the mixture $(c_{23}\nu_\mu - s_{23}\nu_\tau)$ of ν_μ and ν_τ.

The solar ν_e transitions observed by the Super-Kamiokande and SNO experiments are described, as it follows from Eq. (14.88) and Eq. (14.90), approximately by:

$$P^{3\nu}_\odot \cong \sin^4 \theta_{13} + \cos^4 \theta_{13}\ \sin^2 \theta_{12}\,. \tag{14.91}$$

The data show that $P^{3\nu}_\odot \cong 0.3$, which is a strong evidence for matter effects in the solar ν_e transitions [218] since in the case of oscillations in vacuum $P^{3\nu}_\odot \cong \sin^4 \theta_{13} + (1 - 0.5\sin^2 2\theta_{12})\cos^4 \theta_{13} \gtrsim 0.52$, where we have used $\sin^2 \theta_{13} \lesssim 0.0240$ and $\sin^2 2\theta_{12} \lesssim 0.915$ (see Section 14.2).

The analytic expression for the solar ν_e survival probability, Eq. (14.90), with $P^{2\nu}_\odot(\Delta m^2_{21}, \theta_{12}; N_e \cos^2 \theta_{13})$ given by Eq. (14.85) to Eq. (14.87) and the prescriptions

described above, provides a particularly precise description of the solar ν_e survival (and transitions) in the Sun - the results differ by a few percent from those obtained by solving numerically the relevant system of evolution equations using the electron number density distribution in the Sun provided by the standard solar models - if one uses as input in the calculations a "running" value of the scale-height r_0 [209], *i.e.*, if for each given values of $E/\Delta m_{21}^2$ and θ_{12} one finds the resonance density $N^{res} = N^{res}(E/\Delta m_{21}^2, \theta_{12})$, calculates the scale-height parameter $r_0 = N_e(r)/(dN_e(r)/dr)$ at the point in the Sun where $N_e \cos^2\theta_{13} = N^{res}(E/\Delta m_{21}^2, \theta_{12})$ employing the solar electron number density distribution $N_e = N_e(r)$ given by the standard solar models [204], r being the distance from the center of the Sun.

14.8.2.3. *The day-night asymmetry:*

When the solar neutrinos reaching a detector travel through the Earth at night, a partial regeneration of the flux of the solar ν_e is possible due to the inverse Earth matter-enhanced process [219,220] $\nu_{\mu(\tau)} \to \nu_e$. This can lead to a difference between the solar neutrino induced charged current day and night event rates in the detector, R_D and R_N, *i.e.*, to a non-zero day-night asymmetry $A_{D-N} = 2(R_D - R_N)/(R_D + R_N)$. An observation of $A_{D-N} \neq 0$ will be an unambiguous proof of the presence of Earth matter effects in the transitions of solar neutrinos taking place when the neutrinos traverse the Earth: in the absence of the effects of the Earth matter we have $A_{D-N} = 0$.

In the case of two-neutrino mixing, *i.e.*, neglecting the effects of the non-zero $\sin\theta_{13}$, the probability that an electron neutrino produced in the Sun will not be converted into $\nu_{\mu(\tau)}$ when it propagates in the Sun and traverses the Earth on the way to the detector is given by the following simple expression [219]:

$$P_{SE}^{2\nu}(\nu_e \to \nu_e) = \bar{P}_{\odot}^{2\nu}(\nu_e \to \nu_e) + (1 - 2\,\bar{P}_{\odot}^{2\nu}(\nu_e \to \nu_e))\frac{P_{e2} - \sin^2\theta_{12}}{\cos 2\theta_{12}}, \qquad (14.92)$$

where $\bar{P}_{\odot}^{2\nu}(\nu_e \to \nu_e)$ is the average probability of solar ν_e survival in the Sun given in Eq. (14.86) and Eq. (14.87) (with $\theta = \theta_{12}$ and $\Delta m^2 = \Delta m_{21}^2 > 0$) and $P_{e2} = |A(\nu_2 \to \nu_e)|^2$ is the probability of the $\nu_2 \to \nu_e$ transition after the ν_e have left the Sun, *i.e.*, of the $\nu_2 \to \nu_e$ transition in the Earth. For solar neutrinos crossing only the Earth mantle along a trajectory with nadir angle θ_n, the amplitude $A(\nu_2 \to \nu_e)$ in the constant density approximation, has the form:

$$A(\nu_2 \to \nu_e) = \sin\theta_{12} + (e^{-i\varphi^{man}} - 1)\cos(\theta_{12} - \theta_{12}^{man})\sin\theta_{12}^{man}, \qquad (14.93)$$

where $\varphi^{man} = (E_2^m - E_1^m)^{man}2L^{man}$, $(E_2^m - E_1^m)^{man}$ being the relevant difference of the energies of the two matter-eigenstate neutrinos in the Earth mantle and θ_{12}^{man} is the mixing angle in the mantle which coincides in vacuum with θ_{12}. The quantities $(E_2^m - E_1^m)^{man}$ and θ_{12}^{man} can be obtained from Eq. (14.61) and Eq. (14.59) by setting $\theta = \theta_{12}$, $\Delta m^2 = \Delta m_{21}^2$, $N_e^{res} = N_{e21}^{res} = \Delta m_{21}^2 \cos 2\theta_{12}/(2E\sqrt{2}G_F)$ and $N_e = \tilde{N}_e^{man}(\theta_n)$. The two layer constant density approximation expressions for $A(\nu_2 \to \nu_e)$ and P_{e2} for solar neutrinos crossing the Earth core at night were derived and can be found in Ref. 189.

During the day, when the neutrinos do not cross the Earth, $P_{e2} = \sin^2 \theta_{12}$ and we have $P_{SE}^{2\nu}(\nu_e \to \nu_e) = \bar{P}_{\odot}^{2\nu}(\nu_e \to \nu_e)$. For Earth crossing neutrinos at night $P_{e2} \neq \sin^2 \theta_{12}$ due to the Earth matter effect and $P_{SE}^{2\nu}(\nu_e \to \nu_e) \neq \bar{P}_{\odot}^{2\nu}(\nu_e \to \nu_e)$.

Detailed calculations of the day-night asymmetry $A_{D-N} \neq 0$ for the solar neutrino detectors Super-Kamiokande, SNO and BOREXINO have been performed, *e.g.*, in Refs. [221]. In Refs. [222] the effects of a $\theta_{13} \neq 0$ on the predictions for the asymmetry A_{D-N} were taken into account. The results of these calculations showed that for the experimentally determined current values of Δm_{21}^2 and θ_{12}, the predicted values of the asymmetry A_{D-N} for the SNO and BOREXINO experiments are below the sensitivity of these experiments. For the Super-Kamiokande detector an asymmetry $A_{D-N} \sim -3\%$ was predicted.

14.9. Neutrino oscillation experiments

14.9.1. *Solar neutrino experiments* :

So far, solar neutrinos have been observed by chlorine (Homestake) [6] and gallium (SAGE [8], GALLEX [9,10], and GNO [11]) radiochemical detectors, water Cherenkov detectors using light water (Kamiokande [223,7] and Super-Kamiokande [224–228]) and heavy water (SNO [13,14,229,230]) , and liquid scintillation detectors (Borexino [231–237] and KamLAND [238,239]) .

A pioneering solar neutrino experiment by R. Davis, Jr. and collaborators at Homestake using the ^{37}Cl - ^{37}Ar method proposed by B. Pontecorvo [240] started in the late 1960s. This experiment exploited ν_e absorption on ^{37}Cl nuclei followed by the produced ^{37}Ar decay through orbital e^- capture,

$$\nu_e + {}^{37}\text{Cl} \to {}^{37}\text{Ar} + e^- \quad (\text{threshold } 814 \text{ keV}). \tag{14.94}$$

Note that ν_e absorption reactions on nuclei are CC reactions. The detector contained 615 tons of tetrachloroethylene, C_2Cl_4. The ^{37}Ar atoms produced are radioactive, with a half life ($\tau_{1/2}$) of 34.8 days. After an exposure of the detector for two to three times $\tau_{1/2}$, the reaction products were chemically extracted and introduced into a low-background proportional counter, where they were counted for a sufficiently long period to determine the exponentially decaying signal and a constant background. Solar-model calculations [124] predict that the dominant contribution in the chlorine experiment come from ^{8}B neutrinos, the second to the dominant from ^{7}Be neutrinos, with *pep*, ^{13}N, and ^{15}O neutrinos also giving additional subdominant contributions.

Gallium experiments (GALLEX and GNO at Gran Sasso in Italy and SAGE at Baksan in Russia) utilized the reaction

$$\nu_e + {}^{71}\text{Ga} \to {}^{71}\text{Ge} + e^- \quad (\text{threshold } 233 \text{ keV}), \tag{14.95}$$

which is sensitive to the most abundant *pp* solar neutrinos. The solar-model calculations [124] predict that more than 80% of the capture rate in gallium is due to low energy *pp* and ^{7}Be solar neutrinos with the *pp* rate being about twice the ^{7}Be rate. The

^{71}Ge atoms decay through electron capture with a half life ($\tau_{1/2}$) of 11.43 days. SAGE used approximately 50 tons of liquid gallium metal as a target. GALLEX used 101 tons of GaCl$_3$, containing 30.3 tons of gallium. Both experiments used natural gallium, containing 39.9% of ^{71}Ga isotope. SAGE started measurement from December, 1989. GALLEX experiment had been conducted between 1991 and 1997. Since April, 1998, a newly defined collaboration, GNO (Gallium Neutrino Observatory) continued the gallium experiment at Gran Sasso until April 2003.

Both GALLEX [241] and SAGE [242] tested their detectors using intense ^{51}Cr radioactive sources with known activities. Low energy neutrinos relevant to test the gallium experiments (~ 750 keV and ~ 320 keV neutrinos) are emitted from decays of ^{51}Cr.

In 1987, the Kamiokande experiment at Kamioka in Japan succeeded in real-time solar neutrino observation, utilizing νe scattering,

$$\nu_x + e^- \rightarrow \nu_x + e^- \, , \tag{14.96}$$

in a 3,000-ton water-Cherenkov detector. This experiment took advantage of the directional correlation between the incoming neutrino and the recoil electron. This feature greatly helps the clear separation of the solar-neutrino signal from the background. The Kamiokande result gave the first direct evidence that neutrinos come from the direction of the Sun [223]. In 1996, the high-statistics Super-Kamiokande experiment [224–228] with a 50-kton water Cherenkov detector replaced the Kamiokande experiment. Due to the high thresholds (recoil-electron total energy of 7 MeV in Kamiokande and 4 MeV at present in Super-Kamiokande) the experiments observe pure ^{8}B solar neutrinos. It should be noted that the reaction (Eq. (14.96)) is sensitive to all active neutrinos, $x = e$, μ, and τ. However, the sensitivity to ν_μ and ν_τ is smaller than the sensitivity to ν_e since $\sigma(\nu_{\mu,\tau}e) \approx 0.16\,\sigma(\nu_e e)$.

In 1999, a new real time solar-neutrino experiment, SNO (Sudbury Neutrino Observatory), in Canada started observation. This experiment used 1000 tons of ultra-pure heavy water (D$_2$O) contained in a spherical acrylic vessel, surrounded by an ultra-pure H$_2$O shield. SNO measured ^{8}B solar neutrinos via the CC and NC reactions

$$\nu_e + d \rightarrow e^- + p + p \qquad \text{(CC)}\,, \tag{14.97}$$

and

$$\nu_x + d \rightarrow \nu_x + p + n \qquad \text{(NC)}\,, \tag{14.98}$$

as well as νe scattering, (Eq. (14.96)). The CC reaction, (Eq. (14.97)), is sensitive only to ν_e, while the NC reaction, (Eq. (14.98)), is sensitive to all active neutrinos. This is a key feature to solve the solar neutrino problem. If it is caused by flavour transitions such as neutrino oscillations, the solar neutrino fluxes measured by CC and NC reactions would show a significant difference.

The Q-value of the CC reaction is -1.4 MeV and the e^- energy is strongly correlated with the ν_e energy. Thus, the CC reaction provides an accurate measure of the shape

of the ^{8}B neutrino spectrum. The contributions from the CC reaction and νe scattering can be distinguished by using different $\cos\theta$ distributions, where θ is the angle of the e^- momentum with respect to the Sun-Earth axis. While the νe scattering events have a strong forward peak, CC events have an approximate angular distribution of $(1 - 1/3\cos\theta)$.

The neutrino energy threshold of the NC reaction is 2.2 MeV. In the pure D$_2$O [13,14], the signal of the NC reaction was neutron capture in deuterium, producing a 6.25-MeV γ-ray. In this case, the capture efficiency was low and the deposited energy was close to the detection threshold of 5 MeV. In order to enhance both the capture efficiency and the total γ-ray energy (8.6 MeV), 2 tons of NaCl was added to the heavy water in the second phase of the experiment [229]. Subsequently NaCl was removed and an array of ^{3}He neutron counters were installed for the third phase measurement [230]. These neutron counters provided independent NC measurement with different systematics from that of the second phase, and thus strengthened the reliability of the NC measurement. The SNO experiment completed data acquisition in 2006.

Another real time solar neutrino experiment, Borexino at Gran Sasso, started solar neutrino observation in 2007. This experiment measures solar neutrinos via νe scattering in 300 tons of ultra-pure liquid scintillator. With a detection threshold as low as 250 keV, the flux of monochromatic 0.862 MeV ^{7}Be solar neutrinos has been directly observed for the first time [231]. Further, Borexino measured the fluxes of monochromatic 1.44 MeV *pep* solar neutrinos [232] and pp solar neutrinos [233], both for the first time. Measurements of these low energy solar neutrinos are important not only to test the SSM further, but also to study the MSW effect over the energy region spanning from sub-MeV to 10 MeV. Borexino published the final results of the Phase-I (May 2007 to May 2010) low-energy solar-neutrino measurement in [235]. After Phase-I data-taking, Borexino conducted an extensive purification of its liquid scintillator, and started Phase-II data-taking in December 2011. Recently, Borexino has reported the Phase II results of the low-energy solar-neutrino measurement [236]. Borexino has also reported the ^{8}B solar-neutrino measurement between January 2008 and December 2016 [237].

The solar neutrino survival probability, relevant for the interpretation of the solar neutrino data in the terms of the MSW effect is discussed in subsection 14.8.2.2.

KamLAND is a 1-kton ultra-pure liquid scintillator detector located at the old Kamiokande's site. This experiment also measured the ^{7}Be solar neutrino flux [238]. As KamLAND is a multi-purpose experiment whose one of the primary goals was a long-baseline neutrino oscillation studies using electron antineutrinos emitted from nuclear power reactors, further description of the KamLAND experiment is given later in Section 14.9.4.

14.9.2.   *Atmospheric neutrino oscillation experiments* :

Almost all large underground detectors can observe atmospheric neutrinos. In the early history of neutrino oscillation studies using atmospheric neutrinos, water Cherenkov detectors for Kamiokande [243,244] and IMB [245] (experiment in the US) and iron tracking calorimeters for the Frejus experiment [246] in France and the Soudan 2 experiment [247] at the Soudan mine in the US, measured atmospheric neutrinos, in particular, the flux ratio $\nu_\mu/\nu_e \equiv \Phi(\nu_\mu + \bar{\nu}_\mu)/\Phi(\nu_e + \bar{\nu}_e)$. The main purpose of all these experiments was search for nucleon decay, and atmospheric neutrinos were backgrounds for the main purpose. Following these initial experiments, Super-Kamiokande discovered the atmospheric neutrino oscillation [17], and a multi-purpose detector MACRO [248] at Gran Sasso obtained results consistent with neutrino oscillation. Subsequently, Soudan 2 also observed the atmospheric neutrino oscillation effects [249].   Later, the far detector of the MINOS long baseline neutrino oscillation experiment also measured atmospheric neutrinos [250], and obtained results consistent with atmospheric neutrino oscillation. This detector is a 5.4 kton iron-scintillator tracking calorimeter with toroidal magnetic field.

Atmospheric neutrino oscillations have also been observed by the neutrino telescopes for high-energy neutrino astronomy (TeV $\sim$ PeV) using Cherenkov technique, ANTARES and IceCube-DeepCore, based on the measurement of ν_μ charged-current events having an upward-going muon track to avoid contamination from atmospheric muon background. ANTARES [251] is an open water detector deployed deep under the Mediterranean Sea (depth $\sim$ 2500 m) 40 km off-shore from Toulon, France, while IceCube [252] is a detector deployed in the ice at the South Pole at the depth from 1450 m to 2450 m. Though both experiments are optimized to high-energy neutrino interactions in the TeV range, they need to measure muon neutrinos with energies as low as $\sim$ 20 GeV in order to be sensitive to atmospheric neutrino oscillations. ANTARES could reconstruct upward-going muons from ν_μ interactions down to 20 GeV [253], while IceCube used the low-energy sub-detector DeepCore, a region of denser IceCube instrumentation, to lower the muon neutrino energy threshold down to $\sim$ 6 GeV [254]   (also see Ref. 255 with higher thresholds).

All these detectors, with the exception of the MINOS far detector, cannot measure the charge of the final-state leptons, and, therefore, neutrino and antineutrino induced events cannot be discriminated; the MINOS far detector can measure the charge of the muon track, and, therefore, identify ν_μ and $\bar{\nu}_\mu$ charged-current events. However, all these detectors can identify the final-state leptons to be μ-like or e-like. Taking Super-Kamiokande as an example, neutrino events having their vertex in the 22.5 kton fiducial volume are classified into fully contained (FC) events and partially contained (PC) events. The FC events are required to have no activity in the anti-counter. Single-ring events have only one charged lepton which radiates Cherenkov light in the final state, and particle identification is particularly clean for single-ring FC events. A ring produced by an e-like ($e^\pm$, γ) particle exhibits a more diffuse pattern than that produced by a μ-like ($\mu^\pm$, $\pi^\pm$) particle, since an e-like particle produces an electromagnetic shower and low-energy electrons suffer considerable multiple Coulomb scattering in water. All the PC events are assumed to be μ-like since the PC events comprise a 98% pure charged-current

ν_μ sample.

In the near future, Super-Kamiokande will continue atmospheric neutrino measurements. In addition, currently several large underground detectors are proposed for construction (liquid argon detectors with a total mass of 10 - 40 kton as the far detector of the DUNE experiment [93] in the US, and a 2×0.258 Mton water Cherenkov detector, Hyper-Kamiokande (2TankHK-staged design) [200], as the far detector of the T2HK experiment [94] in Japan) or approved (a 50 kton magnetized iron tracking calorimeter, ICAL at the INO (India-based Neutrino Observatory) [85] in the southern Indian state of Tamil Nadu). Analytic expressions for the relevant atmospheric neutrino oscillation probabilities are given in subsection 14.8.1.

As high-statistics atmospheric neutrino observations in the energy region of a few to $\sim$ 10 GeV are considered to be promising for the determination of the neutrino mass ordering (see subsection 14.8.1, Fig. 14.7 and the related discussion), there are two proposed densely-instrumented neutrino telescopes PINGU (Precision IceCube Next-Generation Upgrade) [82] and ORCA (Oscillation Research with Cosmics in the Abyss) [83], both having a multi-megaton total mass. PINGU will be deployed inside the DeepCore, and will be sensitive to > 1 GeV. ORCA is proposed as part of the second phase of the KM3NeT [84], a network of neutrino telescopes deep under the Mediterranean Sea. ORCA will have sensitivity down to a few GeV, its site being Toulon, France.

14.9.3. *Accelerator neutrino oscillation experiments* :

For earlier accelerator neutrino oscillation experiments before the discovery of the atmospheric neutrino oscillation, see, *e.g.*, Ref. 257. The $\Delta m^2 \geq 2 \times 10^{-3}$ eV^2 region can be explored by accelerator-based long-baseline experiments with typically $E \sim 1$ GeV and $L \sim$ several hundred km. K2K [19], MINOS [20,21] and MINOS+ [256], OPERA [173,174], ICARUS [258], T2K [22,23], and NOνA [40,60] are completed or currently running experiments, and DUNE [93] and T2HK [94] are proposed future experiments. For analytic expressions of relevant neutrino oscillation probabilities see Eq. (14.44) and Eq. (14.74) and the discussions related to these equations. With a fixed baseline distance and a narrower, well understood neutrino energy spectrum, the value of $|\Delta m^2_{31(32)}|$ and, with higher statistics, also the relevant neutrino mixing angle, are potentially better constrained in accelerator experiments than from atmospheric neutrino observations. With $\nu_\mu \to \nu_e$ appearance measurements, accelerator long-baseline experiments can measure θ_{13} within an uncertainty related, in particular, to the CPV phase δ. In the early phase of the accelerator long-baseline experiments, K2K used an approximate $\nu_\mu \to \nu_e$ appearance probability given by Eq. (14.46),

$$P(\nu_\mu \to \nu_e) = \sin^2 2\theta_{13} \cdot \sin^2 \theta_{23} \cdot \sin^2(1.27 \Delta m^2_{31} L/E). \tag{14.99}$$

to set an upper limit to $\sin^2 2\theta_{13}$ [175]. More accurate expression for the $\nu_\mu \to \nu_e$ appearance probability relevant for the accelerator long baseline experiments, Eq. (14.74), shows that subleading terms could have rather large effects and the unknown CPV phase δ causes uncertainties if one wishes to determining the value of θ_{13} from accelerator measurements of $\nu_\mu \to \nu_e$ appearance. Now that θ_{13} has been precisely measured by

reactor experiments, accelerator long-baseline experiments can potentially determine or constrain δ and the neutrino mass ordering, from the measurement of $\nu_\mu \to \nu_e$ appearance, using precise reactor results on θ_{13}, depending on the experimental conditions such as baseline distance.

The K2K (KEK-to-Kamioka) long-baseline neutrino oscillation experiment [19] is the first accelerator-based experiment with a neutrino path length extending hundreds of kilometers. A horn-focused wide-band muon neutrino beam having an average $L/E_\nu \sim 200$ ($L = 250$ km, $\langle E_\nu \rangle \sim 1.3$ GeV), was produced by 12-GeV protons from the KEK-PS and directed to the Super-Kamiokande detector. A near detector was located 300 m downstream of the production target. K2K experiment started data-taking in 1999 and was completed in 2004.

MINOS [20,21] is the second long-baseline neutrino oscillation experiment with near and far detectors. Neutrinos are produced by the NuMI (Neutrinos at the Main Injector) facility using 120 GeV protons from the Fermilab Main Injector. The far detector is a 5.4 kton (total mass) iron-scintillator tracking calorimeter with toroidal magnetic field, located underground in the Soudan mine. The baseline distance is 735 km. The near detector, located 1.04 km downstream of the production target, is also an iron-scintillator tracking calorimeter with toroidal magnetic field, with a total mass of 0.98 kton. The NuMI neutrino beam is a horn-focused wide-band beam. Its energy spectrum can be varied by moving the target position relative to the first horn and changing the horn current. MINOS started the neutrino-beam run in 2005 and was completed in 2012. Almost all the MINOS data were taken with the low-energy beam spectrum which peaked at 3 GeV. Part of the MINOS data were taken with the $\bar{\nu}_\mu$-enhanced beam by inverting the current in magnetic horns. In September, 2013, the MINOS+ experiment [256] started with the same near and far detectors as the MINOS experiment, but with the medium-energy beam spectrum which peaks at ~ 6 GeV on axis (zero degree). At zero degree, the NuMI medium-energy beam has much higher intensity than the NuMI low-energy beam. The MINOS+ experiment had run for 3 years and ended in 2016.

The T2K experiment [22,23] is the first off-axis long-baseline neutrino oscillation experiment. The baseline distance is 295 km between the J-PARC in Tokai, Japan and Super-Kamiokande. A narrow-band ν_μ beam with a peak energy of 0.6 GeV, produced by 30 GeV protons from the J-PARC Main Ring, is directed 2.5° off-axis to SK. With this configuration, the ν_μ beam is tuned to the first oscillation minimum of the ν_μ survival probability. T2K started the first physics run in 2010.

The NOνA experiment [40,41] is an off-axis long-baseline neutrino oscillation experiment using the the NuMI medium-energy beam. Its detectors are positioned 14.6 mrad off-axis. With this configuration, the neutrino beam has a narrow spectrum which peaks at around 2 GeV. The 14 kton total active mass far detector is located on the surface at Ash River, Minnesota, 810 km from the production target. The 193 ton total active mass near detector is located 100 m underground at Fermilab, approximately 1km from the target. Both detectors are fine-grained tracking calorimeters consisting of arrays of PVC cells filled with liquid scintillator. NOνA started physics run in 2014.

Although the atmospheric neutrino oscillations and accelerator long-baseline ν_μ disappearance data are fully consistent with the dominance of $\nu_\mu \to \nu_\tau$ oscillations for ν_μ

at GeV energies, ν_τ appearance in the muon neutrino beam has to be demonstrated. As the τ production threshold is $E_\nu \sim 3.5$ GeV, a high-energy neutrino beam is needed for this purpose. The only experiment of this kind is OPERA [173,174] with a muon neutrino source at CERN and a detector at Gran Sasso with a baseline distance of 730 km. OPERA does not have a near detector. The CNGS (CERN Neutrinos to Gran Sasso) neutrino beam with $\langle E_\nu \rangle = 17$ GeV is produced by high-energy protons from the CERN SPS. OPERA received the CNGS neutrino beam between 2008 and 2012. The detector is a combination of the "Emulsion Cloud Chamber" and magnetized spectrometer, having a target mass of 1,290 tons. At Gran Sasso, another neutrino experiment, ICARUS [258], with a 600-ton liquid argon detector, was located and received the CNGS neutrino beam from 2010 to 2012. The ICARUS detector was transported to Fermilab in July 2017, and will be used in a short baseline experiment.

DUNE (Deep Underground Neutrino Experiment) [93] is a projected future experiment with a 1,300 km baseline. A $10 \sim 34$ kton liquid-argon far detector will be located deep underground at the Sanford Lab in South Dakota, the U.S. A fine-grained near neutrino detector will be installed at Fermilab. Based on the existing NuMI beamline and a MW class proton source, a wide-band, high-intensity ν_μ beam with a peak flux at 2.5 GeV is considered for this experiment. T2HK [94] is another future long baseline experiment from J-PARC to the 2×0.258 Mton water Cherenkov detector, Hyper-Kamiokande (2TankHK-staged design) [200], which is at the proposal stage, at Kamioka. An upgrade of the J-PARC Main Ring to achieve a MW-class beam power is also proposed.

In the context of possible hints for the existence of sterile neutrinos at the eV scale, short-baseline accelerator neutrino oscillation experiments have been drawing attention. LSND [259], Karmen 2 (and Karmen 1) [260], and MiniBooNE [261,262] are completed experiments. At Fermilab, the Short-Baseline Neutrino (SBN) Program is ongoing [263]. It consists of three new short-baseline experiments, SBND, MicroBooNE, and ICARUS in the Booster Neutrino Beamline. The detectors of all these new experiments use liquid-argon TPC technology. MicroBooNE is running, and SBND and ICARUS are in preparation.

The LSND (Liquid Scintillation Neutrino Detector) experiment [259] used the LANSE (Los Alamos Neutron Science Center, formerly known as the LAMPF) 800 MeV proton linac as a neutrino source. At this energy, kaon production is negligible. Most of the produced positive pions stop in the massive target and decay at rest, with decay muons also stop in the target and decay. Most of the produced negative pions also stop in the target and are absorbed by the target nuclei. Therefore, this neutrino source emits ν_μ, $\bar\nu_\mu$, and ν_e, with very small contamination of $\bar\nu_e$ which comes from π^- decay in flight followed by the μ^- decay at rest. Because of this small $\bar\nu_e$ component in the neutrino flux, LSND made a sensitive search for $\bar\nu_\mu \to \bar\nu_e$ appearance with 167 tons of diluted liquid scintillator in a tank located about 30 m from the neutrino source, using the reaction $\bar\nu_e + p \to e^+ + n$. Also, LSND studied $\nu_\mu \to \nu_e$ appearance above the Michel electron endpoint energy using the reaction $\nu_e + C \to e^- + N$, as the ν_e flux from μ^+ decay in flight is suppressed due to the long muon lifetime and that from π^+ decay in flight is suppressed by the small $\pi^+ \to e^+ + \nu_e$ branching ratio. The Karmen 2 experiment [260] used the 800 MeV proton synchrotron at the neutron spallation facility of the Rutherford

Appleton Laboratory, also to produce low-energy $\bar{\nu}_\mu$ flux from μ^+ decay at rest. The Karmen 2 detector is a segmented liquid scintillator calorimeter located at a distance of 17.7 m from the neutrino source. MiniBooNE used a conventional horn-focused neutrino beam produced by 8 GeV protons from the Fermilab booster synchrotron. MiniBooNE investigated both ν_e [261] and $\bar{\nu}_e$ [262] appearance in ν_μ and $\bar{\nu}_\mu$ beams, respectively, with a detector containing 806 tons of mineral oil and located 541 m downstream of the production target.

14.9.4.   *Reactor neutrino oscillation experiments* :

As nuclear reactors produce $\bar{\nu}_e$ flux with energy < 10 MeV, $\bar{\nu}_e$ disappearance is the only neutrino oscillation channel that can be studied using reactors and liquid scintillator detectors. To identify low-energy inverse β-decay events $\bar{\nu}_e + p \rightarrow e^+ + n$, detection of a prompt positron signal and delayed neutron signal in coincidence is important to reject natural backgrounds. For detecting neutrons effectively, gadolinium-loaded liquid scintillator is widely used. While neutron capture on a hydrogen produces a 2.2 MeV γ, neutron capture on Gd produces multiple γ, each having average energy of ~ 2 MeV, giving a ~ 8 MeV signal in total.

For short baseline reactor neutrino oscillation experiments in the 1980s or earlier, see, *e.g.*, Refs. [264,52].   Reactor neutrino oscillation experiments with $L \sim 1$ km, $\langle E \rangle \sim 3$ MeV are sensitive down to $E/L \sim 3 \times 10^{-3}$ eV$^2 \sim \Delta m^2$. At this baseline distance, the reactor $\bar{\nu}_e$ oscillations driven by Δm_{21}^2 are negligible in the three neutrino oscillation framework. The $\bar{\nu}_e$ survival probability is given in Eq. (14.45). Therefore, reactor $\bar{\nu}_e$ disappearance experiments with ~ 1 km baseline allow direct measurement of $\sin^2 \theta_{13}$.

In 1990's, two experiments of this kind, Chooz [57] and Palo Verde [265],   were constructed to study a possibility of rather large $\nu_\mu - \nu_e$ mixing in the Δm^2 region down to $10^{-2} \sim 10^{-3}$ eV^2 as a possible solution for the anomalous atmospheric ν_μ/ν_e ratio reported by several experiments (see, Section 14.11.1). Both Chooz and Palo Verde were single-detector experiments. The Chooz detector was located in an underground laboratory with 300 mwe (meter water equivalent) rock overburden, at about 1 km from the neutrino source. It consisted of a central 5-ton target filled with 0.09% Gd-loaded liquid scintillator, surrounded by an intermediate 17-ton and outer 90-ton regions filled with Gd-free liquid scintillator. Another experiment at the Palo Verde Nuclear Generating Station in Arizona, United States, also searched for $\bar{\nu}_e$ disappearance using 11.34 tons of Gd-loaded liquid scintillator located at a shallow (32 mwe) underground site, about 800 m from the neutrino source [265].   These two experiments found no evidence for $\bar{\nu}_e$ disappearance. The CHOOZ collaboration set a limit of $\sin^2 2\theta_{13} < 0.1$ at 90% CL. Somewhat less stringent limit was obtained by the Palo Verde collaboration.

After establishment of atmospheric and solar neutrino oscillations the importance of the reactor neutrino oscillation experiment to measure θ_{13} was widely recognized, and this led to the realization of the three new reactor experiments, Double Chooz in France, RENO in Korea, and Daya Bay in China. Given a small disappearance probability expected from the $\sin^2 2\theta_{13}$ limit reported by Chooz and Palo Verde and an uncertainty of a few% with which reactor $\bar{\nu}_e$ flux was predicted, all these experiments proposed to have near and far detectors to reduce the systematic error due to $\bar{\nu}_e$ flux uncertainty.

These modern reactor neutrino oscillation experiments were approved around 2005. For their histories, see, *e.g.*, Ref. 266 for Double Chooz, Ref. 267 for Daya Bay, and Ref. 268 for RENO.

The Double Chooz experiment [32,35] measures electron antineutrinos from two 4.25 GW_{th} reactors with two identical detectors: a near detector and a far detector located at average distances of 400 m and 1050 m, respectively, from the two reactor cores. Although the far detector was completed in 2010, there was a substantial delay in the construction of the near detector, and it was completed at the end of 2014. The Daya Bay experiment [33,37] measures electron antineutrinos from the Daya Bay nuclear power complex (six 2.9 GW_{th} reactors), initially with six functionally identical detectors deployed in two near (470 m and 576 m of flux-weighted baselines) and one far (1648 m) underground halls. The first Daya Bay result [33] was obtained with this detector configuration. Later, two detectors were further installed, one in one of the near detector hall and the other in the far detector hall. The RENO experiment [34] measures electron antineutrinos from four 2.8 GW_{th} and two 2.66 GW_{th} reactors at Yonggwang Nuclear Power Plant with two identical detectors located at 294 m and 1383 m from the reactor array center (or flux-weighted baseline distance of 408.56 m and 1443.99 m, respectively). Antineutrino detectors of these experiments have similar structures. They consist of three layers and an optically independent outer veto detector. The innermost layer of the antineutrino detector is filled with Gd-loaded liquid scintillator, which is surrounded by a "γ-catcher" layer filled with Gd-free liquid scintillator, and outside the γ-catcher is a buffer layer filled with mineral oil. An outer veto detector is filled with purified water (Daya Bay and RENO) or liquid scintillator (Double Chooz). In addition, the Double Chooz near detector tank is shielded by a 1 m thick water buffer. RENO and Daya Bay started measurements with both the near and far detectors from the beginning. All these experiments published their first results on reactor $\bar{\nu}_e$ disappearance in 2012.

For longer baseline distance of $L \sim$ a few hundred km, a reactor neutrino oscillation experiment is sensitive to Δm^2 down to $\sim 10^{-5}$ eV^2. In this case the reactor $\bar{\nu}_e$ survival probability is given in Eq. (14.51). Therefore, such an experiment can test the LMA (Large Mixing Angle) solution of the solar neutrino problem, assuming CPT invariance.

However, a higher $\bar{\nu}_e$ flux and a larger target mass are needed compared to short-baseline reactor experiments to obtain statistically significant event rate. So far, KamLAND is the only experiment of this kind. It is located at the old Kamiokande's site in Japan. Its neutrino target is 1-kton ultra-pure liquid scintillator contained in a transparent balloon, which is hold inside a spherical tank with buffer oil filled between the baloon and the tank. The tank is surrounded by an outer water Cherenkov detector. Before the Great East Japan Earthquake in March 2011, many nuclear reactors were operating in Japan, and more than 79% of the $\bar{\nu}_e$ flux at KamLAND was coming from 26 reactors between 138 - 214 km away, with a flux-weighted average distance of ~ 180 km.

In future, medium baseline (~ 50 km) reactor neutrino oscillation experiments with neutrino target mass of ~ 20 kton and with a very good energy resolution of $3\%/\sqrt{E_\nu(\text{MeV})}$, not reached in any previous experiment with liquid scintillator, are aiming, in particular, to determine the type of spectrum the neutrino masses obey, *i.e.*, the neutrino mass ordering (see Section 14.2). The relevant $\bar{\nu}_e$ survival probability is given

in Eq. (14.47). These experiments have additional rich physics program. The Jiangmen Underground Neutrino Observatory (JUNO) [269] at Kaiping, Jiangmen in Southern China will be located at 53 km from both of the planned Yangjiang and Taishan nuclear power plants. The neutrino target of this experiment will be 20 kton liquid scintillator. JUNO is a funded project, and its construction started in January, 2015.

14.10. Results of solar neutrino experiments and KamLAND

In 1967, analyzing the possible effects of neutrino oscillations on the solar neutrino flux measurements, B. Pontecorvo predicted the solar neutrino "deficit" in experiments detecting solar neutrinos via a CC reaction [1] before the first solar neutrino data were available. The solar-neutrino problem, *i.e.*, the problem of understanding the origin of the observed deficit of solar neutrinos, remained unsolved for more than 30 years since the late 1960s, but solar neutrino experiments have achieved remarkable progress since the beginning of the new century, and the solar-neutrino problem has been understood as due to neutrino flavour conversion.

14.10.1. *Measurements of* Δm_{21}^2 *and* θ_{12} :

From the very beginning of the solar-neutrino observation by the Homestake chlorine experiment [270] in the late 1960s, it was recognized that the observed flux was significantly smaller than the SSM prediction. The subsequent radiochemical solar neutrino experiments using ^{71}Ga, SAGE [271] and GALLEX [9] also reported smaller solar neutrino fluxes than the SSM predictions in the early 1990s. final results of these experiments [272] are compared with the SSM predictions in Table 14.5. Experiments with water Cherenkov detectors, Kamiokande and Super-Kamiokande, observed almost pure ^{8}B solar neutrinos through νe elastic scattering, and they also reported a clear deficit of ^{8}B solar neutrino flux.

In 2001, the initial SNO CC result combined with the Super-Kamiokande's high-statistics νe elastic scattering result [273] provided direct evidence for flavour conversion of solar neutrinos [13]. Later, SNO's NC measurements further strengthened this conclusion [14,229,230]. From the salt-phase measurement [229], the fluxes measured with CC, ES, and NC events were obtained as

$$\phi_{\text{SNO}}^{\text{CC}} = (1.68 \pm 0.06^{+0.08}_{-0.09}) \times 10^6 \text{cm}^{-2}\text{s}^{-1} \ , \tag{14.100}$$

$$\phi_{\text{SNO}}^{\text{ES}} = (2.35 \pm 0.22 \pm 0.15) \times 10^6 \text{cm}^{-2}\text{s}^{-1} \ , \tag{14.101}$$

$$\phi_{\text{SNO}}^{\text{NC}} = (4.94 \pm 0.21^{+0.38}_{-0.34}) \times 10^6 \text{cm}^{-2}\text{s}^{-1} \ , \tag{14.102}$$

where the first errors are statistical and the second errors are systematic. In the case of $\nu_e \rightarrow \nu_{\mu,\tau}$ transitions, Eq. (14.102) is a mixing-independent result and therefore tests solar models. It shows good agreement with the ^{8}B solar-neutrino flux predicted by the solar model [125]. Fig. 14.8 shows the salt phase result on the $\nu_\mu + \nu_\tau$ flux $\phi(\nu_{\mu,\tau})$ versus the flux of electron neutrinos $\phi(\nu_e)$ with the 68%, 95%, and 99% joint probability

Table 14.5: Results from radiochemical solar-neutrino experiments. The predictions of the standard solar model BPS08(GS) [128] are also shown. The first and the second errors in the experimental results are the statistical and systematic errors, respectively. SNU (Solar Neutrino Unit) is defined as 10^{-36} neutrino captures per atom per second.

	^{37}Cl$\rightarrow^{37}$Ar (SNU)	^{71}Ga$\rightarrow^{71}$Ge (SNU)
Homestake [6]	$2.56 \pm 0.16 \pm 0.16$	–
GALLEX [10]	–	$77.5 \pm 6.2^{+4.3}_{-4.7}$
GNO [11]	–	$62.9^{+5.5}_{-5.3} \pm 2.5$
GNO+GALLEX [11]	–	$69.3 \pm 4.1 \pm 3.6$
SAGE [8]	–	$65.4^{+3.1+2.6}_{-3.0-2.8}$
SSM [BPS08(GS)] [128]	$8.46^{+0.87}_{-0.88}$	$127.9^{+8.1}_{-8.2}$

contours. The flux of non-ν_e active neutrinos, $\phi(\nu_{\mu,\tau})$, can be deduced from these results. It is

$$\phi(\nu_{\mu,\tau}) = \left(3.26 \pm 0.25^{+0.40}_{-0.35}\right) \times 10^6 \text{cm}^{-2}\text{s}^{-1}. \tag{14.103}$$

The non-zero $\phi(\nu_{\mu,\tau})$ is strong evidence for solar ν_e flavor conversion. As it follows from the discussion of the solar ν_e survival and transition probabilities in subsection 14.8.2.2 (see Eq. (14.90)), the parameters which are responsible for the solar neutrino flavour conversion are Δm^2_{21} and θ_{12}. The dependence of the survival probability on $\theta_{13} \cong 0.15$ is extremely weak, leading essentially to a rescaling of the corresponding 2-neutrino mixing ν_e survival probability by a factor of $\cos^4 \theta_{13} = 0.96$ and of N_e by the factor $\cos^2 \theta_{13} \cong 0.98$. The quoted experimental results are consistent with those expected from the LMA (large mixing angle) solution of solar neutrino oscillation in matter [26,27] with $\Delta m^2_{21} \sim 7.5 \times 10^{-5}$ eV^2 and $\tan^2\theta_{12} \sim 0.45$. However, with the SNO data alone, the possibility of other solutions of the solar neutrino problem cannot be excluded with sufficient statistical significance.

The KamLAND experiment solved this problem and finally identified the LMA solution as the true solution of the solar neutrino problem. With the reactor $\bar{\nu}_e$'s energy spectrum (< 8 MeV) and a prompt-energy analysis threshold of 2.6 MeV, this experiment has a sensitive Δm^2 range down to $\sim 10^{-5}$ eV^2. The reactor $\bar{\nu}_e$ survival probability relevant for the interpretation of the KamLAND data is given in Eq. (14.51) and Eq. (14.52). Assuming CPT invariance, it depends on the same parameters Δm^2_{21} and θ_{12}, which drive the solar ν_e transitions, the dependence on θ_{13} having, as in the case of the solar ν_e survival probability, a rather small rescaling effect of the corresponding 2-neutrino $\bar{\nu}_e$ survival probability. Therefore, if the LMA solution is the real solution of the solar neutrino problem, KamLAND should observe reactor $\bar{\nu}_e$ disappearance, assuming CPT invariance.
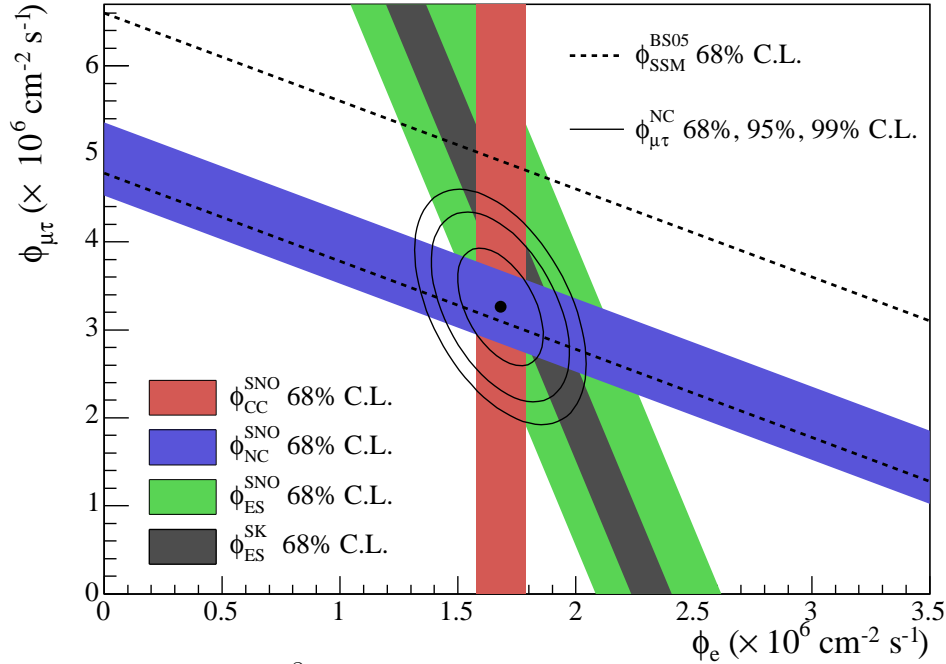
Figure 14.8: Fluxes of ^{8}B solar neutrinos, $\phi(\nu_e)$, and $\phi(\nu_{\mu,\tau})$, deduced from the SNO's CC, ES, and NC results of the salt phase measurement [229]. The Super-Kamiokande ES flux is from Ref. 274. The BS05(OP) standard solar model prediction [125] is also shown. The bands represent the 1σ error. The contours show the 68%, 95%, and 99% joint probability for $\phi(\nu_e)$ and $\phi(\nu_{\mu,\tau})$. The figure is from Ref. 229.

The first KamLAND results [15] with 162 ton·yr exposure were reported in December 2002. The ratio of observed to expected (assuming no $\bar{\nu}_e$ oscillations) number of events was

$$\frac{N_{\text{obs}} - N_{\text{BG}}}{N_{\text{NoOsc}}} = 0.611 \pm 0.085 \pm 0.041 \qquad (14.104)$$

with obvious notation. This result showed clear evidence of an event deficit expected from neutrino oscillations. The 95% CL allowed regions are obtained from the oscillation analysis with the observed event rates and positron spectrum shape. A combined global solar + KamLAND analysis showed that the LMA is a unique solution to the solar neutrino problem with $> 5\sigma$ CL [275]. With increased statistics [16,276,277], KamLAND observed not only the distortion of the $\bar{\nu}_e$ spectrum, but also for the first time the periodic dependence on the neutrino energy of the $\bar{\nu}_e$ survival probability expected from neutrino oscillations (see Fig. 14.9).

It should be noted that with accumulation of precise solar neutrino data, analyses using only solar neutrino data [278,279,235] have attained sufficiently high statistical significance ($> 99.73\%$ or $> 3\sigma$ CL) to show the LMA solution to be the real solution to the solar neutrino problem without resorting to the KamLAND data, namely, without
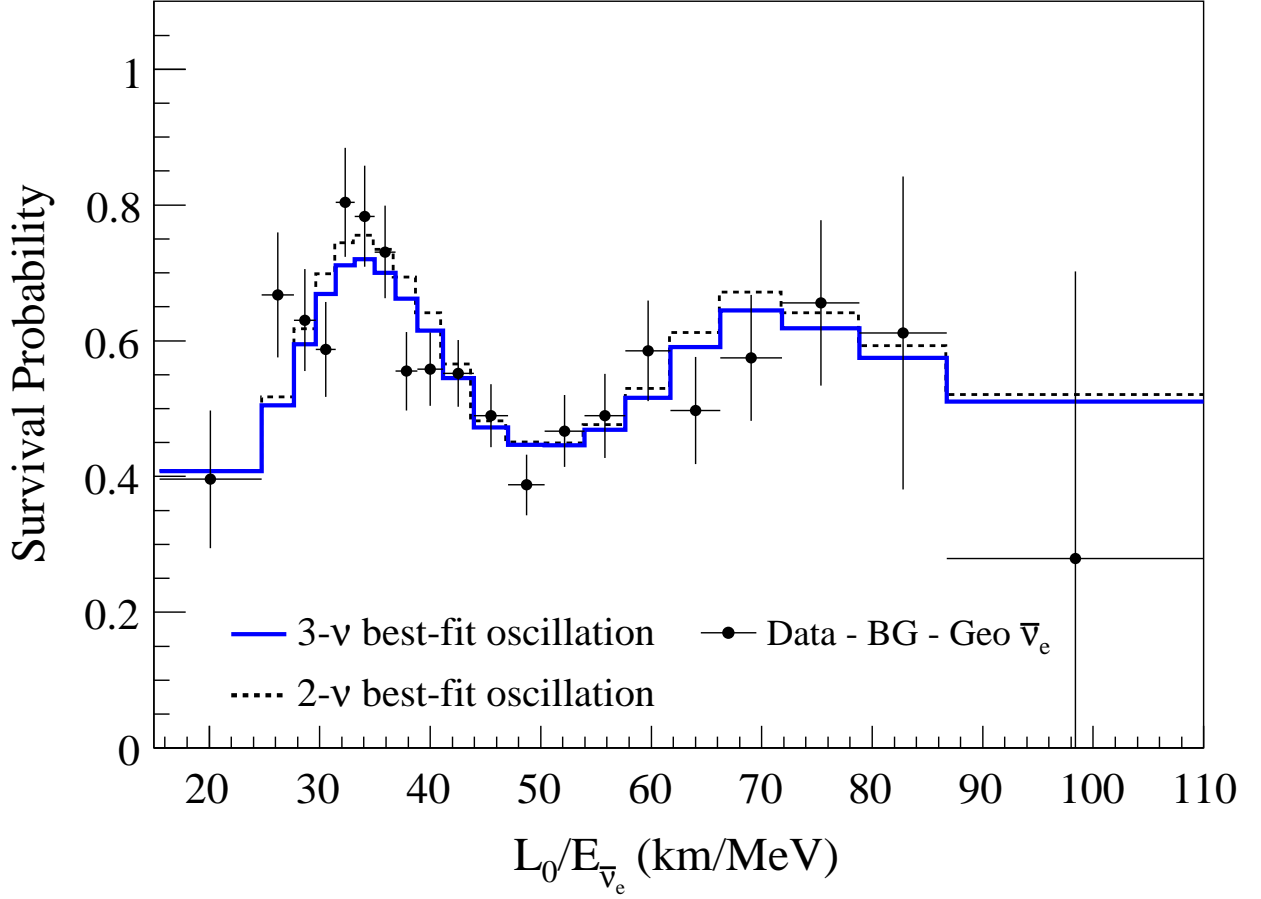
Figure 14.9: The ratio of the background and geoneutrino-subtracted $\bar{\nu}_e$ spectrum, observed in the KamLAND experiment, to the predicted one without oscillations (survival probability) as a function of L_0/E, where L_0=180 km. The histograms show the expected distributions based on the best-fit parameter values from the two- and three-flavor neutrino oscillation analyses. The figure is from Ref. 277.

assuming CPT invariance, though the allowed Δm_{21}^2 range is better determined by the KamLAND data.

The values of Δm_{21}^2 and θ_{12} have been frequently updated by experimental groups or by phenomenological analysis groups, using the global solar neutrino data, or the KamLAND data alone, or the global solar + KamLAND data, or the global neutrino oscillation data. The latest global analysis results found in Ref. 58 are shown in Table 14.1.

Regarding the consistency between the KamLAND and solar neutrino experiments on the values of Δm_{21}^2 and θ_{12}, it has been noted that there is a $\sim 2\sigma$ level tension between the best-fit value of Δm_{21}^2 determined by the KamLAND collaboration and that obtained from analyses using global solar neutrino data [59]. The solar data prefer lower Δm_{21}^2 value. The KamLAND and global solar best-fit values of θ_{12} are consistent.

14.10.2. *Solar neutrino flux measurements and indications of matter effects* :

So far, the pp, pep, ^{7}Be, ^{8}B solar neutrino fluxes have been measured, and upper limits have been set for the hep and CNO solar neutrino fluxes, with various techniques. Chlorine (Homestake) and gallium (SAGE, GALLEX, and GNO) radiochemical experiments measured capture rates of solar neutrinos above threshold (see Table 14.5). Light-water Cherenkov detectors, Kamiokande [7] and Super-Kamiokande [225,227,228], measured the ^{8}B neutrino flux and set an upper limit for the hep neutrino flux using νe elastic scattering [225]. A heavy-water Cherenkov detector, SNO [279], also measured the ^{8}B neutrino flux, but with three different reactions, NC, CC, and νe elastic scattering. Liquid scintillator detectors, Borexino and KamLAND, measured low-energy solar neutrinos using νe elastic scattering. In particular, Borexino successfully measured the pp [233,236], pep [232,235,236], and ^{7}Be [231,235,236] solar neutrino fluxes and set an upper limit for the CNO solar neutrino flux [232,235,236]. KamLAND also measured the ^{7}Be solar neutrino flux [238]. In addition, both Borexino [234,237] and KamLAND [239] measured the ^{8}B neutrino flux. The measured fluxes or upper limits from all these experiments are listed in the Particle Listings at the PDG website [280] except the recently reported Borexino results [236,237].

Fig. 14.10 plots the survival probability of solar ν_e as a function of neutrino energy. The data points are from the Borexino results [236,237] except the SNO+SK ^{8}B data. The theoretical curve shows the prediction of the MSW-LMA solution. As explained in Section 14.8.2.2, matter effects on solar neutrino oscillation is expected to be given by the average two-neutrino vacuum oscillation probability, $1 - \frac{1}{2}\sin^2 2\theta_{12}$ for survival of pp neutrinos. It is ~ 0.58 for $\sin^2\theta_{12} = 0.297$. For ^{8}B neutrinos, transitions are adiabatic and the survival probability is given by $\sin^4\theta_{13} + \cos^4\theta_{13}\sin^2\theta_{12} \sim 0.28$ for $\sin^2\theta_{13} = 0.0215$ (for normal mass ordering) and $\sin^2\theta_{12} = 0.297$. All the data shown in this plot are consistent with the theoretically calculated curve. This indicates that these solar neutrino results are consistent with the MSW-LMA solution of the solar neutrino problem.

In the nighttime, solar neutrino experiments observe neutrinos propagated through the Earth. Therefore, a non-zero day-night flux (or interaction rate) asymmetry implies the Earth matter effects on flavour oscillations of solar neutrinos. In particular, if the nighttime flux is higher than the daytime flux, it implies a ν_e regeneration by the Earth matter effects (see Section 14.8.2.3). Previously, SNO [279] and Borexino [283] searched for day-night flux asymmetries of ^{8}B and ^{7}Be neutrinos, respectively, but they observed no statistically significant asymmetries. In 2014, the Super-Kamiokande experiment has reported [284] a 2.7σ indication of non-zero day-night asymmetry of ^{8}B solar neutrinos, $A_{DN} = 2(R_D - R_N)/(R_D + R_N) = -0.032 \pm 0.011 \pm 0.005$, where R_D and R_N are the average day and average night νe elastic-scattering rates of ^{8}B solar neutrinos. In 2016, Super-Kamiokande updated this day-night asymmetry as $A_{DN} = -0.033 \pm 0.010 \pm 0.005$ [228]. Statistical significance was slightly improved. This result is consistent with the Δm_{21}^2 and θ_{12} values in the LMA region.
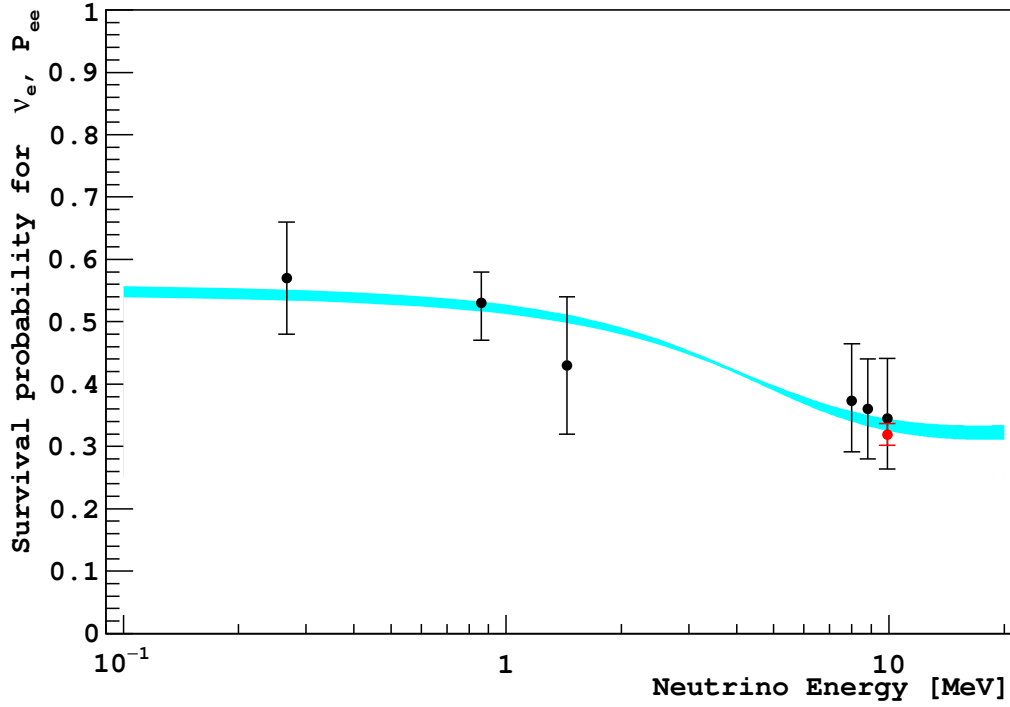
Figure 14.10: Electron neutrino survival probability as a function of neutrino energy. The points represent, from left to right, the Borexino pp, ^{7}Be, pep, and ^{8}B data (black points) and the SNO+SK ^{8}B data (red point). The three Borexino ^{8}B data points correspond, from left to right, to the low-energy (LE) range, LE+HE range, and the high-energy (HE) range. The electron neutrino survival probabilities from experimental points are determined using a high metalliticy SSM from Ref. 281. The error bars represent the $\pm 1\sigma$ experimental + thoretical uncertainties. The curve corresponds to the $\pm 1\sigma$ prediction of the MSW-LMA solution using the parameter values given in Ref. 282. This figure is provided by A. Ianni.

14.11. Measurements of $|\Delta m^2_{31(32)}|$ and θ_{23}, and related topics

The first compelling evidence for the neutrino oscillation was ν_μ disappearance observed by the Super-Kamiokande Collaboration in 1998 [17] in the measurement of atmospheric neutrinos produced by cosmic-ray interactions in the atmosphere. The analysis was performed using the 2-neutrino mixing ν_μ survival probability assuming $\nu_\mu \rightarrow \nu_\tau$ oscillations, Eq. (14.54) with $l = \mu$, $\theta = \theta_{23}$, $\Delta m^2 = \Delta m^2_{31}$ and $x = \tau$ (or Eq. (14.44) with $l = l' = \mu$, $n = 3$, $|U_{\mu 3}|^2 = \cos^2 \theta_{13} \sin^2 \theta_{23} \cong \sin^2 \theta_{23}$). A striking feature of atmospheric neutrino oscillations was a surprisingly large mixing angle θ_{23}. Whether mixing is maximal, *i.e.*, $\theta_{23} = \pi/4$, or, if not, in which octant θ_{23} lies, is one of the questions drawing much interest in neutrino physics because the measurement of certain fundamental physical observables depends on the value of $\sin^2 \theta_{23}$ (see, *e.g.*, Sections 14.2 and 14.8.1). The high precision measurement of $\sin^2 \theta_{23}$ will provide also a test of a large class of theories of neutrino masses and mixing, based, in particular, on discrete symmetries (see, *e.g.*, the first three articles quoted in Ref. 96 and Ref. 285).

14.11.1. ν_μ *disappearance data* :

Prior to the Super-Kamiokande's discovery of atmospheric neutrino oscillations, a deficit of atmospheric $\nu_\mu + \bar{\nu}_\mu$ flux was indicated by the Kamiokande experiment [243]. Actually, Kamiokande reported the double ratio R(ν_μ/ν_e) = (Measured ν_μ/ν_e)/(Expected ν_μ/ν_e)< 1 to reduce systematic effects due to rather large flux uncertainties. The IMB [245] and Soudan 2 [247] experiments also observed $R < 1$, but the Frejus experiment [246] did not see such a tendency. Kamiokande further observed zenith-dependence of $\nu_\mu + \bar{\nu}_\mu$ flux deficit [244].   However, all these results from early experiments did not have conclusive statistical significance.

In 1998, the Super-Kamiokande Collaboration reported a significant zenith-angle (Θ) dependent deficit of μ-like events compared to the no-oscillation expectation [17].   For multi-GeV (visible energy > 1.33 GeV) FC+PC muons, the asymmetry A, defined as $A = (U-D)/(U+D)$, where U is the number of upward-going events ($-1 < \cos\Theta < -0.2$) and D is the number of downward-going events ($0.2 < \cos\Theta < 1$), was observed to be $A = -0.296 \pm 0.048 \pm 0.01$ which deviates from 0 by more than 6σ. This asymmetry is expected to be ~ 0 independent of the atmospheric neutrino flux model for neutrino energy > 1 GeV. On the other hand, the zenith-angle distribution of the e-like events was consistent with the expectation in the absence of oscillations. Fig. 14.11 shows the compilation of zenith-angle distributions of e-like and μ-like events from the Super-Kamiokande atmospheric observation. Events included in these plots are single-ring FC events subdivided into sub-GeV (visible energy < 1.33 GeV) events and multi-GeV events. The zenith-angle distribution of the multi-GeV μ-like events is shown combined with that of the PC events. The final-state leptons in these events have good directional correlation with the parent neutrinos. The dotted histograms show the Monte Carlo expectation for neutrino events. If the produced flux of atmospheric neutrinos of a given flavour remains unchanged at the detector, the data should have similar distributions to the expectation. However, the zenith-angle distribution of the μ-like events shows a strong deviation from the expectation. On the other hand, the zenith-angle distribution of the e-like events is consistent with the expectation. This characteristic feature is interpreted that muon neutrinos coming from the opposite side of the Earth's atmosphere, having travelled $\sim 10,000$ km, oscillate into other neutrinos and disappeared, while oscillations still do not take place for muon neutrinos coming from above the detector, having travelled from a few to a few tens km. These results are in good agreement with $\nu_\mu \leftrightarrow \nu_\tau$ two-flavour neutrino oscillations, because there is no indication of electron neutrino appearance. The atmospheric neutrinos corresponding to the events shown in Fig. 14.11 have $E = 1 \sim 10$ GeV. With $L = 10000$ km, neutrino oscillations suggests $\Delta m^2 \sim 10^{-3} - 10^{-4}$ eV^2. A significant deficit of μ-like events suggests a large mixing angle. Super-Kamiokande's initial results on the oscillation parameters for $\nu_\mu \leftrightarrow \nu_\tau$ were $5 \times 10^{-4} < \Delta m^2 < 6 \times 10^{-3}$ eV^2 and $\sin^2 2\theta > 0.82$ at 90% CL [17].

Although the Super-Kamiokande's atmospheric neutrino data are consistent with $\nu_\mu \leftrightarrow \nu_\tau$ oscillations, this interpretation will be strengthened if ν_τ appearance and characteristic sinusoidal behavior of the ν_μ survival probability as a function of L/E were observed. In fact, other exotic explanations such as neutrino decay [286] and quantum decoherence [287] cannot be completely ruled out from the zenith-angle distributions
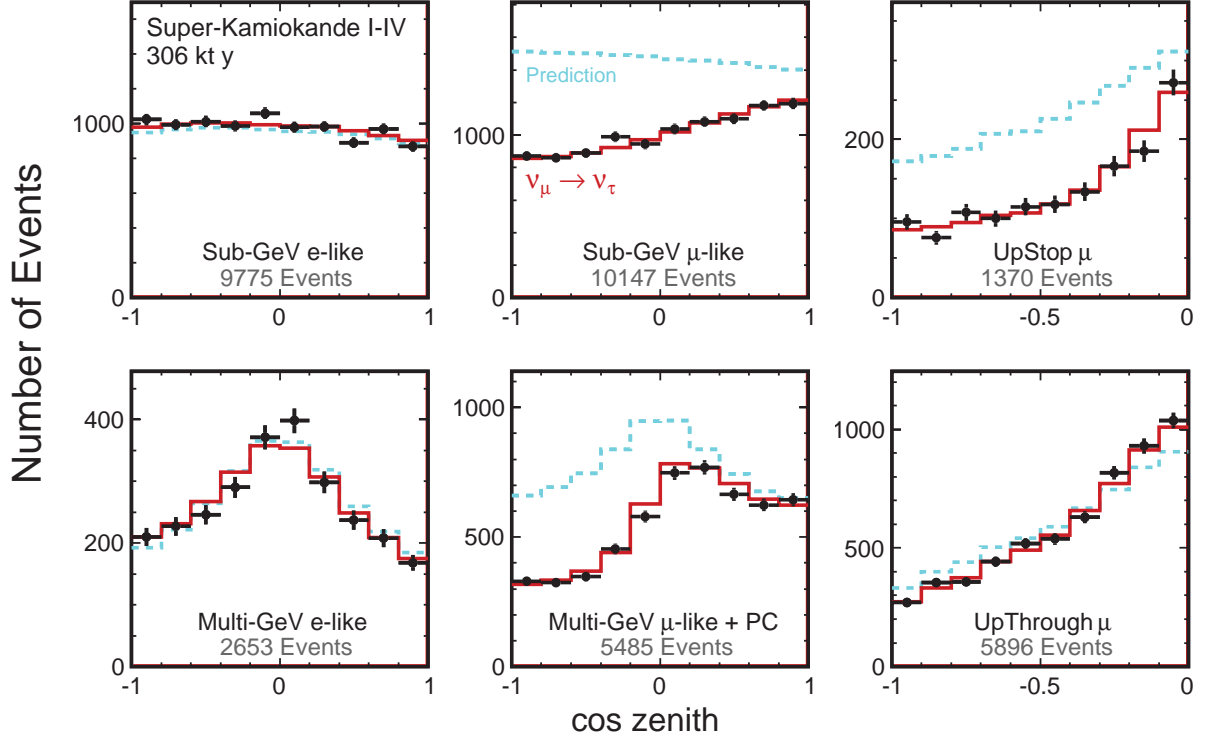
Figure 14.11: The zenith angle distributions for fully contained 1-ring e-like and μ-like events with visible energy < 1.33 GeV (sub-GeV) and > 1.33 GeV (multi-GeV). For multi-GeV μ-like events, a combined distribution with partially contained (PC) events is shown. The dotted histograms show the non-oscillated Monte Carlo events, and the solid histograms show the best-fit expectations for $\nu_\mu \leftrightarrow \nu_\tau$ oscillations. (This figure is provided by the Super-Kamiokande Collab.)

alone. By selecting events with high L/E resolution, evidence for the dip in the L/E distribution was observed at the right place expected from the interpretation of the Super-Kamiokande's data in terms of $\nu_\mu \leftrightarrow \nu_\tau$ oscillations [18], see Fig. 14.12. This dip cannot be explained by alternative hypotheses of neutrino decay and neutrino decoherence, and they are excluded at more than 3σ in comparison with the neutrino oscillation interpretation. For ν_τ appearance, see Section 14.11.4.

The muon neutrino disappearance discovered by Super-Kamiokande has been confirmed by atmospheric neutrino experiments, MACRO [248] and Soudan 2 [249], long baseline accelerator experiments, K2K [19], MINOS [20,21], T2K [22,23], and NOνA [41], and neutrino telescope experiments, ANTARES [253] and IceCube-DeepCore [255]. Fig. 14.13 shows 90% CL allowed regions in the $\sin^2 2\theta_{23}$ - $\Delta m^2_{32(31)}$ plane, for the case of normal mass ordering, reported by the T2K [43], NOνA [60], MINOS [289], Super-Kamiokande [288], and IceCube-DeepCore [254] experiments. All these regions are derived from three-neutrino oscillation analyses.
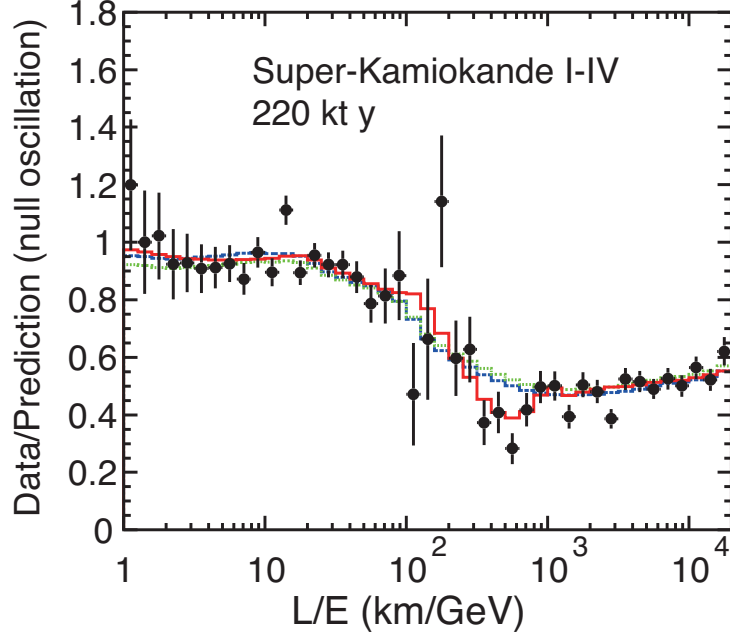
Figure 14.12: Results of the L/E analysis of SK1-SK4 atmospheric neutrino data. The points show the ratio of the data to the Monte Carlo prediction without oscillations, as a function of the reconstructed L/E. The error bars are statistical only. The solid line shows the best fit with 2-flavour $\nu_\mu \leftrightarrow \nu_\tau$ oscillations. The dashed and dotted lines show the best fit expectations for neutrino decay and neutrino decoherence hypotheses, respectively. (This figure is provided by the Super-Kamiokande Collab.)

14.11.2.   *Octant of θ_{23}* :

The two-flavour ν_μ survival probability in vacuum $P^{2\nu}(\nu_\mu \rightarrow \nu_\mu)$ is given by Eq. (14.54) with $l = \mu$, $\theta = \theta_{23}$ and $\Delta m^2 = \Delta m_{31}^2$.   It is symmetric in the mixing angle θ with respect to $\theta = \pi/4$, or degenerate with respect to the interchange $\theta \leftrightarrow \pi/2 - \theta$. In other words, in the leading order the ν_μ disappearance is not sensitive to the octant of the mixing angle θ, namely, whether θ lies in the first octant ($\theta < \pi/4$) or in the second octant ($\theta > \pi/4$). This is the reason why $\sin^2 2\theta_{23}$ has been used in the neutrino oscillation literature until recently. However, as the mixing determined by the angle θ_{23} is known to be nearly maximal, it is important to determine whether $\theta_{23} = \pi/4$, or if not, in which octant θ_{23} lies. As we have seen in Section 14.8, the value of $\sin^2 \theta_{23}$ plays a very important role in the determination of the neutrino mass ordering in the experiments with atmospheric neutrinos and in long baseline neutrino oscillation experiments. It is also one of the important parameters in the interpretation of the data on CP violation in neutrino oscillations. The value of θ_{23} might be related to the existence of a new underlying fundamental symmetry of the neutrino mixing matrix and of the lepton sector of particle physics (see, e.g., the first three articles quoted in Ref. [96]) . Precise determination of θ_{23} requires, *e.g.*, precise measurements of ν_μ disappearance and analyses in terms of full three-neutrino oscillations, or combined analysis of ν_μ disappearance and $\nu_\mu \rightarrow \nu_e$
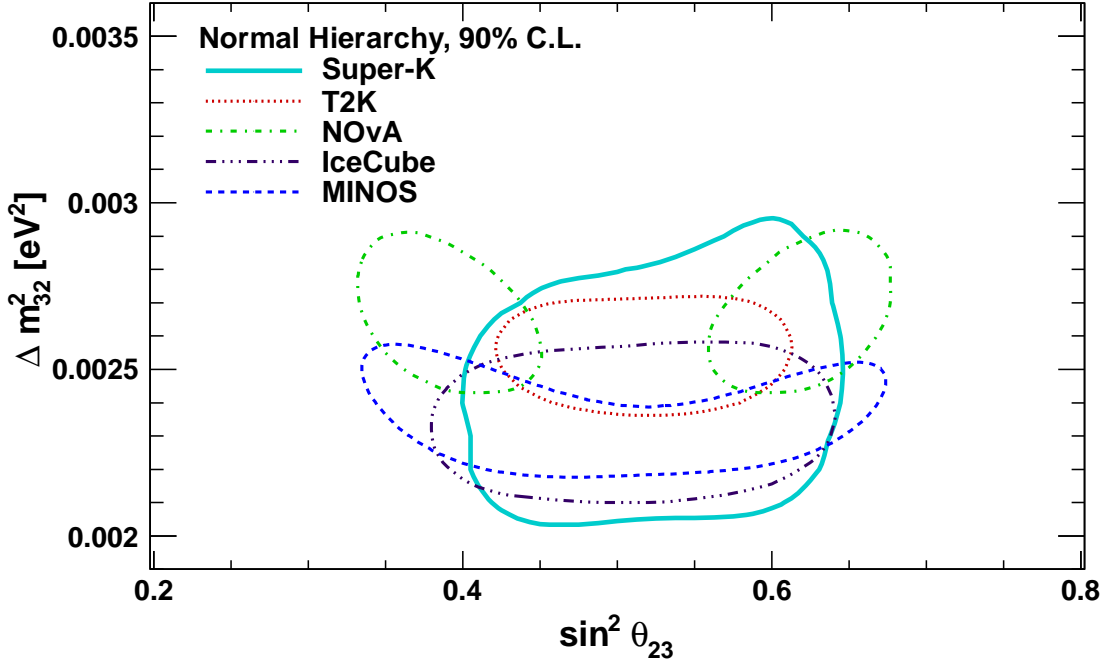
Figure 14.13: The 90% confidence regions for the $\sin^2\theta_{23}$ - Δm_{32}^2 plane assuming normal mass ordering derived from the T2K [43], NOνA [60], MINOS [289], Super-Kamiokande [288], and IceCube [254] experiments. This figure is taken from [288].

appearance for ν_μ and $\bar\nu_\mu$ beams.

MINOS [289] has made a combined analysis of the ν_μ disappearance [290] and $\nu_\mu \to \nu_e$ appearance [47] data using the complete set of accelerator and atmospheric neutrino data. The results obtained are $|\Delta m_{32}^2| = (2.28 - 2.46) \times 10^{-3}$ eV^2 (68% CL) and $\sin^2\theta_{23} = 0.35 - 0.65$ (90% CL) for normal mass ordering and $|\Delta m_{32}^2| = (2.32 - 2.53) \times 10^{-3}$ eV^2 (68% CL) and $\sin^2\theta_{23} = 0.34 - 0.67$ (90% CL) for inverted mass ordering. The best-fit value in this analysis, $\sin^2\theta_{23} < 0.5$ ($\theta_{23} < \pi/4$) is obtained for inverted mass ordering.

Recently, NOνA [60] has made a precise measurement of ν_μ disappearance using the data corresponding to 6.05×10^{20} POT. Assuming the normal mass ordering, $\Delta m_{32}^2 = (2.67 \pm 0.11) \times 10^{-3}$ eV^2 and two statistically degenerate values of $\sin^2\theta_{23} = 0.404^{+0.030}_{-0.022}$ and $0.624^{+0.022}_{-0.030}$ are obtained. The NOνA results disfavor the maximal mixing $\theta_{23} = \pi/2$ at 2.6σ significance.

T2K, on the other hand, has accumulated the neutrino mode data corresponding to 7.482×10^{20} POT and the antineutrino mode data corresponding to 7.471×10^{20} POT, and has made a combined analysis of ν_μ and $\bar\nu_\mu$ disappearance and $\nu_\mu \to \nu_e$ and $\bar\nu_\mu \to \bar\nu_e$ appearance channels [43]. In this analysis, ν_μ, $\bar\nu_\mu$, ν_e, and $\bar\nu_e$ CCQE (charged-current quasielastic event) candidates were selected from the far-detector data, and a joint maximum likelihood fit of these four event samples has been performed to estimate the oscillation parameters, $\sin^2\theta_{23}$, Δm_{32}^2, $\sin^2\theta_{13}$, and δ in the full three

neutrino oscillation framework. (In the fit, the reconstructed neutrino energy $E_{\rm rec}$ is used for ν_μ and $\bar{\nu}_\mu$ samples, and $E_{\rm rec}$ and reconstructed angle between the lepton and the neutrino beam direction $\theta_{\rm rec}$ are used for ν_e and $\bar{\nu}_e$ samples.) The T2K results shown in Fig. 14.13 are obtained from this fit using the "reactor measurement" of $\sin^2 2\theta_{13} = 0.085 \pm 0.005$ [291] and assuming normal mass ordering. The obtained best-fit values are $\Delta m_{32}^2 = 2.545 \times 10^{-3}$ eV^2 and $\sin^2 \theta_{23} = 0.532$. The T2K result is consistent with maximal mixing. However, as the 68% CL interval for $\sin^2 \theta_{23}$ is 0.464 - 0.578, T2K notes [43] that the tension between the the T2K and NOνA [60] measurements is rather mild (1.7 σ).

14.11.3.   *Comparison of ν_μ disappearance and $\bar{\nu}_\mu$ disappearance data* :

The CPT symmetry requires neutrinos and antineutrinos to have the same masses and mixing parameters. In vacuum, this means the same survival probabilities for a neutrino and an antineutrino which have the same energy and which traveled the same distance. In matter, ν_μ and $\bar{\nu}_\mu$ survival probabilities are different, but with the experimental conditions of MINOS and T2K, which reported $\bar{\nu}_\mu$ disappearance in accelerator long baseline experiments, the differences are small.

MINOS first observed muon antineutrino disappearance [292] with the NUMI beam line optimized for $\bar{\nu}_\mu$ production. Actually, MINOS produced a "ν_μ-dominated" or "$\bar{\nu}_\mu$-enhanced" beam by selectively focusing positive or negative pions and kaons. In Ref. 290, MINOS reported the results of the neutrino oscillation analysis based on the data obtained with 10.71×10^{20} POT of the ν_μ-dominated beam and 3.36×10^{20} POT of the $\bar{\nu}_\mu$-enhanced beam. In addition, they used the atmospheric neutrino data based on the MINOS far detector exposure of 37.88 kt·yr [250]. As the MINOS detector has a capability to separate neutrinos and antineutrinos on an event-by-event basis, it can use both ν_μ and $\bar{\nu}_\mu$ contained events from the ν_μ-dominated beam. From the $\bar{\nu}_\mu$-enhanced beam, $\bar{\nu}_\mu$ contained events are used. For the complete data sets used, refer to Ref. 290. Assuming the identical oscillation parameters for neutrinos and antineutrinos, the results of the fit within the two-neutrino oscillation framework using the full MINOS data sample yielded $\Delta m^2 = (2.41^{+0.09}_{-0.10}) \times 10^{-3}$ eV^2 and $\sin^2 2\theta = 0.950^{+0.035}_{-0.036}$, or $\sin^2 2\theta > 0.890$ at 90% CL. Allowing independent oscillations for neutrinos and antineutrinos, characterised respectively by Δm^2, θ and $\Delta\bar{m}^2$, $\bar{\theta}$, the results of the fit are $\Delta\bar{m}^2 = (2.50^{+0.23}_{-0.25}) \times 10^{-3}$ eV^2 and $\sin^2 2\bar{\theta} = 0.97^{+0.03}_{-0.08}$, or $\sin^2 2\bar{\theta} > 0.83$ at 90% CL, and Δm^2 - $\Delta\bar{m}^2 = (0.12^{+0.24}_{-0.26}) \times 10^{-3}$ eV^2. This result shows that the neutrino and antineutrino mass splittings are in agreement, which is compatible with CPT invariance.

T2K also observed $\bar{\nu}_\mu$ disappearance [293,294] using an off-axis quasi-monochromatic $\bar{\nu}_\mu$ beam peaked at $\sim$ 0.6 GeV with the polarity of the horn current set to focus negative pions. Using the same ν_μ and $\bar{\nu}_\mu$ CCQE candidate events as used in Ref. 43, T2K has made a simultaneous analysis of the neutrino and antineutrino disappearance, allowing $\theta_{23} \neq \bar{\theta}_{23}$ and $\Delta m_{32}^2 \neq \Delta\bar{m}_{32}^2$ [294]. This simultaneous analysis is motivated by a significant neutrino background in the antineutrino-mode running. A maximum likelihood fit has been performed to the reconstructed energy spectra of μ-like samples observed in the Super-Kamiokande in the neutrino mode and antineutrino mode. In this fit, δ is fixed to 0 since it has a negligible impact on the disappearance spectra.

Other oscillation parameters, θ_{12}, θ_{13}, and Δm_{21}^2 are assumed to be the same for neutrinos and antineutrinos, and are treated as nuisance parameters. Matter effects, though negligible, are included. Assuming the normal mass ordering, the best-fit values (and 68% CL intervals) obtained for the ν_μ disappearance parameters are $\Delta m_{32}^2 = 2.53$ $(2.40 - 2.68) \times 10^{-3}$ eV^2 and $\sin^2 \theta_{23} = 0.51$ $(0.44 - 0.59)$, and those for $\bar{\nu}_\mu$ disappearance parameters are $\Delta \bar{m}_{32}^2 = 2.55$ $(2.28 - 2.88) \times 10^{-3}$ eV^2 and $\sin^2 \bar{\theta}_{23} = 0.42$ $(0.35 - 0.67)$. These results show that (i) they are consistent with the MINOS $\bar{\nu}_\mu$ disappearance results [292] and (ii) no significant differences are observed between the values of ν_μ and $\bar{\nu}_\mu$ oscillation parameters.

Note also that Super-Kamiokande searched for differences in oscillation parameters for ν_μ and $\bar{\nu}_\mu$ in atmospheric neutrino observations [295]. As Super-kamiokande cannot identify ν_μ and $\bar{\nu}_\mu$ on an event by event basis, this study relied on a statistical method to fit the zenith-angle distributions of various event samples with different mixing parameters between ν_μ and $\bar{\nu}_\mu$ disappearance models. The results of this study showed no difference between neutrino and antineutrino mixing.

14.11.4. ν_τ *appearance data* :

Super-Kamiokande Collaboration searched for the appearance of τ leptons from the CC interactions of oscillation-generated ν_τ in the detector using the atmospheric neutrino data [296,24]. In the 2-neutrino mixing framework, the relevant $\nu_\mu \rightarrow \nu_\tau$ oscillation probability is given by Eq. (14.54) with $l = \mu$, $x = \tau$, $\theta = \theta_{23}$ and $\Delta m^2 = \Delta m_{31}^2$. An excess of τ-like events is expected in the upward-going direction. Though the Super-Kamiokande detector cannot identify a CC ν_τ interaction on an event by event basis, the Super-Kamiokande Collaboration excluded the no-tau-appearance hypothesis at the 3.8σ level through a neural network analysis on the zenith-angle distribution of multi-GeV contained events [24].

For the purpose of demonstrating the appearance of tau neutrinos on an event-by-event basis, a promising method is an accelerator long-baseline experiment using emulsion technique to identify short-lived τ leptons produced in the ν_τ CC interactions. OPERA adopted this strategy and searched for the appearance of ν_τ in the CNGS muon neutrino beam during 2008 and 2012, corresponding to a live exposure of 17.97×10^{19} POT in total. In 2010, OPERA reported observation of the first ν_τ candidate [173]. In 2015, OPERA has reported observation of the fifth ν_τ candidate [297]. The observed candidate events are classified into the four decay channels, $\tau \rightarrow 1h$ (hadronic 1-prong), $\tau \rightarrow 1h$ (hadronic 3-prong), $\tau \rightarrow \mu$, and $\tau \rightarrow e$, and expected signal and background events are calculated for each decay channel. The expected total signal and background events are, respectively, 2.64 ± 0.53 and 0.25 ± 0.05. With 5 events observed, the OPERA Collaboration concludes the discovery of ν_τ appearance with a significance larger than 5σ.

14.12.   Measurements of θ_{13}

The discoveries of atmospheric neutrino oscillations and solar neutrino oscillations naturally led to considerable interests in the measurements of the last neutrino mixing angle θ_{13}, because if θ_{13} is not too small, it will widen the opportunities to measure the unknown CP-violating phase δ in the PMNS matrix and the neutrino mass ordering.

In 2012, the three reactor neutrino oscillation experiments Double Chooz, Daya Bay, and RENO reported their first results on $\bar{\nu}_e$ disappearance. Under the conditions of these experiments the probability of reactor $\bar{\nu}_e$ survival is given to a very good approximation by Eq. (14.45) (the effects of Δm_{21}^2 being negligible) and depends on two parameters $\sin^2 2\theta_{13}$ and Δm_{31}^2. Daya Bay obtained $\sin^2 2\theta_{13} = 0.092 \pm 0.016 \pm 0.005$ from live-time exposure in 55 days, indicating 5.2σ evidence for non-zero θ_{13} [33]. RENO obtained $\sin^2 2\theta_{13} = 0.113 \pm 0.013 \pm 0.019$ from 229 days of exposure, also indicating non-zero θ_{13} with a significance of 4.9σ [34]. Both Daya Bay and RENO results were obtained from rate-only analyses of the $\bar{\nu}_e$ disappearance measurements with near and far detectors. These results established non-zero θ_{13}, and it turned out that the measured value of θ_{13} was relatively large. It should be noted that prior to Daya Bay and RENO, Double Chooz also reported $\sin^2 2\theta_{13} = 0.086 \pm 0.041 \pm 0.030$ with measurements by a far detector, and it ruled out the no-oscillation hypothesis at the 94.6% CL [32].

The latest Daya Bay results [44] are obtained based on the combination of 217 days (December 2011 - July 2012) of measurement with six antineutrino detectors and a subsequent 1013 days (October 2012 - July 2015) of measurement with eight detectors. The Daya Bay collaboration has adopted the three-flavour oscillation scheme and analyzed the relative antineutrino rates and energy spectra between detectors using a method to predict the signal in the far hall based on measurements obtained in the near halls. With this method, they have minimized the model dependence on reactor antineutrino emission. Also, improvements in energy calibration (0.2% between detectors) and background estimation helped reduce systematic errors. Their reported new result, $\sin^2 2\theta_{13} = 0.0841 \pm 0.0027 \pm 0.0019$ is the most precise measurement of θ_{13} to date. To obtain this result, they used $\sin^2 2\theta_{12} = 0.846 \pm 0.021$ and $\Delta m_{21}^2 = (7.53 \pm 0.18) \times 10^{-5}$ eV^2 [291], but the dependence on these parameters is weak. They also found for the effective mass-squared difference $|\Delta m_{ee}^2| = (2.50 \pm 0.06 \pm 0.06) \times 10^{-3}$ eV^2, where $\Delta m_{ee}^2 \simeq \cos^2 \theta_{12} |\Delta m_{31}^2| + \sin^2 \theta_{12} |\Delta m_{32}^2|$. From the measured value of $|\Delta m_{ee}^2|$, they deduce $\Delta m_{32}^2 = (2.45 \pm 0.06 \pm 0.06) \times 10^{-3}$ eV^2 for the normal mass ordering and $\Delta m_{32}^2 = -(2.56 \pm 0.06 \pm 0.06) \times 10^{-3}$ eV^2 for the inverted mass ordering. These results on Δm_{32}^2 are consistent with the T2K and MINOS results.

The latest RENO results are reported at TAUP2017 [45] based on 1500 live days of data. Using the observed IBD prompt rates and spectra in the near and far detectors, $\sin^2 2\theta_{13} = 0.086 \pm 0.006 \pm 0.005$ and $|\Delta m_{ee}^2| = (2.61^{+0.15}_{-0.16} \pm 0.09) \times 10^{-3}$ eV^2 have been obtained.

The latest results from Double Chooz using the data collected by the far detector in 467.90 live days have been published in Ref. 46. From a fit to the observed spectrum ("Rate + Shape analysis") in the two-flavour oscillation scheme, Double Chooz obtained $\sin^2 2\theta_{13} = 0.090^{+0.032}_{-0.029}$ for the normal mass ordering using $\Delta m_{31}^2 = (2.44^{+0.09}_{-0.10}) \times 10^{-3}$ eV^2

from MINOS [289]. For the inverted mass ordering, they obtained $\sin^2 2\theta_{13} = 0.092^{+0.033}_{-0.029}$, using $|\Delta m^2_{31}| = (2.38^{+0.09}_{-0.10}) \times 10^{-3}$ eV^2 [289].

Until θ_{13} was measured by the modern reactor experiments, long-baseline accelerator $\nu_\mu \to \nu_e$ appearance experiments were considered to be another promising method to measure θ_{13}, within uncertainties mainly caused by unknown CPV phase δ. In fact, experimental indications of $\nu_\mu \to \nu_e$ oscillations and a non-zero θ_{13} was reported by the T2K experiment in 2011. T2K observed, with 1.43×10^{20} POT, six ν_e candidate events, while the expectation for $\theta_{13} = 0$ was 1.5 ± 0.3 events. This result implied a non-zero θ_{13} with statistical significance of 2.5σ [30]. However, because of the unfortunate damage of the J-PARC accelerator caused by the big Tohoku earthquake which hit Japan in March 2011, the T2K experiment stopped for more than a year, and it was in 2014 that T2K could establish non-zero θ_{13} at more than 7σ [48]. Thereafter, the focus of long baseline accelerator $\nu_\mu \to \nu_e$ appearance experiments shifted to the measurement of the CPV phase δ.

14.13. $\nu_\mu \to \nu_e$ ($\bar{\nu}_\mu \to \bar{\nu}_e$) appearance data and measurements of δ

As Eq. (14.74) shows, the probability of $\nu_\mu \to \nu_e$ oscillations in matter

is given as a function of all the oscillation parameters including the sign of Δm^2_{31}, *i.e.*, mass ordering. Using the measured values of θ_{13} from the reactor experiments and Δm^2_{21} and θ_{12} from the solar neutrino experiments and KamLAND as constraints, accelerator-based long baseline experiments are able to measure the CPV phase δ and constrain mass ordering through oscillation analyses of $\nu_\mu \to \nu_e$ and $\bar{\nu}_\mu \to \bar{\nu}_e$ appearance. In these analyses, in particular in the simultaneous analyses of ν_e (and $\bar{\nu}_e$) appearance and ν_μ (and $\bar{\nu}_\mu$) disappearance, θ_{23} and $\Delta m^2_{32} \cong \Delta m^2_{31}$ are also better determined.

MINOS first used a combination of the $\nu_\mu \to \nu_e$ (and $\bar{\nu}_\mu \to \bar{\nu}_e$) appearance measurements and the reactor measurements of θ_{13} to study δ, θ_{23} octant, and mass ordering, and placed some constraints on the value of δ [47]. For this study, MINOS extracted $\nu_\mu \to \nu_e$ and $\bar{\nu}_\mu \to \bar{\nu}_e$ appearance signals statistically from the full MINOS data sample corresponding to 10.6×10^{20} POT ν-beam mode and 3.3×10^{20} POT $\bar{\nu}$-beam mode data-taking.

As noted in Section 14.12, T2K first reported observation of $\nu_\mu \to \nu_e$ appearance events in 2011 [30]. After the interruption due to the Tohoku earthquake, the resumed T2K experiment has accumulated $\nu_\mu \to \nu_e$ appearance data. In 2014, T2K reported observation of 28 ν_e events against 4.92 ± 0.55 expected background events with 1.43×10^{20} POT, and established $\nu_\mu \to \nu_e$ appearance signal with statistical significance of more than 7σ [48]. Also, T2K made an oscillation analysis using the ν_e appearance data [48], or joint analyses of ν_e appearance and ν_μ disappearance [298] with a constraint of θ_{13} value from reactor measurements. Later, T2K switched the data-taking with a ν_μ beam to that with a $\bar{\nu}_\mu$ beam. As discussed in Section 14.11.2, T2K further made a combined analysis of ν_μ and $\bar{\nu}_\mu$ disappearance and $\nu_\mu \to \nu_e$ and $\bar{\nu}_\mu \to \bar{\nu}_e$ appearance channels [43] using the neutrino-mode data corresponding to 7.482×10^{20} POT and the antineutrino-mode data corresponding to 7.471×10^{20} POT. As the appearance signal, 32 ν_e and 4 $\bar{\nu}_e$ CCQE event candidates are selected from these data. T2K further added five ν_e CC1π^+

events selected from the same data set used in Ref. 43 and made another combined analysis [299]. Fig. 14.14 shows $-2\Delta \ln \mathcal{L}$ as a function of δ, resulted from a joint maximum-likelihood fit, in which other oscillation parameters and nuisance parameters are marginalized (integrated over the prior probability density function). In this analysis, CP-conserving values $\delta = 0, \pi$ are excluded at 90% CL.

More recently, in August 2017, T2K announced the latest results with doubled POT for the neutrino-mode data taking [300]. With an improved event selection in the Super-Kamiokande in addition, T2K has observed 74 ν_e and 7 $\bar{\nu}_e$ CCQE event candidates. A combined oscillation analysis using the reactor measurement of θ_{13} has now resulted the CP conserving values of $\delta = 0$ and π falling outside of the 2σ CL intervals for both the normal and inverted mass orderings.
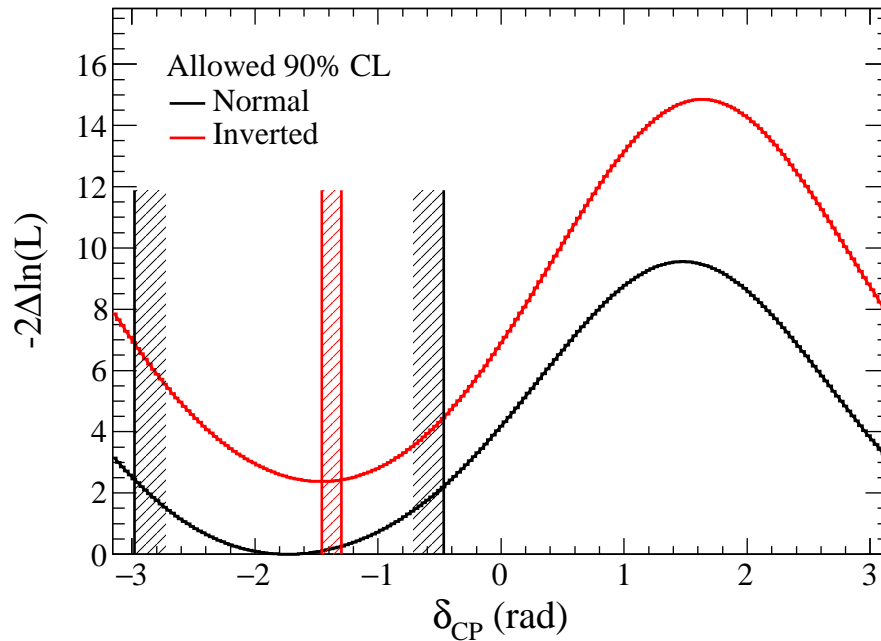

Figure 14.14: T2K's log-likelihood as a function of δ_{CP} for the normal (black) and inverted (red) mass ordering, obtained from a combined analysis of neutrino and antineutrino oscillations using both appearance and disappearance channels. The vertical lines show the corresponding allowed 90% confidence intervals, calculated using the Feldman-Cousins method. $\sin^2 \theta_{13}$ is marginalized using the reactor measurement as prior probability using the value of PDG 2015 [291]. This figure is taken from [299].

NOνA started physics run in February, 2014, and reported its first result of ν_e appearance measurement in 2016 [40]. Since then, NOνA has accumulated more data, and recently reported observation of 33 ν_e candidates withh 8.2 ± 0.8 background events corresponding to 6.05×10^{20} POT [42]. NOνA has made a combined analysis of ν_e appearance and ν_μ disappearance data, using the reactor measurement of θ_{13} as a constraint. Fig. 14.15 shows the significance (σ) at which each value of δ is disfavored.

As the NOνA measurement of $\sin^2\theta_{23}$ has two statistically degenerate values (see Section 14.11.2), the significance is shown for four possible combinations of mass ordering (normal or inverted) and θ_{23} octant (first/lower or second/upper). As seen from this figure, there are two degenerate best-fit points for normal mass ordering, $\sin^2\theta_{23} = 0.404$ and $\delta = 1.48\pi$ and $\sin^2\theta_{23} = 0.623$ and $\delta = 0.74\pi$. The inverted mass ordering in the first octant is disfavored at $> 93\%$ for all the value of δ.
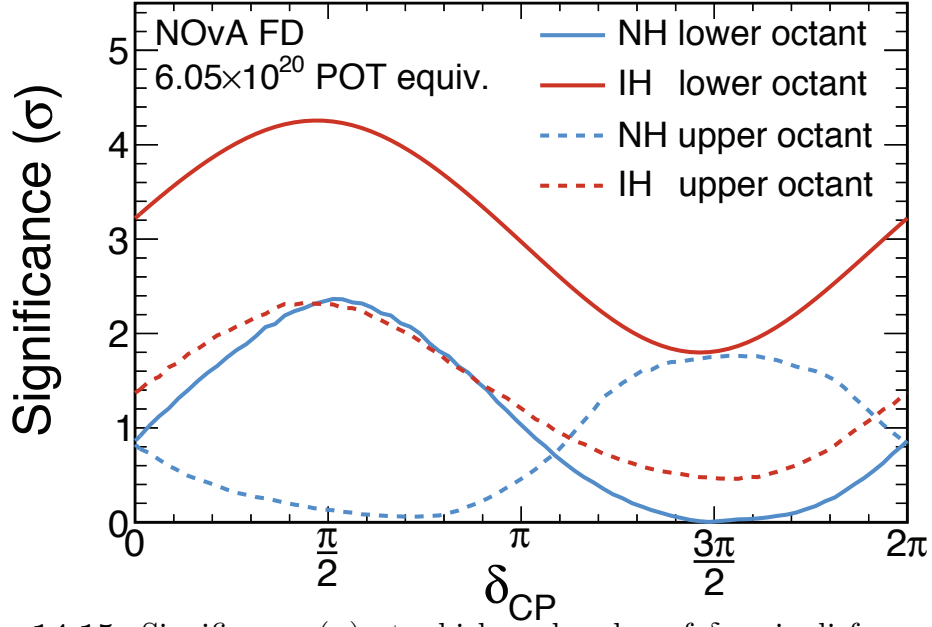

Figure 14.15: Significance (σ) at which each value of δ_{CP} is disfavored for each of the four possible combinations of mass ordering: normal (blue) or inverted (red), and θ_{23} octant: lower (solid) or upper (dashed), by the combination of ν_e appearance and NOνA's latest ν_μ disappearance measurement. This figure is taken from [42].

14.14. Search for Oscillations Involving Light Sterile Neutrinos

Although the mixing of the 3 flavour neutrino states has been experimentally well established, implying the existence of 3 light neutrinos ν_j having masses m_j not exceeding approximately 1 eV, there have been possible hints for the presence in the mixing of one or more additional neutrino states with masses at the eV scale. If these states exist, they must be related to the existence of one or more sterile neutrinos (sterile neutrino fields) which mix with the active flavour neutrinos (active flavour neutrino fields). The hints under discussion have been obtained: i) in the LSND $\bar{\nu}_\mu \rightarrow \bar{\nu}_e$ appearance experiment [259], in which a significant excess of events over the background is claimed to have been observed, ii) from the analysis of the

$\bar{\nu}_\mu \rightarrow \bar{\nu}_e$ [262] and $\nu_\mu \rightarrow \nu_e$ [261] appearance data of the MiniBooNE experiment, iii) from the re-analyses of the short baseline (SBL) reactor neutrino oscillation data using

newly calculated fluxes of reactor $\bar{\nu}_e$ [156,155], which show a possible "disappearance" of the reactor $\bar{\nu}_e$ ("reactor neutrino anomaly"), and iv) from the data of the radioactive neutrino source measurements of the GALLEX [241] and SAGE [242] solar neutrino experiments.

The short baseline neutrino oscillation experiment MiniBooNE at Fermilab investigated ν_e [261] and $\bar{\nu}_e$ [262] appearance in ν_μ and $\bar{\nu}_\mu$ beams, respectively, with a detector containing 800 tons of mineral oil and located 541 m downstream of the production target. With the antineutrino running mode [262], a 2.8σ excess of events over the background was observed in the energy range of $200 < E_\nu < 1250$ MeV in the charged-current quasielastic data. Excess events were observed, in particular, in the interval of energies $200 < E_\nu < 475$ MeV, which corresponds to L/E range outside of that probed in the LSND experiment. The origin of this excess is not understood. Employing a simple 2-neutrino oscillation hypothesis and using the data from the entire neutrino energy interval $200 < E_\nu < 1250$ MeV in the data analysis, this result, interpreted in terms of $\nu_\mu \rightarrow \nu_e$ oscillations, corresponds to an allowed region in the $\sin^2 2\theta - \Delta m^2$ plane, which overlaps with the allowed region obtained from the interpretation of the LSND data in terms of $\bar{\nu}_\mu \rightarrow \bar{\nu}_e$ oscillations. The overlap region at the 90% CL extends over $\Delta m^2 \sim$ a few $\times 10^{-2}$ eV^2 at $\sin^2 2\theta = 1$ to 1 eV^2 at $\sin^2 2\theta =$ a few $\times 10^{-3}$. The MiniBooNE Collaboration studied also the CP conjugate oscillation channel [261], $\nu_\mu \rightarrow \nu_e$, and observed a $3.4\ \sigma$ excess of events in the same energy range. Most of the excess events lie in the interval $200 < E_\nu < 475$ MeV and are incompatible with the $\bar{\nu}_\mu \rightarrow \bar{\nu}_e$ oscillation interpretation of the LSND data. The energy spectra of the excess events observed in the ν_μ [261] and $\bar{\nu}_\mu$ [262] runs are only marginally compatible with each other and thus with the simple 2-neutrino oscillation hypothesis.

The reactor neutrino anomaly [156] is related to the results of a new and very detailed calculation of the reactor $\bar{\nu}_e$ fluxes [155] which were found to be by approximately 3.5% larger than the fluxes calculated in Ref. 153 and widely used in the past in the interpretation of the data of the SBL reactor $\bar{\nu}_e$ oscillation experiments. These data show indications for reactor $\bar{\nu}_e$ "disappearance" when analyzed using the fluxes from [155]. It should be added that there are a number of uncertainties in the calculation of the fluxes under discussion (associated, *e.g.*, with the weak magnetism term contribution to the corresponding β-decay rates [157], the contribution of a relatively large number of "forbidden" β-decays [301], etc.) which can be of the order of the difference between the "old" and "new" fluxes.

Radioactive neutrino source measurements of the GALLEX [241] and SAGE [242] experiments also showed a deficit of the measured fluxes compared to the expected fluxes ("Gallium anomaly"), and therefore might be interpreted as hints for ν_e disappearance.

Significant constraints on the parameters characterizing the oscillations involving sterile neutrinos follow from the negative results of the searches for $\nu_\mu \rightarrow \nu_e$ and/or $\bar{\nu}_\mu \rightarrow \bar{\nu}_e$ oscillations in the Karmen [260], NOMAD [302], ICARUS [258], and OPERA [303] experiments, and from the nonobservation of effects of oscillations into sterile neutrinos in the solar neutrino experiments and in the studies of ν_μ and/or $\bar{\nu}_\mu$ disappearance in the CDHSW [304], MINOS and SuperKamiokande experiments.

In the period May 2016 - May 2017 results of searches for active-sterile neutrino

oscillations with $\Delta m^2 \sim 1$ eV^2 were presented by the IceCube [305], NEOS [306] and DANSS [307] experiments. The IceCube collaboration reported results on disappearance into sterile antineutrinos $\bar{\nu}_s$ of atmospheric $\bar{\nu}_\mu$ with energies in the interval $E_\nu \sim$(300 GeV - 10 TeV), which traverse the Earth before reaching the detector. For Earth core crossing $\bar{\nu}_\mu$, the $\bar{\nu}_\mu \to \bar{\nu}_s$ transitions at small mixing angles and $\Delta m^2 \sim (0.1 - 1.0)$ eV^2 can be maximally enhanced at $E_\nu \sim$3 TeV by the Earth mantle-core amplification (or NOLR) effect [190,196](see also [308]) . This allowed the IceCube collaboration to obtain stringent limits on the relevant $\bar{\nu}_\mu - \bar{\nu}_s$ mixing parameter in the region $\Delta m^2 \sim (0.1 - 0.6)$ eV^2 assuming two-neutrino mixing (for further details see [305,308]) .

The NEOS and DANSS collaborations performed searches of reactor $\bar{\nu}_e$ disappearance into $\bar{\nu}_s$. The NEOS experiment [306] used a 1 ton Gd loaded liquid scintillator detector located at a distance $L = 24$ m from the core of a reactor with thermal power of 2.8 GW, belonging to the Hanbit nuclear power complex in Yeonggwang, South Korea. In the DANSS experiment at the Kalinin nuclear power plant in Russia [307] the measurements were performed with a movable 0.9 ton segmented solid scintillator detector at 3 different distances from the core of a 3 GW reactor, spanning the (center to center) interval (10.7 - 12.7) m. The detector consists of 2500 scintillator strips, covered with gadolinium loaded reflective paint and read out by silicon PMs via wave length shifting fibers.

In the same period the Daya Bay, MINOS and Bugey-3 collaborations published results of a joint analysis of their disappearance data [309].

Two possible "minimal" phenomenological models (or schemes) with light sterile neutrinos are widely used in order to explain the data discussed in this section in terms of neutrino oscillations: the so-called "3 + 1" and "3 + 2" models. They contain respectively one and two sterile neutrinos (right-handed sterile neutrino fields). Thus, the "3 + 1" and "3 + 2" models have altogether 4 and 5 light massive neutrinos ν_j, which in the minimal versions of these models are Majorana particles. The additional neutrinos ν_4 and ν_4, ν_5 should have masses m_4 and m_4, m_5 at the eV scale (see below). It follows from the data that if ν_4 or ν_4, ν_5 exist, they couple to the electron and muon in the weak charged lepton current with couplings U_{ek} and $U_{\mu k}$, $k = 4$; 4, 5, which are approximately $|U_{ek}| \sim 0.1$ and $|U_{\mu k}| \sim 0.1$.

In the context of the "3+1" model, the Daya Bay Collaboration searched for relative spectral distortion in their reactor antineutrino data, due to possible mixing of a light sterile neutrino in the $|\Delta m_{41}^2| < 0.3$ eV^2 region [310]. The result is consistent with no sterile neutrino mixing, leading to the most stringent limits on $\sin^2\theta_{14} = |U_{e4}|^2$ in the 10^{-3} eV$^2 < |\Delta m_{41}^2| < 0.1$ eV^2 region.

Global analysis of all the data (positive evidences and negative results) relevant for the test of the sterile neutrino hypothesis were performed most recently in [311](for earlier results of global fits see, e.g., Ref. [312] and Ref. [313]) . The authors of [311] performed the analysis within the $3 + 1$ scheme employing the so-called "pragmatic approach", i.e., excluding from the data set used the MiniBooNE data at $E_\nu < 0.475$ GeV. As we have already mentioned, these data show an excess of events over the estimated background [261,262] whose nature is presently not well understood. For the best fit values of the parameters $|U_{e4}|^2$, $|U_{\mu 4}|^2$ and $\Delta m_{\mathrm{SBL}}^2 \equiv m_4^2 - m_{min}^2$, where $m_{min} = \min(m_j)$, $j = 1, 2, 3$, characterizing the active-sterile neutrino (antineutrino)

oscillations in the $3 + 1$ scheme, the authors of [311] find:

$$|U_{e4}|^2 = 0.019 \,, \quad |U_{\mu 4}|^2 = 0.015 \,, \quad \Delta m^2_{\text{SBL}} = 1.7 \ \text{eV}^2 \,. \qquad (14.105)$$

The existence of light sterile neutrinos has cosmological implications the discussion of which lies outside the scope of the present article (for a discussion of the cosmological constraints on light sterile neutrinos see, *e.g.*, [314,75]) .

The hypothesis of existence of light sterile neutrinos with eV scale masses and charged current couplings to the electron and muon quoted above, is already being tested, as we have discussed, in a few running experiments, and will be tested in a large number of experiments with reactor and accelerator neutrinos, and neutrinos from artificial sources, some of which are under preparation and are planned to start taking data already this (2017) year (see, *e.g.*, [315] for a detailed list and discussion of the planned experiments).

14.15.   Outlook

The currently available data on neutrino oscillations are summarised in Fig. 14.16.

The program of experimental research in neutrino physics extends beyond 2030 (see, *e.g.*, Refs. [91,93,94,82,83,84,85])

In the coming years we expect a wealth of new data that, it is hoped, will shed light on the fundamental aspects of neutrino mixing: the nature - Dirac or Majorana - of massive neutrinos, the type of spectrum the neutrino masses obey, the status of CP symmetry in the lepton sector, the absolute neutrino mass scale, the origin of the observed patterns of the neutrino masses and mixing, and, eventually, on the mechanism of neutrino mass generation. We are looking forward to these exciting developments in neutrino physics.
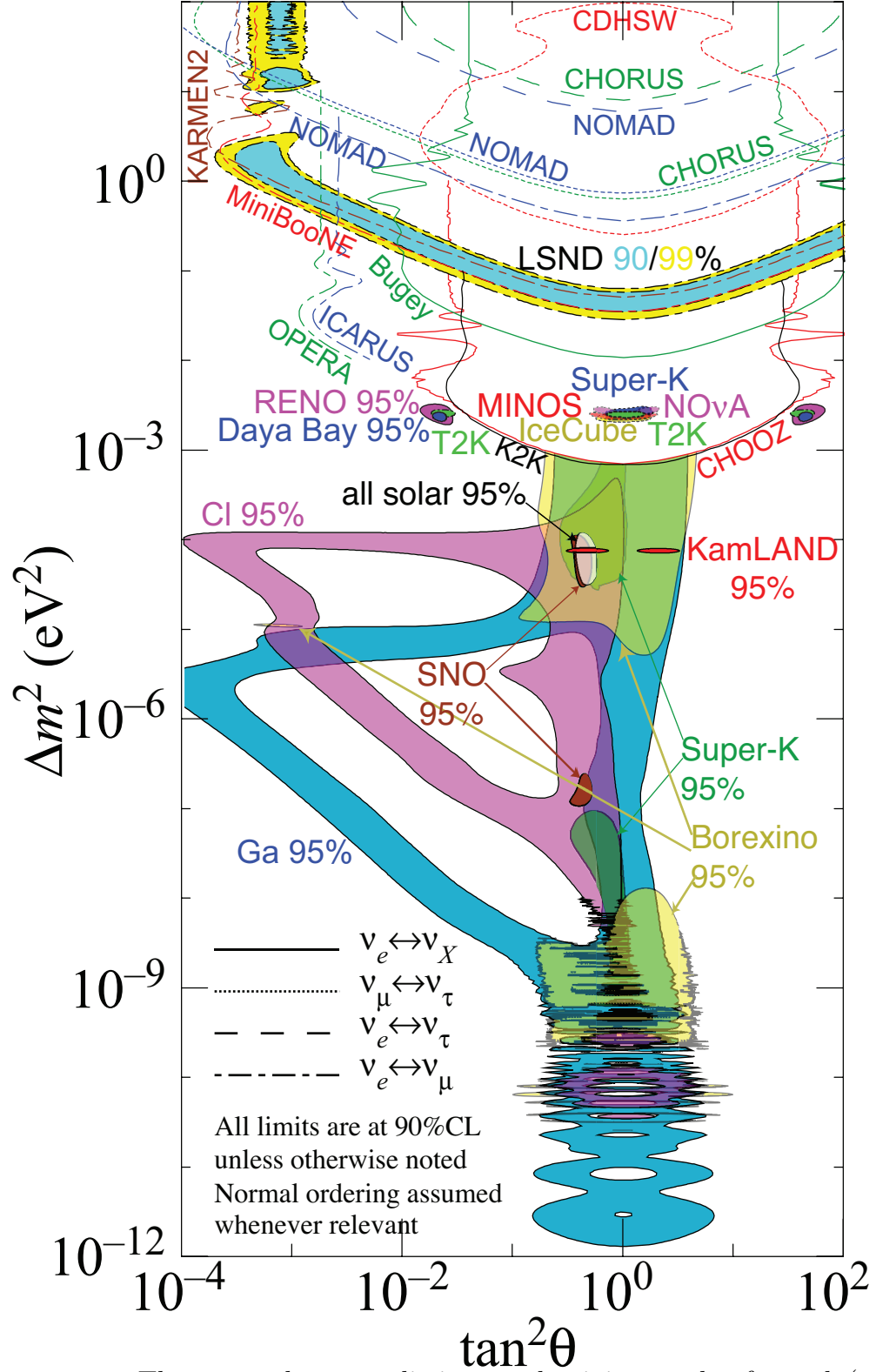
Figure 14.16: The squared-mass splittings and mixing angles favored (solid regions) or excluded (open regions) by existing neutrino oscillation measurements. Results are categorized by channels: ν_e disappearance (solid lines), $\nu_\mu \leftrightarrow \nu_\tau$ (dotted lines), $\nu_e \leftrightarrow \nu_\tau$ (dashed lines), and $\nu_e \leftrightarrow \nu_\mu$ (dashed-dotted lines). The normal mass ordering is assumed where relevant. The figure was contributed by H. Murayama (University of California, Berkeley, and Kavli IPMU, University of Tokyo, 2018).

References:

1. B. Pontecorvo, Zh. Eksp. Teor. Fiz. **53**, 1717 (1967) [Sov. Phys. JETP **26**, 984 (1968)].
2. M. Fukugita and T. Yanagida, Phys. Lett. **B174**, 45 (1986); V.A. Kuzmin, V.A. Rubakov, and M.E. Shaposhnikov, Phys. Lett. **B155**, 36 (1985).
3. P. Minkowski, Phys. Lett. **B67**, 421 (1977); see also: M. Gell-Mann, P. Ramond, and R. Slansky in *Supergravity*, p. 315, edited by F. Nieuwenhuizen and D. Friedman, North Holland, Amsterdam, 1979; T. Yanagida, *Proc. of the Workshop on Unified Theories and the Baryon Number of the Universe*, edited by O. Sawada and A. Sugamoto, KEK, Japan 1979; R.N. Mohapatra and G. Senjanović, Phys. Rev. Lett. **44**, 912 (1980).
4. B. Pontecorvo, Zh. Eksp. Teor. Fiz. **33**, 549 (1957) and **34**, 247 (1958).
5. Z. Maki, M. Nakagawa, and S. Sakata, Prog. Theor. Phys. **28**, 870 (1962).
6. B.T. Cleveland *et al.*, Astrophys. J. **496**, 505 (1988).
7. Y. Fukuda *et al.*, [Kamiokande Collab.], Phys. Rev. Lett. **77**, 1683 (1996).
8. J.N. Abdurashitov *et al.*, [SAGE Collab.], Phys. Rev. **C80**, 015807 (2009).
9. P. Anselmann *et al.*, [GALLEX Collab.], Phys. Lett. **B285**, 376 (1992).
10. W. Hampel *et al.*, [GALLEX Collab.], Phys. Lett. **B447**, 127 (1999).
11. M. Altmann *et al.*, [GNO Collab.], Phys. Lett. **B616**, 174 (2005).
12. S. Fukuda *et al.*, [Super-Kamiokande Collab.], Phys. Lett. **B539**, 179 (2002).
13. Q.R. Ahmad *et al.*, [SNO Collab.], Phys. Rev. Lett. **87**, 071301 (2001).
14. Q.R. Ahmad *et al.*, [SNO Collab.], Phys. Rev. Lett. **89**, 011301 (2002).
15. K. Eguchi *et al.*, [KamLAND Collab.], Phys. Rev. Lett. **90**, 021802 (2003).
16. T. Araki *et al.*, [KamLAND Collab.], Phys. Rev. Lett. **94**, 081801 (2005).
17. Y. Fukuda *et al.*, [Super-Kamiokande Collab.], Phys. Rev. Lett. **81**, 1562 (1998).
18. Y. Ashie *et al.*, [Super-Kamiokande Collab.], Phys. Rev. Lett. **93**, 101801 (2004).
19. M.H. Ahn *et al.*, [K2K Collab.], Phys. Rev. **D74**, 072003 (2006).
20. D.G. Michael *et al.*, [MINOS Collab.], Phys. Rev. Lett. **97**, 191801 (2006); P. Adamson *et al.*, [MINOS Collab.], Phys. Rev. Lett. **101**, 131802 (2008).
21. P. Adamson *et al.*, [MINOS Collab.], Phys. Rev. Lett. **106**, 181801 (2011).
22. K. Abe *et al.*, [T2K Collab.], Phys. Rev. **D85**, 031103 (2012).
23. K. Abe *et al.*, [T2K Collab.], Phys. Rev. Lett. **111**, 211803 (2013).
24. K. Abe *et al.*, [Super-Kamiokande Collab.], Phys. Rev. Lett. **110**, 181802 (2013).
25. A. Pastore, talk at the EPS HEP 2013 Conference, July 18-24, 2013, Stockholm.
26. L. Wolfenstein, Phys. Rev. **D17**, 2369 (1978);
    Proc. of the 8th International Conference on Neutrino Physics and Astrophysics - "Neutrino'78" (ed. E.C. Fowler, Purdue University Press, West Lafayette, 1978), p. C3.
27. S.P. Mikheev and A.Y. Smirnov, Sov. J. Nucl. Phys. **42**, 913 (1985); Nuovo Cimento **9C**, 17 (1986).
28. T. Kajita, "Nobel Diploma", http://www.nobelprize.org/nobel_prizes/physics/laureates/2015/kajita-diploma.html.
29. A.B. McDonald, "Nobel Diploma" http://www.nobelprize.org/nobel_prizes/physics/laureates/2015/mcdonald-diploma.html.

30. K. Abe *et al.*, [T2K Collab.], Phys. Rev. Lett. **107**, 041801 (2011).
31. P. Adamson *et al.*, [MINOS Collab.], Phys. Rev. Lett. **107**, 181802 (2011).
32. Y. Abe *et al.*, [Double Chooz Collab.], Phys. Rev. Lett. **108**, 131801 (2012).
33. F.P. An *et al.*, [Daya Bay Collab.], Phys. Rev. Lett. **108**, 171803 (2012).
34. J.K. Ahn *et al.*, [RENO Collab.], Phys. Rev. Lett. **108**, 191802 (2012).
35. Y. Abe *et al.*, [Double Chooz Collab.], Phys. Rev. **D86**, 052008 (2012).
36. K. Abe *et al.*, [T2K Collab.], Phys. Rev. **D88**, 032002 (2013).
37. F.P. An *et al.*, [Daya Bay Collab.], Chin. Phys. C **37**, 011001 (2013).
38. F.P. An *et al.*, [Daya Bay Collab.], Phys. Rev. Lett. **112**, 061801 (2014).
39. S.-H. Seo [for the RENO Collab.], talk at the TAUP2013 International Workshop, September 9-13, 2013, Asilomar, California, USA.
40. P. Adamson *et al.*, [NOνA Collab.] Phys. Rev. Lett. **116**, 151806 (2016).
41. P. Adamson *et al.*, [NOνA Collab.], Phys. Rev. **D93**, 051104 (2016).
42. P. Adamson *et al.*, [NOνA Collab.], Phys. Rev. Lett. **118**, 231801 (2017).
43. K. Abe *et al.*, [T2K Collab.], Phys. Rev. Lett. **118**, 151801 (2017).
44. F.P. An *et al.*, [Daya Bay Collab.], Phys. Rev. **D95**, 072006 (2017).
45. S.-H. Seo [for the RENO Collab.], talk at the TAUP2017 International Workshop, July 24-28, 2017, Sudbury, Canada; `arXiv:1710.08204`.
46. Y. Abe *et al.*, [Double Chooz Collab.], JHEP **1014**, 086 (2014).
47. P. Adamson *et al.*, [MINOS Collab.], Phys. Rev. Lett. **110**, 171801 (2013).
48. K. Abe *et al.*, [T2K Collab.], Phys. Rev. Lett. **112**, 061802 (2014).
49. D. Karlen in RPP2016 [Chin. Phys. **C40**, No. 10, 646 (2016)].
50. E. Majorana, Nuovo Cimento **5**, 171 (1937).
51. Majorana particles, in contrast to Dirac fermions, are their own antiparticles. An electrically charged particle (like the electron) cannot coincide with its antiparticle (the positron) which carries the opposite non-zero electric charge.
52. S.M. Bilenky and S.T. Petcov, Rev. Mod. Phys. **59**, 671 (1987).
53. S.T. Petcov, Adv. High Energy Phys. **2013**, 852987 (2013), `arXiv:1303.5819`.
54. S.M. Bilenky, J. Hosek, and S.T. Petcov, Phys. Lett. **B94**, 495 (1980).
55. J. Schechter and J.W.F. Valle, Phys. Rev. **D22**, 2227 (1980); M. Doi *et al.*, Phys. Lett. **B102**, 323 (1981).
56. L. Wolfenstein, Phys. Lett. **B107**, 77 (1981); J. Bernabeu and P. Pascual, Nucl. Phys. **B228**, 21 (1983); S.M. Bilenky, N.P. Nedelcheva, and S.T. Petcov, Nucl. Phys. **B247**, 61 (1984); B. Kayser, Phys. Rev. **D30**, 1023 (1984).
57. M. Apollonio *et al.*, [Chooz Collab.], Phys. Lett. **B466**, 415 (1999); Eur. Phys. J. **C27**, 331 (2003).
58. F. Capozzi *et al.*, Phys. Rev. **D95**, 096014 (2017).
59. I. Esteban *et al.*, JHEP **1701**, 087 (2017).
60. P. Adamson *et al.*, [NOνA Collab.], Phys. Rev. Lett. **118**, 151802 (2017).
61. N. Cabibbo, Phys. Lett. **B72**, 333 (1978).
62. V. Barger *et al.*, Phys. Rev. Lett. **45**, 2084 (1980).
63. P.I. Krastev and S.T. Petcov, Phys. Lett. **B205**, 84 (1988).
64. C. Jarlskog, Z. Phys. **C29**, 491 (1985).
65. P. Langacker *et al.*, Nucl. Phys. **B282**, 589 (1987).

66. S.M. Bilenky, S. Pascoli, and S.T. Petcov, Phys. Rev. **D64**, 053010 (2001), and *ibid.*, 113003.

67. S. Pascoli, S.T. Petcov, and A. Riotto, Phys. Rev. **D75**, 083511 (2007); E. Molinaro and S.T. Petcov, Phys. Lett. **B671**, 60 (2009).

68. S. Pascoli, S.T. Petcov, and A. Riotto, Nucl. Phys. **B774**, 1 (2007).

69. In the convention we use, the neutrino masses are not ordered in magnitude according to their index number: $\Delta m^2_{31} < 0$ corresponds to $m_3 < m_1 < m_2$. We can also number the massive neutrinos in such a way that one always has $m_1 < m_2 < m_3$, see, *e.g.*, Ref. 66.

70. F. Perrin, Comptes Rendus **197**, 868 (1933); E. Fermi, Nuovo Cimento **11**, 1 (1934).

71. V. Lobashev *et al.*, Nucl. Phys. **A719**, 153c, (2003).

72. Ch. Kraus *et al.*, Eur. Phys. J. **C40**, 447 (2005).

73. K. Eitel *et al.*, Nucl. Phys. (Proc. Supp.) **B143**, 197 (2005).

74. V.N. Aseev *et al.*, Phys. Rev. **D84**, 112003 (2011).

75. J. Lesgourgues and L. Verde, "Neutrinos in Cosmology" review in PDG 2017 edition at `http://pdg.lbl.gov`.

76. K.N. Abazajian *et al.*, Astropart. Phys. **35**, 177 (2011); K.N. Abazajian and M. Kaplinghat, Ann. Rev. Nucl. Part. Sci. **66**, 401 (2016).

77. P.A.R. Ade *et al.*, [Planck Collab.], Astron. Astrophys. **571**, A16 (2014).

78. P.A.R. Ade *et al.*, [Planck Collab.], Astron. Astrophys. **594**, A13 (2016).

79. S.M. Koksbang and S. Hannestad, JCAP **1709**, 014 (2017); see also, e.g., R. Farpon, A.E. Nelson and N. Weiner, JCAP **0410**, 005 (2004); Z. Chacko *et al.*, Phys. Rev. Lett. **94**, 111801 (2005).

80. K. Abe *et al.*, [T2K Collab.], Prog. Theor. Exp. Phys. **4**, 043C01 (2015), `arXiv:1609.04111`.

81. A. de Gouvea *et al.*, `arXiv:1310.4340`.

82. M. G. Aartsen *et al.*, [IceCube-PINGU Collab.], `arXiv:1401.2046`.

83. U.F. Katz (for the KM3NeT Collaboration), `arXiv:1402.1022`.

84. S. Adrian-Martinez *et al.*, [KM3Net Collab.], J. Phys. **G43**, 084001 (2016), `arXiv:1601.07459`.

85. S. Ahmed *et al.*, [INO Collab.], Pramana **88**, 79 (2017), `arXiv:1505.07380`.

86. S.T. Petcov and M. Piai, Phys. Lett. **B533**, 94 (2002).

87. S. Choubey, S.T. Petcov and M. Piai, Phys. Rev. **D68**, 113006 (2003).

88. J. Learned *et al.*, Phys. Rev. **D78**, 071302 (2008); L. Zhan *et al.*, Phys. Rev. **D78**, 111103 (2008) and Phys. Rev. **D79**, 073007 (2009); P. Ghoshal and S.T. Petcov, JHEP **1103**, 058 (2011); F. Capozzi, E. Lisi and A. Marrone, Phys. Rev. **D92**, 073011 (2016).

89. S.M. Bilenky, F. Capozzi and S.T. Petcov, Phys. Lett. **B772**, 179 (2017).

90. L. Stanco *et al.*, `arXiv:1707.07651`.

91. F. An *et al.*, J. Phys. **G43**, 030401 (2016).

92. R.N. Cahn *et al.*, `arXiv:1307.5487`; X. Qian and P. Vogel, Prog. Part. Nucl. Phys. **83**, 1 (2015).

93. R. Acciarri *et al.*, [DUNE Collab.] `arXiv:1601.05471` and `arXiv:1601.02984`.

94. K. Abe *et al.*, Prog. Theor. Exp. Phys. **5**, 053C02 (2015), `arXiv:1502.05199`.

95. R. Mohapatra *et al.*, Rept. on Prog. in Phys. **70**, 1757 (2007); A. Bandyopadhyay *et al.*, Rept. on Prog. in Phys. **72**, 106201 (2009).

96. G. Altarelli and F. Feruglio, Rev. Mod. Phys. **82**, 2701 (2010); S.F. King *et al.*, New. J. Phys. **16**, 045018 (2014); I. Girardi *et al.*, Nucl. Phys. **B902**, 1 (2016); R. Barbieri *et al.*, JHEP **9812**, 017 (1998); S.T. Petcov, Phys. Lett. **B110**, 245 (1982).

97. A. Morales and J. Morales, Nucl. Phys. (Proc. Supp.) **B114**, 141 (2003); J. Gómez-Cadenas *et al.*, Riv. Nuovo Cimento **40**, 2 (2012).

98. S. Dell'Oro *et al.*, Adv. High Energy Phys. **2016**, 2162659 (2016).

99. J.D. Vergados, H. Ejiri and F. Simkovic, Int. J. Mod. Phys. **E25**, 1630007 (2016).

100. N. Abgrall *et al.* [LEGEND Collab.], AIP Conf. Proc. **1894**, 020027 (2017), `arXiv:1709.01980 [physics.ins-det]`.

101. F. Iachello, J. Kotila and J. Barea, PoS NEUTEL **2015**, 047 (2015).

102. S. Pascoli and S.T. Petcov, Phys. Lett. **B544**, 239 (2002).

103. S.M. Bilenky *et al.*, Phys. Rev. **D54**, 4432 (1996).

104. S.M. Bilenky *et al.*, Phys. Lett. **B465**, 193 (1999); F. Vissani, JHEP **9906**, 022 (1999); K. Matsuda *et al.*, Phys. Rev. **D62**, 093001 (2000); K. Czakon *et al.*, `hep-ph/0003161`; H.V. Klapdor-Kleingrothaus, H. Päs and A.Yu. Smirnov, Phys. Rev. **D63**, 073005 (2001); S. Pascoli, S.T. Petcov and W. Rodejohann, Phys. Lett. **B549**, 177 (2002), and *ibid.* **B558**, 141 (2003); H. Murayama and Peña-Garay, Phys. Rev. **D69**, 031301 (2004); S. Pascoli, S.T. Petcov, and T. Schwetz, Nucl. Phys. **B734**, 24 (2006); M. Lindner, A. Merle, and W. Rodejohann, Phys. Rev. **D73**, 053005 (2006); A. Faessler *et al.*, Phys. Rev. **D79**, 053001 (2009); W. Rodejohann, Int. J. Mod. Phys. **E20**, 1833 (2011).

105. A. S. Barabash, Phys. Atom. Nucl. **74**, 603 (2011).

106. A.Gando *et al.* [KamLAND-Zen Collab.], Phys. Rev. Lett. **117**, 082503 (2016); Addendum: Phys. Rev. Lett. **117**, 109903 (2016).

107. M. Agostini *et al.* [GERDA Collab.], Phys. Rev. Lett. **120**, 132503 (2018).

108. C. Alduino *et al.* [CUORE Collab.], Phys. Rev. Lett. **120**, 132501 (2018).

109. E. Andreotti *et al.* [Cuoricino Collab.], Astropart. Phys. **34**, 822 (2011).

110. K. Alfonso *et al.* [CUORE Collab.], Phys. Rev. Lett. **115**, 102502 (2015).

111. S. Pascoli, S.T. Petcov, and L. Wolfenstein, Phys. Lett. **B524**, 319 (2002); S.M. Bilenky and S.T. Petcov, `hep-ph/0405237`.

112. S. Pascoli and S.T. Petcov, Phys. Rev. **D77**, 113003 (2008).

113. A. Halprin *et al.*, Phys. Rev. **D13**, 2567 (1976); H. Päs *et al.*, Phys. Lett. **B453**, 194 (1999), and Phys. Lett. **B498**, 35 (2001); F.F. Deppisch, M. Hirsch and H. Päs, J. Phys. **G39**, 124007 (2012); L.C. Helo *et al.*, JHEP **1505**, 092 (2015).

114. A. Halprin, S.T. Petcov and S.P. Rosen, Phys. Lett. **B125**, 335 (1983); F. Deppisch and H. Päs, Phys. Rev. Lett. **98**, 232501 (2007); V.M. Gehman and S.R. Elliott, J. Phys. **G34**, 667 (2007), Erratum J. Phys. **G35**, 029701 (2008).

115. S. M. Bilenky, S. Pascoli and S. T. Petcov, Phys. Rev. **D64**, 113003 (2001); J. Barry, W. Rodejohann and H. Zhang, JHEP **1107**, 091 (2011); I. Girardi, A. Meroni and S. T. Petcov, JHEP **1311**, 146 (2013); M. Blennow *et al.*, JHEP **1007**, 096 (2010).

116. F. Deppisch, talk given at "The XXVII International Conference on Neutrino Physics and Astrophysics" (Neutrino 2016), London (UK), 4-9 July, 2016; F. Deppisch, M. Hirsch and H. Paes, J. Phys. **G39**, 12 (2012).

117. A. Faessler *et al.*, Phys. Rev. **D83**, 113003 (2011); A. Faessler *et al.*, Phys. Rev. **D83**, 113015 (2011); F. Simkovic, J. Vergados, and A. Faessler, Phys. Rev. **D82**, 113015 (2010); A. Meroni, S.T. Petcov, and F. Simkovic, JHEP **1302**, 025 (2013).

118. For alternative mechanisms of neutrino mass generation see, *e.g.*, the first article in Ref. 95, the review article Yi Cai *et al.*, Front. Phys. **5**, 63 (2017), `arXiv:1706.08524`, and references quoted therein.

119. S. Davidson and A. Ibarra, Phys. Lett. **B535**, 25 (2002).

120. A. Abada *et al.*, JCAP **0604**, 004 (2006); E. Nardi *et al.*, JHEP **0601**, 164 (2006).

121. C. Hagedorn and E. Molinaro, Nucl. Phys. **B919**, 404 (2017); P. Chen, G.-J. Ding and S.F. King, JHEP **1603**, 206 (2016); C.-Ch. Li and G.-J. Ding, Phys. Rev. **D96**, 075005 (2017).

122. L.C. Stonehill, J.A. Formaggio, and R.G.H. Robertson, Phys. Rev. **C69**, 015801 (2004).

123. F.L. Villante Phys. Lett. **B742**, 279 (2015).

124. J.N. Bahcall and R.K. Ulrich, Rev. Mod. Phys. **60**, 297 (1988); J.N. Bahcall and M.H. Pinsonneault, Rev. Mod. Phys. **64**, 885 (1992); J.N. Bahcall and M.H. Pinsonneault, Rev. Mod. Phys. **67**, 781 (1995); J.N. Bahcall, M.H. Pinsonneault, and S. Basu, Astrophys. J. **555**, 990 (2001);.

125. J.N. Bahcall, A.M. Serenelli, and S. Basu, Astrophys. J. **621**, L85 (2005).

126. J.N. Bahcall, A.M. Serenelli, and S. Basu, Astrophys. J. Supp. **165**, 400 (2006).

127. S. Turck-Chieze *et al.*, Astrophys. J. **335**, 415 (1988).

128. C. Peña-Garay and A.M. Serenelli, `arXiv:0811.2424`.

129. A.M. Serenelli, W.C. Haxton, and C. Peña-Garay, Astrophys. J. **743**, 24 (2011).

130. N. Vinyoles *et al.*, Astrophys. J. **835**, 202 (2017).

131. E.G. Adelberger *et al.*, Rev. Mod. Phys. **83**, 195 (2011).

132. N. Grevesse and A.J. Sauval, Space Sci. Rev. **85**, 161 (1998).

133. M. Asplund *et al.*, Annu. Rev. Astron. Astrophys. **747**, 481 (2009).

134. A.M. Serenelli, Eur. Phys. J. **A52**, 78 (2016).

135. C. Patrignani *et al.*, (PDG), Chin. Phys. **C40**, No. 10 (2016).

136. M. Honda *et al.*, Phys. Rev. **D70**, 043008 (2004); Phys. Rev. **D75**, 043006 (2007); Phys. Rev. **D83**, 123001 (2011).

137. M. Honda *et al.*, Phys. Rev. **D92**, 023004 (2015).

138. G.D. Barr *et al.*, Phys. Rev. **D70**, 023006 (2004).

139. G. Battistoni *et al.*, Astopart. Phys. **19**, 269 (2003).

140. S.E. Kopp, Phys. Rep. **439**, 101 (2007).

141. A. Ambrosini *et al.*, Phys. Lett. **B420**, 225 (1998); Phys. Lett. **B425**, 208 (1998).

142. M.G. Catanesi *et al.*, Nucl. Instrum. Methods **A571**, 527 (2007).

143. R. Raja, Nucl. Instrum. Methods **A553**, 225 (2005).

144. N. Abgrall *et al.*, Phys. Rev. **C84**, 034604 (2011); Eur. Phys. J. **C76**, 84 (2016); Eur. Phys. J. **C76**, 617 (2016).

145. D. Beavis *et al.*, Physics Design Report, BNL 52459 (1995).

146. K. Abe *et al.*, [T2K Collab.], Phys. Rev. **D87**, 012001 (2013).

147. R.B. Patterson [NOνA Collab.], Nucl. Phys. (Proc. Supp.) **B235-236**, 151 (2013).

148. K. Schrenkenbach, ILL technical report 84SC26T, quoted in M. Apollonio *et al.*, Eur. Phys. J. **C27**, 331 (2003).

149. J. Cao, Nucl. Phys. (Proc. Supp.) **B229-232**, 205 (2012).

150. M.F. James, J. Nucl. Energy **23**, 517 (1969); V. Kopeikin *et al.*, Phys. Atom. Nucl. **67**, 1892 (2004).

151. B.R. Davis *et al.*. Phys. Rev. **C19**, 2259 (1979).

152. P. Vogel *et al.*. Phys. Rev. **C24**, 1543 (1981).

153. F. von Feilitzsch *et al.*, Phys. Lett. **B118**, 162 (1982); K. Schreckenbach *et al.*, Phys. Lett. **B160**, 325 (1985); A.A. Hahn *et al.*. Phys. Lett. **B218**, 365 (1989).

154. N. Haag *et al.*. Phys. Rev. Lett. **112**, 122501 (2014).

155. T.A. Mueller *et al.*, Phys. Rev. **C83**, 054615 (2011).

156. G. Mention *et al.*, Phys. Rev. **D83**, 073006 (2011).

157. P. Huber, Phys. Rev. **C84**, 024617 (2011).

158. F.P. An *et al.*, [Daya Bay Collab.], Phys. Rev. Lett. **116**, 061801 (2016).

159. F.P. An *et al.*, [Daya Bay Collab.], Phys. Rev. Lett. **118**, 251801 (2017).

160. C. Giunti, Phys. Lett. **B764**, 145 (2017); Phys. Rev. **D96**, 033005 (2017).

161. D.A. Dwyer and T.J. Langford, Phys. Rev. Lett. **114**, 012502 (2014); A.A. Sonzogni, T.D. Johnson, and E.A. McCutchan, Phys. Rev. **C91**, 011301R (2015); A.C. Hayes *et al.*, Phys. Rev. **D92**, 033015 (2015); A.A. Zakari-Issoufou *et al.*, Phys. Rev. Lett. **115**, 102503 (2015); A.A. Sonzogni *et al.*, Phys. Rev. Lett. **116**, 132502 (2016); B.C. Rasco *et al.*, Phys. Rev. Lett. **117**, 092501 (2016); C. Buck *et al.*, Phys. Lett. **B765**, 159 (2017); P. Huber, Phys. Rev. Lett. **118**, 042502 (2017).

162. C. Bemporad, G. Gratta, and P. Vogel, Rev. Mod. Phys. **74**, 292 (2002).

163. S. Nussinov, Phys. Lett. **B63**, 201 (1976); B. Kayser, Phys. Rev. **D24**, 110 (1981); J. Rich, Phys. Rev. **D48**, 4318 (1993); H. Lipkin, Phys. Lett. **B348**, 604 (1995); W. Grimus and P. Stockinger, Phys. Rev. **D54**, 3414 (1996); L. Stodolski, Phys. Rev. **D58**, 036006 (1998); W. Grimus, P. Stockinger, and S. Mohanty, Phys. Rev. **D59**, 013011 (1999); L.B. Okun, Surv. High Energy Physics **15**, 75 (2000); J.-M. Levy, `hep-ph/0004221` and `arXiv:0901.0408`; A.D. Dolgov, Phys. Reports **370**, 333 (2002); C. Giunti, Phys. Scripta **67**, 29 (2003) and Phys. Lett. **B17**, 103 (2004); M. Beuthe, Phys. Reports **375**, 105 (2003); H. Lipkin, Phys. Lett. **B642**, 366 (2006); S.M. Bilenky, F. von Feilitzsch, and W. Potzel, J. Phys. **G34**, 987 (2007); C. Giunti and C.W. Kim, *Fundamentals of Neutrino Physics and Astrophysics* (Oxford University Press, Oxford, 2007); E.Kh. Akhmedov, J. Kopp, and M. Lindner, JHEP **0805**, 005 (2008); E.Kh. Akhmedov and A.Yu. Smirnov, Phys. Atom. Nucl. **72**, 1363 (2009).

164. For the subtleties involved in the step leading from Eq. (14.1) to Eq. (14.28) see, *e.g.*, Ref. 165.

165. A.G. Cohen, S.L. Glashow, and Z. Ligeti, Phys. Lett. **B678**, 191 (2009).

166. The neutrino masses do not exceed approximately 1 eV, $m_j \lesssim 1$, while in neutrino oscillation experiments neutrinos with energy $E \gtrsim 100$ keV are detected.

167. E. K. Akhmedov, J. Kopp and M. Lindner, JHEP **0805**, 005 (2008).

168. S.M. Bilenky and B. Pontecorvo, Phys. Reports **41**, 225 (1978).

169. In Eq. (14.33) we have neglected the possible instability of neutrinos ν_j. In most theoretical models with nonzero neutrino masses and neutrino mixing, the predicted half life-time of neutrinos with mass of 1 eV exceeds the age of the Universe, see, *e.g.*, S.T. Petcov, Yad. Fiz. **25**, 641 (1977), (E) *ibid.*, **25**, 1336 (1977) [Sov. J. Nucl. Phys. **25**, 340 (1977), (E) *ibid.*, **25**, 698 (1977)], and Phys. Lett. **B115**, 401 (1982); W. Marciano and A.I. Sanda, Phys. Lett. **B67**, 303 (1977); P. Pal and L. Wolfenstein, Phys. Rev. **D25**, 766 (1982).

170. L.B. Okun (2000), J.-M. Levy (2000) and H. Lipkin (2006) quoted in Ref. 163 and Ref. 165.

171. The articles by L. Stodolsky (1998) and H. Lipkin (1995) quoted in Ref. 163.

172. A. De Rujula *et al.*, Nucl. Phys. **B168**, 54 (1980).

173. N. Agafonova *et al.*, [OPERA Collab.], Phys. Lett. **B691**, 138 (2010); New J. Phys. **14**, 033017 (2012).

174. N. Agafonova *et al.*, [OPERA Collab.], JHEP **1311**, 036 (2013).

175. M.H. Ahn *et al.*, [K2K Collab.], Phys. Rev. Lett. **93**, 051801 (2004); S. Yamamoto *et al.*, [K2K Collab.], Phys. Rev. Lett. **96**, 181801 (2006).

176. S.M. Bilenky, D. Nicolo and S.T. Petcov, Phys. Lett. **B538**, 77 (2002).

177. V. Gribov and B. Pontecorvo, Phys. Lett. **B28**, 493 (1969).

178. S. Goswami *et al.*, Nucl. Phys. (Proc. Supp.) **B143**, 121 (2005).

179. These processes are important, however, for the supernova neutrinos see, *e.g.*, G. Raffelt, *Proc. International School of Physics "Enrico Fermi", CLII Course "Neutrino Physics"*, 23 July-2 August 2002, Varenna, Italy [`hep-ph/0208024`]), and articles quoted therein.

180. We standardly assume that the weak interaction of the flavour neutrinos ν_l and antineutrinos $\bar{\nu}_l$ is described by the Standard Model (for alternatives see, *e.g.*, Ref. 26; M.M. Guzzo *et al.*, Phys. Lett. **B260**, 154 (1991); E. Roulet, Phys. Rev. **D44**, R935 (1991) and Ref. 95).

181. V. Barger *et al.*, Phys. Rev. **D22**, 2718 (1980).

182. P. Langacker, J.P. Leveille, and J. Sheiman, Phys. Rev. **D27**, 1228 (1983).

183. The difference between the ν_μ and ν_τ indices of refraction arises at one-loop level and can be relevant for the $\nu_\mu - \nu_\tau$ oscillations in very dense media, like the core of supernovae, *etc.*; see F.J. Botella, C.S. Lim, and W.J. Marciano, Phys. Rev. **D35**, 896 (1987).

184. The relevant formulae for the oscillations between the ν_e and a sterile neutrino ν_s, $\nu_e \leftrightarrow \nu_s$, can be obtained from those derived for the case of $\nu_e \leftrightarrow \nu_{\mu(\tau)}$ oscillations by Refs. [65,182] replacing N_e with $(N_e - 1/2N_n)$, N_n being the neutron number density in matter.

185. T.K. Kuo and J. Pantaleone, Phys. Lett. **B198**, 406 (1987).

186. A.D. Dziewonski and D.L. Anderson, Physics of the Earth and Planetary Interiors **25**, 297 (1981).

187. The first studies of the effects of Earth matter on the oscillations of neutrinos were performed numerically in Refs. [181,188] and in E.D. Carlson, Phys. Rev. **D34**,

1454 (1986); A. Dar *et al.*, *ibid.*, **D35**, 3607 (1988); in Ref. 63 and in G. Auriemma *et al.*, *ibid.*, **D37**, 665 (1988).

188. A.Yu. Smirnov and S.P. Mikheev, *Proc. of the VIth Moriond Workshop* (eds. O. Fackler, J. Tran Thanh Van, Frontières, Gif-sur-Yvette, 1986), p. 355.

189. S.T. Petcov, Phys. Lett. **B434**, 321 (1998), (E) *ibid.* **B444**, 584 (1998); see also Nucl. Phys. (Proc. Supp.) **B77**, 93 (1999) and `hep-ph/9811205`.

190. M.V. Chizhov, M. Maris, and S.T. Petcov, `hep-ph/9810501`.

191. E.Kh. Akhmedov *et al.*, Nucl. Phys. **B542**, 3 (1999).

192. S.T. Petcov, Phys. Lett. **B214**, 259 (1988).

193. J. Hosaka *et al.*, [Super-Kamiokande Collab.], Phys. Rev. **D74**, 032002 (2006).

194. I. Mocioiu and R. Shrock, Phys. Rev. **D62**, 053017 (2000).

195. E.Kh. Akhmedov, Nucl. Phys. **B538**, 25 (1999).

196. M.V. Chizhov and S.T. Petcov, Phys. Rev. Lett. **83**, 1096 (1999) and Phys. Rev. Lett. **85**, 3979 (2000); Phys. Rev. **D63**, 073003 (2001).

197. J. Bernabéu, S. Palomares-Ruiz, and S.T. Petcov, Nucl. Phys. **B669**, 255 (2003); S. Palomares-Ruiz and S.T. Petcov, Nucl. Phys. **B712**, 392 (2005); S.T. Petcov and T. Schwetz, Nucl. Phys. **B740**, 1 (2006); R. Gandhi *et al.*, Phys. Rev. **D76**, 073012 (2007); E.Kh. Akhmedov, M. Maltoni, and A.Yu. Smirnov, JHEP **0705**, 077 (2007).

198. The mantle-core enhancement maxima, *e.g.*, in $P_m^{2\nu}(\nu_\mu \to \nu_\mu)$, appeared in some of the early numerical calculations, but with incorrect interpretation (see, *e.g.*, the articles quoted in Ref. 187).

199. M. Honda *et al.*, Phys. Rev. **D52**, 4985 (1995); V. Agraval *et al.*, Phys. Rev. **D53**, 1314 (1996); G. Fiorentini *et al.*, Phys. Lett. **B510**, 173 (2001).

200. K. Abe *et al.*, [Hyper-Kamiokande Proto-Collab.], KEK Report 2016-21; ICRR-Report-701-2016-1.

201. O.L.G. Peres and A.Y. Smirnov, Phys. Lett. **B456**, 204 (1999), and Nucl. Phys. Proc. Suppl. **110**, 355 (2002).

202. M. Freund, Phys. Rev. **D64**, 053003 (2001).

203. M.C. Gonzalez-Garcia and Y. Nir, Rev. Mod. Phys. **75**, 345 (2003); S.M. Bilenky, W. Grimus, and C. Giunti, Prog. in Part. Nucl. Phys. **43**, 1 (1999).

204. J.N. Bahcall, *Neutrino Astrophysics*, Cambridge University Press, Cambridge, 1989; J.N. Bahcall and M. Pinsonneault, Phys. Rev. Lett. **92**, 121301 (2004); J.N. Bahcall, A.M. Serenelli and S. Basu, Astrophys. J. Supp. **165**, 400 (2006).

205. N. Cabibbo, summary talk at the International Workshop on Weak Interaction and Neutrinos (WIN), June 1985, Savonlina, Finland.

206. A. Messiah, *Proc. of the VIth Moriond Workshop* (eds. O. Fackler, J. Tran Thanh Van, Frontières, Gif-sur-Yvette, 1986), p. 373.

207. S.J. Parke, Phys. Rev. Lett. **57**, 1275 (1986).

208. S.T. Petcov, Phys. Lett. **B200**, 373 (1988).

209. P.I. Krastev and S.T. Petcov, Phys. Lett. **B207**, 64 (1988); see also M. Bruggen, W.C. Haxton, and Y.-Z. Quian, Phys. Rev. **D51**, 4028 (1995).

210. T. Kaneko, Prog. Theor. Phys. **78**, 532 (1987); S. Toshev, Phys. Lett. **B196**, 170 (1987); M. Ito, T. Kaneko, and M. Nakagawa, Prog. Theor. Phys. **79**, 13 (1988), (E) *ibid.*, **79**, 555 (1988).

211. S.T. Petcov, Phys. Lett. **B406**, 355 (1997).

212. C. Cohen-Tannoudji, B. Diu, and F. Laloe, *Quantum Mechanics*, Vol. 1 (Hermann, Paris, and John Wiley & Sons, New York, 1977).

213. S.T. Petcov, Phys. Lett. **B214**, 139 (1988); E. Lisi *et al.*, Phys. Rev. **D63**, 093002 (2000); A. Friedland, Phys. Rev. **D64**, 013008 (2001).

214. S.T. Petcov and J. Rich, Phys. Lett. **B224**, 401 (1989).

215. An expression for the "jump" probability P' for N_e varying linearly along the neutrino path was derived in W.C. Haxton, Phys. Rev. Lett. **57**, 1271 (1986) and in Ref. 207 on the basis of the old Landau-Zener result: L.D. Landau, Phys. Z. USSR **1**, 426 (1932), C. Zener, Proc. R. Soc. **A137**, 696 (1932). An analytic description of the solar ν_e transitions based on the Landau-Zener jump probability was proposed in Ref. 207 and in W.C. Haxton, Phys. Rev. **D35**, 2352 (1987). The precision limitations of this description, which is less accurate than that based on the exponential density approximation, were discussed in S.T. Petcov, Phys. Lett. **B191**, 299 (1987) and in Ref. 209.

216. A. de Gouvea, A. Friedland, and H. Murayama, JHEP **0103**, 009 (2001).

217. C.-S. Lim, Report BNL 52079, 1987; S.P. Mikheev and A.Y. Smirnov, Phys. Lett. **B200**, 560 (1988).

218. G.L. Fogli *et al.*, Phys. Lett. **B583**, 149 (2004).

219. S.P. Mikheyev and A.Yu. Smirnov, *Proc. of the VIth Moriond Workshop* (eds. O. Fackler, J. Tran Thanh Van, Frontières, Gif-sur-Yvette, 1986), p. 355.

220. M. Cribier *et al.*, Phys. Lett. **B182**, 89 (1986); J. Bouchez et al., Z. Phys. **C32**, 499 (1986).

221. E. Lisi and D. Montanino, Phys. Rev. **D56**, 1792 (1997); Q.Y. Liu, M. Maris and S.T. Petcov, Phys. Rev. **D56**, 5991 (1997); M. Maris and S.T. Petcov, Phys. Rev. **D56**, 7444 (1997); J.N. Bahcall and P.I. Krastev, Phys. Rev. **C56**, 2839 (1997); J.N. Bahcall, P.I. Krastev and A.Y. Smirnov, Phys. Rev. **D60**, 093001 (1999); M. Maris and S.T. Petcov, Phys. Rev. **D62**, 093006 (2000); J.N. Bahcall, P.I. Krastev and A.Y. Smirnov, Phys. Rev. **D62**, 093004 (2000); M.C. Gonzalez-Garcia, C. Pena-Garay and A.Y. Smirnov, Phys. Rev. **D63**, 113004 (2001); P.I. Krastev and A.Y. Smirnov, Phys. Rev. **D65**, 073022 (2002).

222. A. Bandyopadhyay *et al.*, Phys. Lett. **B583**, 134 (2004); M. Blennow, T. Ohlsson and H. Snellman, Phys. Rev. **D69**, 073006 (2004); E.K. Akhmedov, M.A. Tortola and J.W.F. Valle, JHEP **0405**, 057 (2004).

223. K.S. Hirata *et al.*, [Kamiokande Collab.], Phys. Rev. Lett. **63**, 16 (1989).

224. Y. Fukuda *et al.*, [Super-Kamiokande Collab.], Phys. Rev. Lett. **81**, 1158 (1998).

225. J. Hosaka *et al.*, [Super-Kamiokande Collab.], Phys. Rev. **D73**, 112001 (2006).

226. J.P. Cravens *et al.*, [Super-Kamiokande Collab.], Phys. Rev. **D78**, 032002 (2008).

227. K. Abe *et al.*, [Super-Kamiokande Collab.], Phys. Rev. **D83**, 052010 (2011).

228. K. Abe *et al.*, [Super-Kamiokande Collab.], Phys. Rev. **D94**, 052010 (2016).

229. B. Aharmim *et al.*, [SNO Collab.], Phys. Rev. **C72**, 055502 (2005).

230. B. Aharmim *et al.*, [SNO Collab.], Phys. Rev. Lett. **101**, 111301 (2008); Phys. Rev. **C87**, 015502 (2013).

231. G. Bellini *et al.*, [Borexino Collab.], Phys. Rev. Lett. **107**, 141302 (2011).

232. G. Bellini *et al.*, [Borexino Collab.], Phys. Rev. Lett. **108**, 051302 (2012).

233. G. Bellini *et al.*, [Borexino Collab.], Nature **512**, 383 (2014).

234. G. Bellini *et al.*, [Borexino Collab.], Phys. Rev. **D82**, 033006 (2010).

235. G. Bellini *et al.*, [Borexino Collab.], Phys. Rev. **D89**, 112007 (2014).

236. M. Agostini *et al.*, [Borexino Collab.], `arXiv:1707.09279`.

237. M. Agostini *et al.*, [Borexino Collab.], `arXiv:1709.00756`.

238. A. Gando *et al.*, [KamLAND Collab.], Phys. Rev. **C92**, 055808 (2015).

239. S. Abe *et al.*, [KamLAND Collab.], Phys. Rev. **C84**, 035804 (2011).

240. B. Pontecorvo, Chalk River Lab. report PD-205, 1946.

241. P. Anselmann *et al.*, [GALLEX Collab.], Phys. Lett. **B342**, 440 (1995); W. Hampel *et al.*, [GALLEX Collab.], Phys. Lett. **B420**, 114 (1998).

242. J.N. Abdurashitov *et al.*, [SAGE Collab], Phys. Rev. Lett. **77**, 4708 (1996); Phys. Rev. **C59**, 2246 (1999).

243. K.S. Hirata *et al.*, [Kamiokande Collab.], Phys. Lett. **B205**, 416 (1988) and Phys. Lett. **B280**, 146 (1992).

244. Y. Fukuda *et al.*, [Kamiokande Collab.], Phys. Lett. **B335**, 237 (1994).

245. D. Casper *et al.*, [IMB Collab.], Phys. Rev. Lett. **66**, 2561 (1991).

246. K. Daum *et al.*, [Frejus Collab.], Z. Phys. **C66**, 417 (1995).

247. W.W.M. Allison *et al.*, [Soudan 2 Collab.], Phys. Lett. **B391**, 491 (1997).

248. M. Ambrosio *et al.*, [MACRO Collab.], Phys. Lett. **B434**, 451 (1998); Phys. Lett. **B566**, 35 (2003).

249. M. Sanchez *et al.*, [Soudan 2 Collab.], Phys. Rev. **D68**, 113004 (2003); W.W.M. Allison *et al.*, [Soudan 2 Collab.], Phys. Rev. **D72**, 052005 (2005).

250. P. Adamson *et al.*, [MINOS Collab.], Phys. Rev. **D86**, 052007 (2012).

251. M. Ageron *et al.*, [ANTARES Collab.], Nucl. Instrum. Methods **A656**, 11 (2011).

252. M.G. *et al.*, [IceCube Collab.], Astropart. Phys. **35**, 615 (2012).

253. S. Adrián-Martínez *et al.*, [ANTARES Collab.], Phys. Lett. **B714**, 224 (2012).

254. M.G. Aartsen *et al.*, [IceCube Collab.], Phys. Rev. Lett. **120**, 071801 (2018).

255. M.G. Aartsen *et al.*, [IceCube Collab.], Phys. Rev. Lett. **111**, 081801 (2013); Phys. Rev. **D91**, 072004 (2015).

256. G. Tzanakos *et al.*, [MINOS+ Collab.], FERMILAB-PROPOSAL-1016 (2011).

257. S. Wojcicki, *Proc. of the 1997 SLAC Summer Institute.*

258. M. Antonello *et al.*, [ICARUS Collab.], Eur. Phys. J. **C73**, 2345 (2013); Eur. Phys. J. **C73**, 2599 (2013).

259. A. Aguilar *et al.*, [LSND Collab.], Phys. Rev. **D64**, 112007 (2001).

260. B. Armbruster *et al.*, [Karmen Collab.], Phys. Rev. **D65**, 112001 (2002).

261. A.A. Aguilar-Arevalo *et al.*, [MiniBooNE Collab.], Phys. Rev. Lett. **98**, 231801 (2007); Phys. Rev. Lett. **102**, 101802 (2009).

262. A.A. Aguilar-Arevalo *et al.*, [MiniBooNE Collab.], Phys. Rev. Lett. **105**, 181801 (2010); Phys. Rev. Lett. **110**, 161801 (2013).

263. For the Fermilab short-Baseline Neutrino (SBN) Program, we refer to S. Tufanli, Talk at the EPS International Conference on High Energy Physics, July 2017, Venice, Italy.

264. F. Boem and P. Vogel, *Physics of Massive Neutrinos*, Cambridge Univ. Press, 1987.

265. F. Boehm *et al.*, Phys. Rev. **D64**, 112001 (2001).

266. F. Suekane and T.J.C. Bezerra, Nucl. Phys. **B908**, 74 (2016).

267. J. Cao and K. B. Luk, Nucl. Phys. **B908**, 62 (2016).

268. S. B. Kim, Nucl. Phys. **B908**, 94 (2016).

269. Y.-F. Li Int. J. Mod. Phys.: Conf. Ser. **31**, 1460300 (2014).

270. D. Davis, Jr., D.S. Harmer, and K.C. Hoffman, Phys. Rev. Lett. **20**, 1205 (1968).

271. A.I. Abazov *et al.*, [SAGE Collab.], Phys. Rev. Lett. **67**, 3332 (1991).

272. Note that after publication of Ref. 8, the SAGE results including an extended observation period are reported by V.N. Gavrin in Phys.-Usp. **54**, 941 (2011). Also, F. Kaether *et al.*, Phys. Lett. **B685**, 47 (2010) reanalyzed a complete set of the GALLEX data with a method providing a better background reduction than that adopted in Ref. 10. The resulting GALLEX and GNO+GALLEX capture rates are slightly different from, but consistent with, those reported in Table 14.5.

273. Y. Fukuda *et al.*, [Super-Kamiokande Collab.], Phys. Rev. Lett. **86**, 5651 (2001).

274. Y. Fukuda *et al.*, [Super-Kamiokande Collab.], Phys. Lett. **B539**, 179 (2002).

275. G. L. Fogli *et al.*, Phys. Rev. **D67**, 073002 (2003); M. Maltoni, T. Schwetz, and J.W. Valle, Phys. Rev. **D67**, 093003 (2003); A. Bandyopadhyay *et al.*, Phys. Lett. **B559**, 121 (2003); J.N. Bahcall, M.C. Gonzalez-Garcia, and C. Peña-Garay, JHEP **0302**, 009 (2003); P.C. de Holanda and A.Y. Smirnov, JCAP **0302**, 001 (2003).

276. S. Abe *et al.*, [KamLAND Collab.], Phys. Rev. Lett. **100**, 221803 (2008).

277. A. Gando *et al.*, [KamLAND Collab.], Phys. Rev. **D83**, 052002 (2011).

278. B. Aharmim *et al.*, [SNO Collab.], Phys. Rev. **C81**, 055504 (2010).

279. B. Aharmim *et al.*, [SNO Collab.], Phys. Rev. **C88**, 025501 (2013).

280. http://pdg.lbl.gov/2017/listings/contents_listings.html.

281. B. Geytenbeek *et al.*, JCAP **1703**, 029 (2017).

282. J. Bergstrom *et al.*, JHEP **1603**, 132 (2016).

283. G. Bellini *et al.*, [Borexino Collab.], Phys. Lett. **B707**, 22 (2012).

284. A. Renshaw *et al.*, [Super-Kamiokande Collab.], Phys. Rev. Lett. **112**, 091805 (2014).

285. S. T. Petcov, Nucl. Phys. **B892**, 400 (2015); C. Hagedorn, A. Meroni, and E. Molinaro, Nucl. Phys. **B891**, 499 (2015); I. Girardi, S.T. Petcov, and A.V. Titov, Nucl. Phys. **B894**, 733 (2015), and Eur. Phys. J. **C75**, 345 (2015); P. Ballett, S. Pascoli, and J. Turner, Phys. Rev. **D92**, 093008 (2015); C.C. Li and G.J. Ding, JHEP **1505**, 100 (2015); J.T. Penedo, S.T. Petcov and A.V. Titov, JHEP **1712**, 022 (2017).

286. V. Barger *et al.*, Phys. Rev. Lett. **82**, 2640 (1999).

287. E. Lisi *et al.*, Phys. Rev. Lett. **85**, 1166 (2000).

288. K. Abe *et al.*, [Super-Kamiokande Collab.], Phys. Rev. **D97**, 072001 (2018).

289. P. Adamson *et al.*, [MINOS Collab.], Phys. Rev. Lett. **112**, 191801 (2014).

290. P. Adamson *et al.*, [MINOS Collab.], Phys. Rev. Lett. **110**, 251801 (2013).

291. K.A. Olive *et al.*, (PDG), Chin. Phys. **C38**, 090001 (2014) and 2015 update (http://pdg.lbl.gov/2015/).

292. P. Adamson *et al.*, [MINOS Collab.], Phys. Rev. Lett. **107**, 021801 (2011); Phys. Rev. Lett. **108**, 191801 (2012).

293. K. Abe *et al.*, [T2K Collab.], Phys. Rev. Lett. **116**, 181801 (2016).

294. K. Abe *et al.*, [T2K Collab.], Phys. Rev. **D96**, 011102 (2017).

295. K. Abe *et al.*, [Super-Kamiokande Collab.], Phys. Rev. Lett. **107**, 241801 (2011).

296. K. Abe *et al.*, [Super-Kamiokande Collab.], Phys. Rev. Lett. **97**, 171801 (2006).

297. N. Agafonova *et al.*, [OPERA Collab.], Phys. Rev. Lett. **115**, 121802 (2015).

298. K. Abe *et al.*, [T2K Collab.], Phys. Rev. **D91**, 072010 (2015).

299. K. Abe *et al.*, [T2K Collab.], Phys. Rev. **D96**, 092006 (2017).

300. M. Hartz, talk at KEK colloquium, August 2017.

301. A.C. Hayes *et al.*, Phys. Rev. Lett. **112**, 202501 (2014).

302. P. Astier *et al.*, [NOMAD Collab.], Phys. Lett. **B570**, 19 (2003).

303. N. Agafanova *et al.*, [OPERA Collab.], JHEP **1307**, 004 (2013); JHEP **1307**, 085 (2013).

304. F. Dydak *et al.*, [CDHSW Collab.], Phys. Lett. **B134**, 281 (1984).

305. M.G. Aartsen *et al.*, [IceCube Collab.], Phys. Rev. Lett. **117**, 071801 (2016).

306. Y. Ko *et al.*, [NEOS Collab.], Phys. Rev. Lett. **118**, 121802 (2017).

307. M. Danilov *et al.*, [DANSS Collab.], talk given at the Moriond Workshop on Electroweak Physics, March 2017.

308. S.T. Petcov, Int. J. Mod. Phys. **A32**, 1750018 (2017), `arXiv:1611.09247`.

309. P.A. Adamson *et al.*, Phys. Rev. Lett. **117**, 151801 (2016).

310. F.P. An *et al.*, [Daya Bay Collab.], Phys. Rev. Lett. **113**, 141802 (2014).

311. S. Gariazzo *et al.*, JHEP **1706**, 135 (2017).

312. J. Kopp *et al.*, JHEP **1305**, 050 (2013).

313. C. Giunti *et al.*, Phys. Rev. **D88**, 073008 (2013).

314. M. Archidiacono *et al.*, Phys. Rev. **D86**, 065028 (2012).

315. S. Gariazzo *et al.*, J. Phys. **G43**, 033001 (2016).